Mo-Si-B Alloys for Ultrahigh-Temperature Structural Applications

*J. A. Lemberg and R. O. Ritchie**

A continuing quest in science is the development of materials capable of operating structurally at ever-increasing temperatures. Indeed, the development of gas-turbine engines for aircraft/aerospace, which has had a seminal impact on our ability to travel, has been controlled by the availability of materials capable of withstanding the higher-temperature hostile environments encountered in these engines. Nickel-base superalloys, particularly as single crystals, represent a crowning achievement here as they can operate in the combustors at ~1100 °C, with hot spots of ~1200 °C. As this represents ~90% of their melting temperature, if higher-temperature engines are ever to be a reality, alternative materials must be utilized. One such class of materials is Mo-Si-B alloys; they have higher density but could operate several hundred degrees hotter. Here we describe the processing and structure versus mechanical properties of Mo-Si-B alloys and further document ways to optimize their nano/microstructures to achieve an appropriate balance of properties to realistically compete with Ni-alloys for elevated-temperature structural applications.

1. Introduction

The quest for new, ultrahigh temperature structural materials is principally driven by the ever present need to improve the efficiency of aerospace and power-generation gas-turbine engines by operating at higher temperatures. Currently, turbine blades made from single-crystal nickel-base superalloys can function at temperatures nearing 1150 °C, i.e., close to 90% of their melting points.[1] Using complex cooling systems and thermal barrier coatings, these materials can exist in the hottest regions of a turbine engine where temperatures can approach 1500 °C. However, the necessity for coatings and forced-air cooling greatly reduces the efficiency gained from operating at the higher temperatures, as shown in **Figure 1**. To combat growing inefficiency losses, a preferred solution is the development of new ultrahigh temperature structural materials capable of operating at such temperatures; one such class of materials which shows potential in this regard is based on the silicides of refractory metals, in particular involving the Mo-Si-B system.

Mo-Si-B alloys have been the subject of a number of reviews that have been published since the early 1990s,[1–12] but many of these works either focused solely on one alloy system[3,4,9–11] or on one specific property of the alloys.[8] The only truly comprehensive review of the research on Mo-Si-B alloys was published in 2007 by Perepezko et al.,[2] but that review does not contain information about the cutting-edge processing techniques which have been developed since its publication.

Here, the development of Mo-Si-B alloys is reviewed from the initial work of Nowotny et al.[13] who developed the first phase diagram for the Mo-Si-B ternary system, to the most recent studies[14,15] on ultra-fine grained Mo-3Si-1B alloys. We highlight the processing methods used to produce Mo-Si-B alloys, as well as their oxidation and mechanical response, focusing on alloys in the α-Mo-Mo_3Si-Mo_5SiB_2 and Mo_3Si-Mo_5Si_3-Mo_5SiB_2 phase regimes, although other systems are discussed. A brief description of the thermodynamics and phase stability of the Mo-Si-B system is also included, although for a more detailed discussion of this particular topic, the reader is referred to the excellent review of research in this area by Perepezko et al.[2]

2. Single Phase Properties

We begin by reviewing the properties of individual phases within the Mo-Si-B system. Unless otherwise noted, all quantities are expressed as wt.%. **Figure 2** shows the Mo-rich portion of the 1600 °C isotherm of the Mo-Si-B phase diagram, as developed by Nowotny et al.[13] and later refined by Nunes et al.[16] We will focus on the properties of the α-Mo phases and the intermetallic phases Mo_3Si, Mo_5Si_3 (T1) and Mo_5SiB_2 (T2).

2.1. Molybdenum and α-Mo Solid Solutions

Pure molybdenum cannot be used in oxidative environments above ~500 °C as a result of the rapid formation and

Prof. R. O. Ritchie, Dr. J. A. Lemberg
Materials Sciences Division
Lawrence Berkeley National Laboratory
Berkeley, CA 94720, USA
E-mail: RORitchie@lbl.gov
Prof. R. O. Ritchie, Dr. J. A. Lemberg
Department of Mater. Sci. Eng.
University of California Berkeley
Berkeley, CA 94720, USA

DOI: 10.1002/adma.201200764

volatilization of MoO_3.[17] Thus it is necessary to limit the α-Mo content for the best oxidation performance. However, as described in Section 5.2, α-Mo is required for any measure of ductility and damage tolerance in Mo-Si-B alloys, as the intermetallic phases are inherently brittle. (Damage-tolerance here represents resistance to crack propagation or more generally a tolerance to the presence of cracks. An essential requirement of almost all structural materials, it is afforded by the often mutually exclusive mechanical properties of strength combined with ductility and toughness.) One strategy to limit the amount of α-Mo is to improve the room temperature ductility of α-Mo. In that way, the same damage tolerance can be afforded by less α-Mo (thus improving the oxidation resistance of the alloy).

The strength and ductility of body-centered cubic molybdenum is strongly influenced by impurities and solid solution strengthening. Silicon is well known[18–20] as a solid solution strengthener of Mo, but as it segregates to dislocation cores[18] and grain boundaries,[19–22] this can lead to the embrittlement of α-Mo based alloys. Numerous strategies have been employed to combat this embrittlement, including alloying with zirconium,[9,10,21–23] rhenium[24] (which realized significant gains in ductility, but required nearly equal weights of molybdenum and rhenium), or $MgAl_2O_4$ spinel.[25–30]

The influence of Si on the ductility and toughness of Mo was investigated by Sturm et al.,[20] who reported negligible room temperature ductility with the addition of only 0.1 wt.% Si. Dramatic increases by as much as a factor of six in yield strength, however, were realized with small amounts of Si additions (**Figure 3**), with strength levels in each alloy being insensitive to grain size. The insensitivity of yield strengths to grain size was ascribed to a failure in the case of these alloys of the underlying assumption of a single dislocation pile-up in the Hall-Petch model.[20] Concomitant with the elevated yield strength with increasing Si content, the authors saw a precipitous drop in the room-temperature fracture toughness from ~24 MP$\alpha\sqrt{m}$ with no silicon to ~ 4 MP$\alpha\sqrt{m}$ with the addition of only 1 wt.% Si.[20] A weakening of the grain boundaries by Si segregation, as indicated by a transition to intergranular fracture, was blamed for this significant reduction in fracture toughness.

Zirconium has been shown[21,22] to be an effective ductilizing agent in molybdenum alloys. Miller et al.,[21] for example, reported a marked increase, by nearly a factor of seven, in the ductility of Mo weldments with a transition from an intergranular to a transgranular fracture mode. They attributed this increase in ductility to the presence of small amounts of Zr (0.16 at.%) which was added to getter oxygen and nitrogen impurities, as well as small (<100 appm) C and B additions meant to strengthen the grain boundaries. These additions prevented the segregation of oxygen to the grain boundaries, where it is known to embrittle. Specifically, Zr segregates to grain boundaries, where it competes with O, and possibly N and Si, for grain boundary sites.[22]

Following the studies of Miller et al.,[21,22] a number of recent publications[9,10,23] have concentrated on Zr additions as a means to prevent Si segregation to grain boundaries in Mo-Si alloys (and thus the α-Mo phase in Mo-Si-B alloys). Saage et al.[23] added 1 at.% Zr to mechanically-alloyed Mo-1.5Si (at.%) and saw a reduction in grain size of ~50% with the addition of Zr. Even without added Zr, they observed a reduction in grain size of more than an order of magnitude for their mechanically alloyed material, as compared to a traditionally blended-powder alloy. Bend tests on their alloys revealed limited ductility (0.1% plastic strain) at room temperature in the Zr-doped material, while the Mo-Si alloy and an alloy containing 0.7 vol.% Y_2O_3 (added to reduce the grain size below 1 μm) exhibited no ductility even at 538°C. At higher temperatures, the Y_2O_3-added material did show some ductility, but the strength of this alloy was diminished compared to the Zr-added material. These results are reproduced in **Figure 4**. The authors attributed these effects to increased grain boundary cohesion and a reduction in grain size, both resulting from the addition of Zr.[23] Auger electron spectra of the grain boundaries in their Zr-added material showed a depletion of Si at the grain boundaries, which was attributed to a competition between Zr and Si for residence within grain boundaries,[23] confirming the earlier work of Miller et al.[21,22] Saage et al. also reported a roughly 14% increase in the amount of transgranular cleavage with the addition of Zr (93% intergranular in undoped condition, ~80%

Joseph A. Lemberg graduated from Cornell University magna cum laude with a B.S. with Honors in Materials Science & Engineering in 2005. He continued his studies in Materials Sciences & Engineering at the University of California, Berkeley, where he was awarded a National Defense Science and Engineering Graduate Fellowship. He completed his Ph.D. in 2012, which focused on the fracture of Mo-Si-B alloys at ultra-high temperatures. Dr. Lemberg now serves as an engineering consultant with Exponent, Inc., Menlo Park, California.

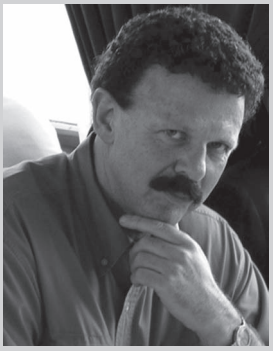

Robert O. Ritchie is the Chua Distinguished Professor of Engineering in the Materials Science & Engineering Department at the University of California Berkeley; he is also Senior Faculty Scientist at the Lawrence Berkeley National Laboratory. He received B.A. (1969), M.A. (1972), Ph.D. (1973) and Sc.D. (1990) degrees in physics/materials science from Cambridge University, and is known for his research into the mechanics and mechanisms of fracture and fatigue of structural and biological materials. He is a member of the U.S. National Academy of Engineering, the U.K. Royal Academy of Engineering, and the Russian Academy of Sciences.

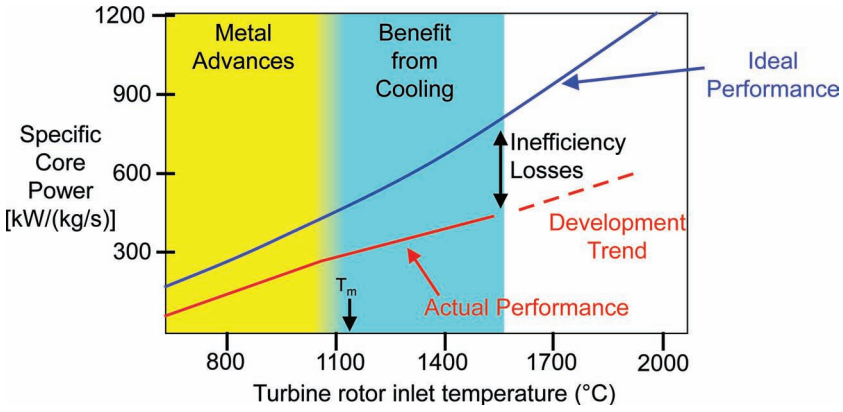

Figure 1. Specific core power *vs.* turbine inlet temperature for gas turbine engines. Current engines operate above the melting temperature of the Ni-based superalloys used within the hottest regions of the engine. As a result of complex cooling schemes and thermal barrier coatings, these turbine blade materials operate at ~1150 °C, nearly 90% of the melting temperature (0.9 T_m). As the operating temperature has increased, an increasing large amount of the power generated is required to cool the turbine blades, drastically reducing the actual engine performance. New materials must be developed that can operate at high (>1300 °C) temperatures without the need for cooling. Refractory metal silicides, such as Mo-Si-B, are potential replacements for Ni-based superalloys. Note, the term "ideal performance" refers to a condition of maximum thermodynamic efficiency. After Dimiduk and Perepezko.[1]

intergranular in the Zr-added condition),[23] which represents a further indication of increased grain boundary strength.

Another additive which has been shown to increase the ductility of Mo alloys is $MgAl_2O_4$, as shown in **Figure 5**.[25–29] Scruggs, in his 1967 patent,[27] attributed this increased ductility in Mo and Cr alloys to gettering of oxygen by the brittle spinel particles, much in the same way that Zr is thought to act as a gettering agent.[21–23] An increased ductility was verified for Cr alloys by Brady et al.[30] with the addition of $MgCr_2O_4$ spinel, but the impurities (nitrogen) did not directly incorporate into the spinel; instead, nitrides precipitated at the Cr/spinel boundaries. They found similar behavior for non-spinel-forming additions, and claimed that the impurity segregation behavior is not unique to spinels.

With this understanding, Sun[25] studied the thermomechanical response of Mo alloys containing fine dispersions of $MgAl_2O_4$ spinel and MgO. She found that the spinel distribution and particle size was an important factor in the ductility of her alloys. Alloys containing large spinel particles failed in brittle fashion at room temperature, while an alloy containing small spinel particles with nearly the same composition exhibited room temperature ductility. No explanation was given as to why this might be the case except to quote the earlier work of Scruggs.[27] She also claimed that processing time was critical for developing ductility, as longer processing times would lead to stronger bonding between the spinel and matrix. She used the work of Schneibel et al.[28] as a basis for comparison, as their alloy had nearly the same composition as one of the alloys studied by Sun,[25] but was hot-pressed for four times as long. However, Sun[25] did not report mechanical properties for her alloy with a composition comparable to that studied by Schneibel et al.[28] except to say that her alloy failed in a brittle manner in room temperature bending, while the Schneibel alloy exhibited room temperature ductility. Sun goes so far as to state that her 3 wt% spinel alloy is not comparable to the Schneibel et al. material.[25] As a result of the differing compositions and processing conditions of the alloys for which mechanical properties were reported by these authors, it is difficult to directly compare the two results.

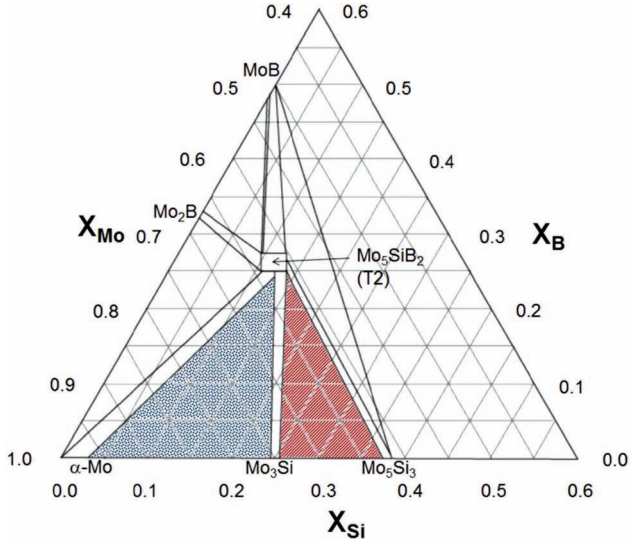

Figure 2. Mo-rich portion of the 1600 °C isotherm of the Mo-Si-B phase diagram. Two phase fields have received a lot of attention: Mo_3Si-Mo_5Si_3-Mo_5SiB_2 (red) and α-Mo-Mo_3Si-Mo_5SiB_2 (blue).

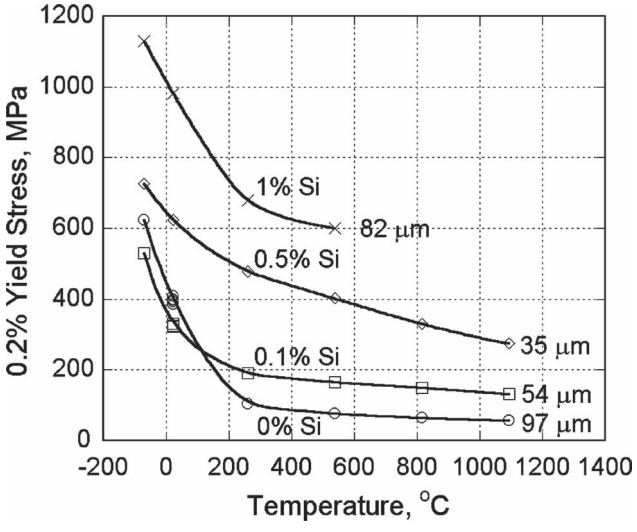

Figure 3. Yield strength of Mo as a function of Si content and temperature.[20] The addition of only 0.1 wt.% Si can significantly increase the yield strength of Mo. Si segregates to dislocation cores[19] and acts as a potent solid-solution strengthener.

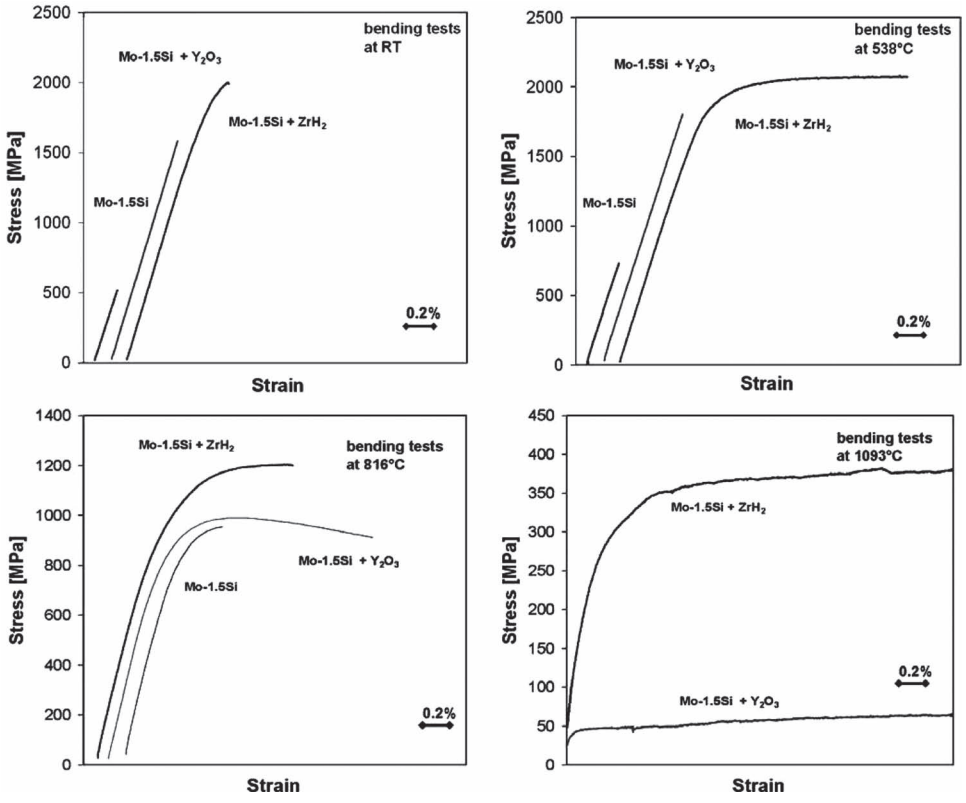

Figure 4. Influence of Zr and Y_2O_3 on the stress-strain behavior of Mo-1.5 Si at various temperatures.[10] Y_2O_3, by reducing the grain size, is an effective ductilizing agent above 800 °C. Small additions of Zr can increase the ductility of Mo-1.5Si and can even impart marginal room temperature ductility. In Mo alloys, Zr competes with Si for grain boundary sites,[21,22] thereby reducing Si segregation and increasing grain boundary adhesion.

Lee[26] expanded upon Sun's work, however, and after thermal cycling observed surface microcracking in alloys containing spinel. He attributed this cracking to the differing coefficients of thermal expansion for Mo and $MgAl_2O_4$. Microcracks were seen to emanate from large spinel particles, with fewer microcracks visible in samples containing a finer distribution of spinel. He also noted an increase in brittle failure with "excessive" spinel inclusions, mirroring the results of Sun.[25] Lee blamed gettering of "excessive" amounts of MoO_x for the decreased ductility of the high spinel content alloys, though little proof was provided to support this argument. More likely, the brittle spinel particles act as crack initiation sites and fail prematurely. Lee[26] showed evidence of particle/matrix decohesion after thermal cycling in air at 650 and 1000 °C, which he credited to oxygen gettering by the spinel particle, leading to the formation of MoO_x which then volatilized, for the formation of the gaps between the spinel and matrix phases. However, what is a more likely is the absorption of oxygen from the air atmosphere during the thermal cycling test. The gaps between spinel particles and the matrix are formed as the bonds between the particles and matrix are broken by thermal stresses.

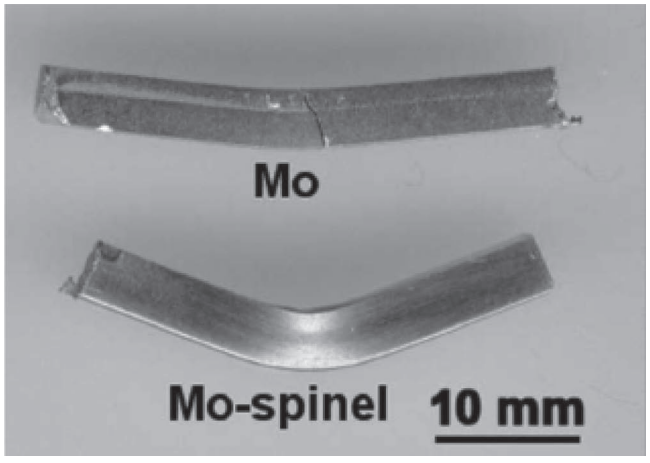

Figure 5. Influence of $MgAl_2O_4$ on the room temperature ductility of Mo. Room temperature ductility was displayed by a Mo-9 vol.% $MgAl_2O_4$ spinel alloy. This effect has been attributed to grain size refinement.[28,29] After Schneibel et al.[141]

Schneibel et al.[28] showed a fifteen-fold increase in ductility for a Mo alloy containing 2.5 vol% $MgAl_2O_4$ spinel, but the ductility subsequently decreased as more spinel was added. While the authors felt an increase in ductility caused by oxygen gettering could not be discounted, they claimed that grain size refinement was likely a larger contributor. They argued that the ductility gains outweigh the increase in crack initiation sites (the brittle spinel particles), at least at low spinel contents. As the spinel content is raised, eventually the embrittling nature of the spinel particles overtakes the ductilization afforded by a refined grain size.

This effect was verified by Gunter et al.[29] who showed that the increased ductility afforded by spinel additions was not accompanied by an increase in fracture toughness. In fact, the fracture toughness of alloys containing as little as 0.1 vol.% and as much as 5 vol.% spinel was identical. As depletion of oxygen at grain boundaries is known to increase crack blunting,[31] an increase in the toughness is expected if oxygen gettering is taking place. Since no toughening with increased spinel content was observed, oxygen gettering was reasoned to be not the cause of increased Mo ductility with the addition of spinel. Instead, Gunter et al.[29] proposed that grain refinement, and the subsequent ductility increase, can be achieved via alternate means without embrittlement. Spinel inclusions can act as crack initiation sites, in much the same way as the Y_2O_3 particles studied by Saage et al.[23] and Brady et al.[30] In fact, Brady et al.[30] do not provide any grain sizes for their materials, so it is possible that some of the ductility gains that they realized were caused by grain refinement. Specifically, Zr limits oxygen segregation (and acts as a gettering agent),[23] although some of the ductility gains are likely attributable to the accompanying grain refinement observed with the addition of Zr. However, Saage et al.[23] also showed that grain refinement alone is not enough to allow for room temperature ductility in α-Mo solid solutions. Silicon and oxygen in the grain boundaries are highly detrimental, and any ductilizing agent added to Mo must prevent their segregation, as well as refine the grain size in order to be truly useful.

Jain et al. and Jain and Kumar have studied the high temperature compressive,[32] tensile[19] and tensile creep[18] responses of model Mo-0.9Si-0.15B alloys developed to mimic the expected composition of the solid solution phase in two- or three-phase Mo-Si-B alloys. Their arc-melted, cast, extruded and forged alloy consisted of a saturated α-Mo solid solution with minor (3–5 vol.%) Mo_5SiB_2 inclusions. Jain et al.[32] reported a significant increase in the compressive yield strength of their solid solution alloy (550 MPa compared to 170 MPa for pure Mo) at 1000 °C with a strain rate of 10^{-4} s^{-1}. They also observed gradual work hardening for their solid solution alloy, while pure Mo exhibited no work hardening. However, Jain and Kumar[19] found that the composition of the samples tested by Jain et al.[32] varied along the extruded direction. As a result, the dissolved Si level varied from sample to sample. In the two single phase materials tested, the Si content varied from 1 to 2 at.% in a bimodal distribution. Tensile tests at 1200 °C at a strain rate of 10^{-4} s^{-1} revealed a yield strength in the 2 at.% Si samples (220 MPa) that was twice that of the 1 at.% Si samples (110 MPa). Long anneals at both 800 °C and 1200 °C were unable to relieve the microsegregation present in these alloys. However, it should be noted that their Si content is approximately one quarter to one half the Si content found in the α-Mo phase in two- or three-phase alloys.[19]

The high creep strengths of these Mo solid solution alloys was rationalized in terms of Si segregation to dislocation cores, which was verified using atom probe field ion microscopy and Auger electron spectroscopy. Si was also found to segregate to grain boundaries; indeed, precipitation of Mo_5SiB_2 particles on these boundaries during creep tests provided further evidence of such segregation.

2.2. Mo_3Si

As $MoSi_2$ cannot exist in thermodynamic equilibrium with α-Mo,[13,16] more Mo-rich silicides such as Mo_3Si, Mo_5Si_3 and Mo_5SiB_2 must act as the oxidation- and creep-resistant phases in high Mo content Mo-Si-B alloys. Owing to its higher Mo content, Mo_3Si has lower oxidation resistance than $MoSi_2$. Mo_3Si forms in the A15 cubic structure and was initially thought to be a line compound.[33] Rosales and Schneibel,[34] however, showed that some compositional flexibility is possible, as compositions with a narrow "window" of less than 0.5 at.% Si around 24 at.% Si (i.e., Mo_3Si is not a stoichiometric compound) produced single phase Mo_3Si. They also reported no trend in hardness or fracture toughness with varying Si content. The average fracture toughness of Mo_3Si is 3 MP$\alpha\sqrt{m}$,[34] though Rosales[35] measured a slightly lower indentation toughness of 2.4 MPa$\sqrt{m}$ for directionally solidified single crystals. (Although a convenient means to quickly estimate the toughness of brittle materials, the indentation toughness test can only yield approximate values of the fracture toughness, as the assumptions of the nature of the cracking modes beneath the indenter are not always realized and the test does not incorporate a consistent consideration of subcritical cracking and resistance-curve behavior.) For single crystals of Mo_3Si grown using an optical floating zone furnace, Swadener et al.[36] reported highly anisotropic elastic behavior from nanoindentation measurements; specifically, they measured the elastic constants as C_{11} = 505 ±35 GPa, C_{12} = 80 ±60 GPa and C_{44} = 130 ±15 GPa). Slip was found to occur in both {110}<100> and {100}<010> systems.

With respect to high temperature behavior, compression tests of Mo_3Si at 1325 °C *in vacuo* revealed significant yield points in some crystallographic directions attributed to few mobile dislocations.[37] Slip was seen to occur on {001} and {012} planes, with similar critical resolved shear stresses. Since only three slip systems are active, even at 1325 °C, Mo_3Si displays very little plasticity. Alloying Mo_3Si with Nb, however, increases both the strength and ductility of Mo_3Si at 1400 °C, based on measurements at a strain rate of 10^{-5} s^{-1}.[38] Mo_3Si forms a solid solution with Nb, via a diffusional substitution process, so an increase in strength at 1400 °C is not unexpected. Rosales and Martinez[38] rationalized the increase in ductility in terms of a reduction in the ductile-brittle transition temperature due to the addition of Nb.

There are only limited data on the oxidation behavior of Mo_3Si as a single phase, apart from the studies of Ochiai[39] and Rosales et al.[40] on the influence of Al additions. For an alloy containing 15 mol.%, Al, Ochiai[39] reported a significant decrease in mass loss after 1 and 10 h at 900 °C; the mass loss increased though as the Al content was raised above 15 mol.%. This was rationalized in terms of the formation of a mixed Al_2O_3-SiO_2 scale which was postulated to act as a better oxygen barrier than either a pure Al_2O_3 or SiO_2 scale. Chromium additions of less than 15 mol.% were shown to improve the oxidation resistance of both Mo_3Si and Mo_3Al at 900 °C by more than an order of magnitude.

Rosales et al.[40] conducted a much more comprehensive study on the effect of Al on the oxidation resistance of Mo_3Si. Cyclic oxidation experiments were performed at temperatures ranging from 700–1000 °C on directionally solidified Mo_3Si

alloys containing 8–16 at.% Al. The oxidation resistance of Mo_3Si was found to increase with increasing Al content. Unalloyed Mo_3Si failed catastrophically by a pesting reaction, while the highest Al-content alloy displayed the two-stage oxidation kinetics typical of MoO_3 volatilization followed by subsequent formation of a passivating Al_2O_3-SiO_2 scale. The oxide was found to form in two layers: Al_2O_3 on the outer surface of the material and SiO_2 between the substrate material and the outer Al_2O_3 scale. The SiO_2 layer was proposed to form after oxygen diffusion through the Al_2O_3 layer allowed some Mo_3Si to oxidize.

2.3. Mo_5Si_3 (T1)

Mo_5Si_3, often referred to as the T1 phase, exhibits highly anisotropic thermal expansion,[41–43] so much so that the residual stresses that develop during cooling can exceed the fracture strength of the material. Mo_5Si_3 forms in a tetragonal structure; as a result of this and the highly covalent nature of the basal plane bonds, the coefficient of thermal expansion ratio, CTE(c)/CTE(a) is as high as ~2.[41–43] Additions of Nb or V can reduce this anisotropy. Nb reduces CTE(c) by substituting for Mo in *16k* sites, elongating Mo chains along the *c*-axis and reducing the anharmonicity of the chains;[42] V substitutes for *c*-axis Mo, directly reducing the *c/a* ratio and thus the thermal expansion anisotropy. CTE(c)/CTE(a) ratios as low as 1.0 and ~1.25 have been reported for highly V-alloyed[41] or Nb-alloyed[42] materials.

Mechanical properties for Mo_5Si_3 have been determined at both ambient[52] and elevated temperatures.[48,53–55] Ström[52] found a solubility range of ~2 at.% Si, implying that Mo_5Si_3 is also not a line compound and can exist at lower silicon contents than originally posited by Nowotny et al.[13] He also found that the indentation toughness and Vickers hardness of Mo_5Si_3 depended upon Si content. At both hypo- and hyper-stoichiometric compositions (no exact compositions were given), the indentation toughness of the material was lower than in the stoichiometric composition, though the scatter was very large, nearly 50% of the reported value of 2.4 MPa$\sqrt{m}$. The relatively low hardness and toughness of the off-stoichiometric compositions was associated with CTE mismatch cracking, as well as the much lower hardness of $MoSi_2$ in the case of the hyper-stoichiometric composition. The hypo-stoichiometric composition contained second phase Mo_3Si particles while $MoSi_2$ was found in the hyper-stoichiometric alloy.

Yoshimi et al.[55] investigated the high temperature compression behavior of Mo_5Si_3 single crystals. They found that temperatures in excess of 1300 °C were required for plastic deformation. They tested the compression behavior along four crystallographic axes: [001], near -[101], near -[111] and [100]. At all testing temperatures above 1200 °C, a large drop in flow stress after yielding was observed for the near -[101], near -[111] and [100] orientations. Compression along the [001] axis did not exhibit a yield drop, and the post-test sample was heavily sheared. This behavior was ascribed to insufficient slip systems in this direction. For the near -[101], near -[111] and [100] orientations, after the initial yield drop, the flow stress remained relatively constant, which the authors modeled as constant stress creep. They found that the activation energy varied with orientation; with the somewhat questionable assumption of no variation in stress exponent with orientation, they obtained values of 458 kJ/mol for the near-[111] orientation and 490 kJ/mol for the near-[101] orientation.

The compressive creep behavior of Mo_5Si_3 and B-doped Mo_5Si_3 was studied in more depth by Meyer et al.[54] who performed constant stress creep tests over the range 1220–1320 °C and 140–180 MPa. Samples were held under load and at temperature until the sample strained ~1%, then the temperature was increased by 20 °C and another data point was recorded. The authors tested samples consisting of nominally pure Mo_5Si_3, as well as the B-doped material which consisted of ~54 vol.% Mo_5Si_3 with the balance of the material consisted of nearly equal volume fractions of Mo_5SiB_2 and Mo_3Si. They reported an average stress exponent of 4.3,[54] indicating dislocation climb as the dominant creep mechanism, though no clearly defined primary or secondary creep regimes could be discerned. The activation energies for all test conditions fell between 386 and 412 kJ/mol, implying no change in the dominant creep process over the test regime. While the Mo_5Si_3 phase in the B-doped material exhibited no dislocation activity, moderate dislocation activity was observed in the Mo_5SiB_2 phase. A much higher dislocation density was observed in the Mo_3Si phase and polygonization occurred after 5% strain, which the authors claim resulted from dislocation climb. The lack of dislocations in the Mo_5Si_3 phase was contradicted by the work of Yoshimi et al.[55] who found evidence of slip in single crystals of Mo_5Si_3, but no explanation as to why Meyer et al. did not see dislocations in the Mo_5Si_3 phase is given by either set of authors. Significant cracking was observed in the Mo_5Si_3 phase at the highest loads and temperatures. Meyer et al.[54] proposed cracking and sliding of Mo_5Si_3 grains as the means by which Mo_5Si_3 accommodates creep deformation.

Mo_5Si_3, with a high Mo content, has poor oxidation resistance[44] although it performs better than Mo_3Si. Boron, however, has been shown[45–49] to be highly effective at improving the oxidation resistance of Mo_5Si_3. Meyer and Akinc studied the isothermal oxidation behavior of Mo_5Si_3 and B-Mo_5Si_3 between 600 °C[45,46] and 1450 °C.[47] At 800 °C, their undoped Mo_5Si_3 suffered from rapid oxidation and a pest reaction. The oxidation resistance of Mo_5Si_3 was shown to be the best at 900 °C,[47] though the SiO_2 scale that formed was always porous and weight loss was always linear. They found that outward transport of MoO_3 through the SiO_2 scale was rate-limiting in the 900–1100°C temperature regime. Similar behavior was noted by Natesan and Deevi[49] for undoped Mo_5Si_3 (hot pressed) alloys and single crystals.

Small amounts (~1–2 wt.%) of B can radically improve the oxidation resistance of Mo_5Si_3, by more than five orders of magnitude.[47] Meyer and Akinc[47] reported no pesting reaction at 800 °C and parabolic weight gain above 1050 °C. The transition to parabolic oxidation kinetics implies that oxygen diffusion through a dense scale is the rate-limiting step. The oxidation behavior of B-Mo_5Si_3 exhibits two stages: (i) initial transient mass loss as Mo is oxidized and escapes as MoO_3 and (ii) passivation by a dense SiO_2 scale. The mass loss decreased with increasing B content.[45] Boron is a well-known flux of silica;[50] increasing the boron content lowers the viscosity of the SiO_2 scale, allowing for quicker surface coverage and a shorter

transient period. As a result, the overall mass loss of the alloy will be lower, even though B increases the diffusivity of oxygen through the scale.[51] The superior oxidation performance of B-doped Mo_5Si_3 has led researchers to explore Mo_5SiB_2 as a phase of interest for creating oxidation resistant refractory silicide alloys.

2.4. Mo_5SiB_2 (T2)

Mo_5SiB_2, or T2 phase, forms in the $D8_l$ body-centered tetragonal structure, with a unit cell containing 32 atoms (20 Mo, 4 Si, 8 B).[56,57] The atoms arrange into four distinct layer types: layer A containing only Mo atoms, layer B containing only Si, layer C containing Mo and B atoms and another layer containing only Mo atoms, but shifted by one half the base diagonal in relation to the A layer, labeled as layer $A_{1/21/2}$.[57] Layers are stacked in a $BACA_{1/21/2}BA_{1/2/1/2}CAB$ structure, as shown in **Figure 6**. The two different A-type layers are required to accommodate the significant difference in atomic radii between Si and B. As a result of this complicated crystal structure, the coefficient of thermal expansion of Mo_5SiB_2 is nearly isotropic. Rawn et al.[56] reasoned that the differing thermal response of the various bond types led to low CTE anisotropy; they observed a CTE of ~7.7×10^{-6} K^{-1} for polycrystalline Mo_5SiB_2, on par with the values reported by Ito et al.[58] for single crystals and by Field et al.[59] for a polycrystalline alloy.

Mo_5SiB_2, like Mo_3Si and Mo_5Si_3, is not a line compound and exhibits some compositional flexibility around the stoichiometric concentrations (Figure 2). In fact, Sakidja et al.[60] demonstrated the potential of α-Mo precipitation from supersaturated Mo_5SiB_2 as a means of ductile phase reinforcement of Mo_5SiB_2. Studies of the effects of a number of transition[57,61,62] and refractory metal[63] alloying additions on the stability of Mo_5SiB_2 and multiphase regions containing Mo_5SiB_2 (i.e., the α-Mo-Mo_3Si-Mo_5SiB_2 three phase region) have recently been published. A combination of geometric and electronic factors was shown[57,61] to increase the stability of Mo_5SiB_2. A valance electron per atom (e/a) ratio of 5.5 was indicated[61] to exhibit a minimum gap in total density of states. Mo has an e/a ratio of 6, while transition metals like Ti, Zr and Hf have e/a ratios of 4. All of these transition metals form extended solid solutions with Mo_5SiB_2, but only Ti has been shown[62] to be effective at stabilizing a three-phase equilibrium. Both Hf and Zr are known[62] to limit the stability of a α-Mo-Mo_3Si-Mo_5SiB_2 three-phase equilibrium as a result of the formation of MoSiHf and MoSiZr ternary phases. It was argued by Sakidja and Perepezko[61] though that a favorable e/a ratio was not the only factor driving the extended solubility of transition metal additions. These authors claimed that rare-earth metal substitutions would not form extended solid solutions in Mo_5SiB_2, even though rare-earth metals have favorable e/a ratios, because of the large size difference between atoms like Y and Mo.

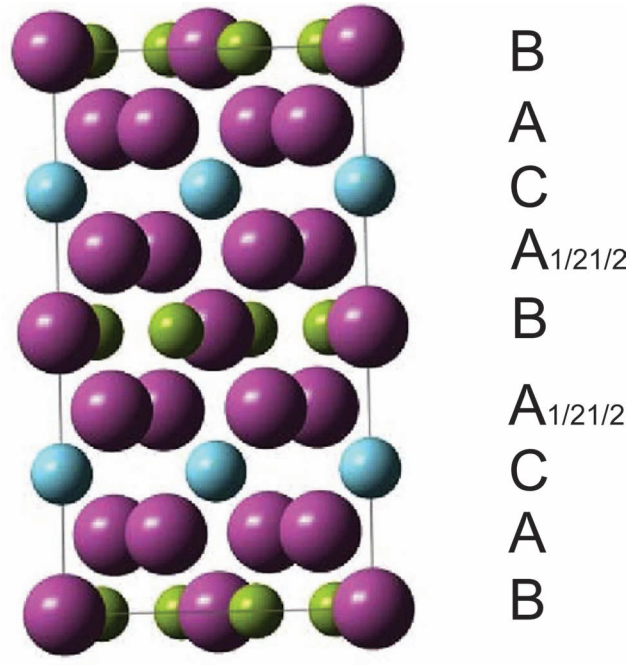

Figure 6. Crystal structure of Mo_5SiB_2.[2] The unit cell contains 32 atoms (20 Mo, 4 Si and 8B) arranged in a body-centered tetragonal $D8_\lambda$ structure. Atoms arrange in three layer types: A and $A_{1/21/2}$ containing only Mo atoms, B containing Mo and B atoms and C containing only Si atoms. Atoms on the $A_{1/21/2}$ layers are translated by one half of the basal plane diagonal in relation to A layers.

Sakidja et al.[63] showed a larger α-Mo/Mo_5SiB_2 two-phase equilibrium regime could be obtained by substitution of Nb or Cr for Mo in Mo_5SiB_2. Nb increased the c/a ratio of Mo_5SiB_2 as a result of its larger atomic radius, thus allowing more Si to substitute for B and lowering the B/Si ratio. Cr, by contrast, lowered the c/a ratio as a result of its smaller atomic radius, allowing more Si to be replaced by B. In both situations, altering the c/a ratio of Mo_5SiB_2, and, by extension, the effective atomic ratios of the metalloid components (i.e., altering the B/Si ratio), stabilized the α-Mo-Mo_5SiB_2 two-phase field over a larger compositional range.[63] Further details on the thermodynamics and phase stability of the Mo-Si-B system can be found elsewhere.[2]

Only limited data are available on the mechanical properties of Mo_5SiB_2.[58,59,64,65] While few dislocations have been observed in Mo_5SiB_2, slip has been observed on the <100>{010} slip system.[59,64,65] Ihara et al.[65] reported an indentation toughness of Mo_5SiB_2 of ~ 2 MP$\alpha\sqrt{m}$, comparable to other Mo-Si intermetallics. Hayashi et al.[64] and Ito et al.[58] studied the creep response of Mo_5SiB_2 in compression. The creep rate for [021] oriented Mo_5SiB_2 single crystals at 1300 °C was reported[58,64] to be three orders of magnitude lower than that for the hardest orientation of $MoSi_2$, highlighting the excellent creep resistance afforded by Mo_5SiB_2; the creep mechanism for polycrystalline Mo_5SiB_2, however, was not fully characterized,[64] possibly because plastic anisotropy of Mo_5SiB_2, grain boundary sliding and the presence of small amounts of second phases contributed to confusion about the dominant process. The authors did report a stress exponent of 4.6, however.

Similarly, little information exists on the oxidation behavior of pure Mo_5SiB_2. Yoshimi et al.[66] have published the only study to date, although their samples contained small amounts of MoB, Mo_2B and Mo_5Si_3 as secondary phases. As Nunes et al. showed,[16] direct solidification of pure Mo_5SiB_2 is very difficult, and these secondary phases will remain even after long heat treatments. Yoshimi et al.[66] tested the short-term isothermal

response of their material between 700 and 1400 °C. Below 800 °C, MoO_3 formed and then volatilized, leading to a slight mass gain followed by a subsequent mass loss. Above 1000 °C, two-stage oxidation kinetics were observed and two layers of oxidation product covered the base material. They described the process in the following way: during an initial transient period, Mo, B and Si simultaneously oxidizes forming volatile MoO_3 and B_2O_3 as well as a dense SiO_2 scale. As MoO_3 and B_2O_3 volatilizes, the formation SiO_2 is accelerated by the rising Si activity. When a SiO_2 scale completely covers the substrate, surface oxygen transport through the scale becomes the rate-limiting step and parabolic oxidation kinetics dominate. At this point, the oxygen partial pressure at the oxide interface is governed by the equilibrium between Si and SiO_2. Si is selectively oxidized at these oxygen partial pressures, leaving behind an interlayer of α-Mo. The oxidation resistance for Mo_5SiB_2 is not as good as B-doped Mo_5Si_3 since the B content (and thus oxygen diffusivity through the borosilicate scale) is much higher in the former case.

As intermetallic compounds, Mo_3Si and Mo_5SiB_2 display excellent oxidation and creep resistance. The limited plasticity of both of these compounds, even above 1300 °C, implies good strength retention at temperatures of industrial interest. Si and B preferentially oxidize, forming a passivating oxide scale. While the oxidation and creep resistance of these compounds are excellent, they are very brittle and consequently exhibit very poor toughness. As a result, an alloy consisting solely of these brittle phases is unlikely to be ever successfully used for structural applications. Alloying with a ductile phase, such as α-Mo, is required for the creation of an alloy exhibiting optimal oxidation, creep and fracture resistance. For this reason, much recent research on Mo-Si-B alloys has focused on processing techniques to make such α-Mo-Mo_3Si-Mo_5SiB_2 and α-Mo-Mo_5SiB_2 alloys.

3. Processing

Many strategies have been employed to process Mo-Si-B alloys. There are problems though as, for example, direct solidification of Mo-rich alloys can be frustrated by a high degree of solute segregation during solidification, and segregation of B during solidification can lead to the precipitation of unwanted phases like MoB and Mo_2B.[16] As stated above in Section 2.4, significant effort has been directed to finding alloying additions that can stabilize Mo_5SiB_2 over a wider compositional range and reduce solidification segregation.

Despite the disadvantages noted above, direct solidification of Mo-Si-B alloys via repeated arc-melting and casting has been the processing method most utilized in the study of Mo-Si-B alloys owing to its relative processing ease. Directional solidification has also been used by some researchers to produce high aspect ratio grains. Powder metallurgy methods have recently been developed to process Mo-Si-B alloys using solid-state reactions. Hot pressing and sintering of blended powders, reaction hot pressing, plasma spraying, rapid solidification via gas atomization, plasma rotating electrode processing, vacuum annealing Mo-Si-B powders to create material with a continuous α-Mo phase, mechanical alloying and reaction synthesis of Mo, Si_3N_4 and BN powders have all been used with great success to process Mo-Si-B alloys. A number of these processing methods and their resultant phase morphologies are summarized below.

3.1. Ingot Metallurgy

Arc-melting has been used by many researchers to directly solidify Mo-Si-B alloys[61,67–85] or to generate a precursor material which is then pulverized and reconsolidated.[82–87] Elemental Mo, Si and B are generally melted using a very high ampere DC current arc. A variety of microstructures are possible using this method, as the equilibrium microstructure is obtained from the melt. By changing the composition of the alloy, it is possible to alter the phase morphology. For example, small, isolated islands of α-Mo form within an intermetallic matrix for Mo-4Si-1B,[84] while a mixture of two-phase α-Mo/Mo_5SiB_2 eutectic and α-Mo/Mo_5SiB_2/Mo_3Si three-phase eutectic forms for Mo-5.1Si-1.3B.[61] Arc-melting and direct solidification has been successfully used to form both α-Mo-Mo_3Si-Mo_5SiB_2[84] and Mo_5SiB_2-Mo_3Si-Mo_5Si_3[45] alloys.

The optical floating zone technique has recently been used[88–91] to directionally solidify Mo-Si-B alloys. A halogen or xenon light beam is focused on a precast Mo-Si-B rod, creating a small molten zone;[92] the light beam, and thus the molten zone is then slowly moved along the sample, resulting in a directionally solidified alloy[88–91] or a single crystal.[58] Ito et al.[88] pioneered the use of an optical floating zone furnace to grow directionally solidified two-phase Mo-3.4Si-2.6B eutectic alloys. These authors obtained a Mo_5SiB_2 matrix surrounding fine (~10 μm) α-Mo grains, interspersed with some coarser α-Mo dendrites at a growth rate of 5 mm/h. Wang et al.[90,91] directionally solidified a Mo-5Si-1.4B alloy at growth rates of 10 and 30 mm/h and found slight microstructural alignment along the growth direction, with the degree of alignment increasing with increasing growth rate. Transverse sections revealed a two-phase α-Mo-Mo_5SiB_2 dendritic microstructure, whereas a finer, three-phase eutectic (α-Mo-Mo_5SiB_2-Mo_3Si) was found in the interdendritic regions with a coarse and inhomogeneous grain morphology. The coarsest α-Mo dendrites were ~50 μm long in the case of the slower growth rate and ~40 μm in the case of the faster growth rate.

Both of these techniques require extremely high temperatures, globally in the case of arc-melting and locally in the case of the optical floating zone technique. Berczik[95,96] has reported the necessity of temperatures in excess of 1750 °C to form wrought Mo-Si-B alloys. The extremely high temperatures required for these processes limit the scalability of direct solidification. As a result, powder metallurgy processes have been developed to create Mo-Si-B alloys which are potentially easier to manufacture on an industrial scale.

3.2. Powder Metallurgy

Powders rapidly solidified from the melt[11,18,19,32,93–101] can avoid the formation of deleterious boride phases. Small, spherical particles consisting of either an intermetallic matrix phase surround primarily solidified α-Mo[93,94] or an α-Mo matrix phase[95–97] can be produced, depending on the atomizing

gas (and thus the cooling rate). Plasma rotating electrode processing (PREP), another rapid solidification technique, utilizes electric arc heating to melt a rotating electrode. Centrifugal forces eject the molten melt, which solidify into spheres in flight. The PREP process has proven effective at forming α-Mo matrix powders containing Mo_5SiB_2 dispersions.[18,19,32,98–101] Consolidation of these powders by hot pressing and sintering can lead to the formation of dense, well bonded three-phase microstructures.

Low pressure plasma spraying has been used with some success to deposit Mo_5Si_3-MoB-$MoSi_2$ coatings on stainless steel[102–104] and for Mo_3Si-Mo_5Si_3-Mo_5SiB_2 coatings on Mo-ZrC alloys.[105] Argon carrier gas is used to inject Mo-Si-B powders into a DC plasma flame. The powders melt and then splat cool upon contact with the substrate. Initial experiments[102] using air as a carrier gas showed unacceptable levels of silicon loss and oxygen impurities, and so inert atmospheres and carrier gases must be used. A high degree of variation in the grain size and composition of individual splats implies that the solidification undercooling and composition can vary from layer to layer in the coating. High temperature (>1800 °C) annealing is required to recrystallize the microstructure and improve the coating homogeneity.[102] Approximately 8 wt.% of the Mo_5Si_3-MoB-$MoSi_2$ coating is silica, reducing its high-temperature strength of the coating but improving its ductility.[104] Dense coatings are possible with this technique,[105] highlighting the potential for using low pressure plasma spraying to apply oxidation-resistant coatings to ductile-phase toughened α-Mo-based alloys.

Reactive hot-pressing combines the increased reactivity experienced by a material as it undergoes a phase transformation with the application of pressure to create a dense and strongly bonded material.[106] Although only a few researchers[107–112] have pursued this processing path, reactive hot pressing has been found to be particularly useful for the manufacture of Mo-Si-B-Al alloys.[107–111] For example, Mitra et al.[107] added Al to their material as a means to scavenge oxygen impurities from their starting materials. They held their Mo-Si-B-Al powder blends at 700 °C for 1 h before hot-pressing to allow liquid Al to react with any SiO_2, MoO_3 or B_2O_3 to form α-Al_2O_3. In this way, the starting materials are purified, and oxygen impurities in the alloy are tied up in Al_2O_3 inclusions. A relatively low reaction temperature was required to limit the fluidity of the Al liquid and prevent its escape from the hot press die during the reaction step. The free energy of Al_2O_3 formation is lower than that for SiO_2 or MoO_3, driving the formation of Al_2O_3. Li and Peng[112] have shown that this technique can also be used to create Mo-Si-B alloys without the addition of Al. They held their material at 1400 °C for 2 h before raising the temperature to 1600 °C and applying pressure. Utilizing this method, fully dense Mo_3Si-Mo_5SiB_2-matrix materials were created with 18-31 vol.% discontinuous α-Mo, with the α-Mo content scaling inversely with increasing B content.[112]

Hot pressing of blended powders provides a relatively simple means of creating a two- or three-phase microstructure without the pitfalls of direct solidification; for this reason it is now widely used in processing of Mo-Si-B alloys. The technique has been used to successfully compact and sinter mixtures of molybdenum silicides, Mo and B,[81,113] precast Mo-Si-B powders,[82–87] elemental Mo, Si and B[114] as well as rapidly-solidified,[18,19,32,95–101] surface-modified,[115–118] reaction synthesized[15,119–123] or mechanically alloyed[4,10,11,14,123–137] Mo-Si-B powders. Heat treatment is required after hot pressing to further homogenize the material. The resultant microstructure depends greatly on the chosen powder mixture and the particle size of the starting material. Schneibel et al.[80] synthesized a Mo_5Si_3-Mo_5SiB_2-Mo_3Si alloy from $MoSi_2$, Mo and B, while the elemental Mo, Si and B powders hot pressed by Nieh et al.[114] were used to produce an alloy containing discontinuous islands of α-Mo within an Mo_3Si-Mo_5SiB_2 matrix.

In their work to demonstrate the effects of initial powder size on the microstructure of their continuous α-Mo matrix material, Kruzic et al.[116–118] found it possible to produce microstructures with varying grain sizes while maintaining an equal volume fraction of α-Mo solely by varying the initial powder size. The powders that they used were produced utilizing the novel surface-modification technique pioneered by Schneibel et al.[115] After pulverizing arc-cast ingots of Mo-20Si-10B (at.%), the resultant powder was annealed at 1600 °C for 16 h in a vacuum better than 10^{-3} Pa. At this temperature and oxygen partial pressure Si preferentially oxidized to form volatile SiO[115] leaving behind an α-Mo-enriched surface layer. Compaction, hot pressing and subsequent annealing produces a continuous α-Mo matrix decorated with second phase intermetallic particles.

Reaction synthesis of Mo-Si-B alloys from Mo, Si_3N_4 and BN powders has attracted interest[15,119–122] as a means of manufacturing Mo-Si-B alloys on an industrial scale. This simple processing method relies on reactions between the nitride phases and Mo to form intermetallic Mo_3Si and Mo_5SiB_2 during free sintering in an Ar-10% H_2 atmosphere. Specifically, the intermetallic phases form according to the following reactions:

$$3\,Mo + 2/3\,Si_3N_4 \rightarrow Mo_3Si + 2/3\,N_2 \quad (1)$$

$$5\,Mo + 1/3\,Si_3N_4 + 2\,BN \rightarrow Mo_5SiB_2 + 5/3\,N_2 \quad (2)$$

At a sintering temperature of 1600 °C, 95% of theoretical density was achieved after a soak of 6 h. While Middlemas and Cochran[119] postulated that an increased sintering temperature would increase the density of the alloy further, the accompanying grain growth was seen as unacceptable. Hot isostatic pressing was chosen as the final consolidation step, as it resulted in nearly 100% dense compacts which retained the desired fine grain structure. Hot isostatic pressing is not possible directly from the unfired powders, as the evolution of N_2 gas during processing prevents full densification. As this process may not require the application of load during sintering, many complex shapes, which cannot be made using other powder metallurgy processes, are possible. Ultra-fine grain sizes are also possible if submicrometer starting materials are used.[121]

Mechanical alloying has received much attention recently[4,10,11,14,124–137] as a method for producing ultra-fine grained *in situ* Mo-Si-B composites. High energy collisions during mechanical alloying lead to repeated cold welding and fracturing of powder particles.[138] This high-energy processing method allows for the formation of non-equilibrium materials, such as supersaturated α-Mo.

Krüger et al.[14] demonstrated complete dissolution of 10 at.% Si into a supersaturated α-Mo solid solution, far beyond the equilibrium 1-2 at.% Si proposed by Nunes et al.[16] and Nowotny et al.[13] This process is also useful for creating ultra-fine grain sizes, as extended milling reduces the grain size into the sub-micrometer regime.

The effectiveness of mechanical alloying as a method for producing Mo-Si-B alloys appears to be sensitive to composition. Krüger et al.[14] were able to synthesize Mo-3Si-1B ultrafine grained materials (grain size ~ 1 μm) with a continuous α-Mo phase[124] after 20 h of milling at 200 rpm and a 3 h anneal at 1400 °C to precipitate the intermetallic phases. Abbasi and Shamanian[125–127] found that a composite structure consisting of nanoscale Si and B particles embedded within a Mo matrix formed from a 5:1:2 (mol.%) mixture of Mo, Si and B powders after 10 h of milling. Subsequent heat treatment led to the precipitation of Mo_5SiB_2, $MoSi_2$ and Mo_3Si.[125] However, an increase in milling time to 20 h led to the direct formation of a two-phase α-Mo/Mo_5SiB_2 composite with Mo_5SiB_2 particles embedded in a continuous α-Mo matrix.[126] The authors were also able to produce a three-phase α-Mo-Mo_5SiB_2-Mo_3Si alloy in a two-step mechanical alloying process.[127] After milling a Si-43.62B (wt.%) mixture for 20 h, Mo was added to create a 5:1:2 Mo:Si:B molar ratio. The powder was milled for an additional 20 h at 300 rpm to form an α-Mo/$MoSi_2$ nanocomposite. After the second milling step, the powder was annealed for 1 h at 1100 °C to precipitate Mo_3Si from the α-Mo/$MoSi_2$ composite. An increase in secondary milling time reduces the amount of Mo_3Si that forms on subsequent annealing, stabilizing an α-Mo-Mo_5SiB_2-$MoSi_2$ structure. It was postulated by Abbasi and Shamanian[127] that the extremely short diffusion pathways that result from extended mechanical alloying cause this shift in phase structure. By contrast, Yamauchi et al.[128] were unable to directly synthesize Mo_5SiB_2 via mechanical alloying, even after milling a 5:1:2 molar mixture of Mo, Si and B at 500 rpm for 100 h. A two-step mechanical alloying process, where Mo and Si were milled for 50 h, then B was added and the mixture was milled for another 50 h, followed by spark plasma sintering, was required to obtain an α-Mo-Mo_5SiB_2*in situ* composite. Yamauchi et al.[128] were unable to form an α-Mo-Mo_5SiB_2 composite from Mo-3.3Si-2.5B. Similarly, in their initial work on Mo-5Si-1.4B, Bakhshi et al.[129] were unable to produce a Mo solid solution, even after 20 h of mechanical alloying at 365 rpm and 10 h of annealing at 1100 °C. In their subsequent study, Bakhshi et al.[130] were able to form intermetallic phases in Mo-57Si-10B and Mo-47Si-23B (at.%) but could not synthesize a solid solution phase for a Mo-5Si-1.4B alloy.

Both mechanical alloying and reaction synthesis are attractive powder processing techniques. As will be shown in Section 5.1, mechanical alloying can be used to form ultra-fine grained materials that exhibit superplastic behavior at temperatures as low as 1400 °C. Extended plasticity at 1400 °C allows for manufacturing processes such as deep drawing to be used successfully to create near-net shapes. Reaction synthesis can produce 95% dense material without the necessity for external pressure. Pressureless sintering allows for complex geometries to be created with a minimum of machining necessary. As a result, reaction synthesis has the potential to form net shape products directly.

4. Oxidation Behavior

4.1. Mechanisms

Parthasarathy et al.[67] recently published a comprehensive study of the oxidation mechanisms in α-Mo-Mo_5SiB_2-Mo_3Si alloys, examining the cyclic oxidation response of Mo-4.3Si-1.7B alloys at temperatures ranging from 500° to 1300 °C. They identified four temperature regimes with differing oxidation kinetics. At low (500–600 °C) temperatures, Mo, Si and B all oxidize, as evidenced by the formation of a solid MoO_3(Si,B) scale. While the formation of a SiO_2 is thermodynamically preferred, owing to its more favorable free energy of formation, its high viscosity at low temperatures prevents SiO_2 from forming a protective scale. As a result, Mo is free to oxidize and form MoO_3. In this temperature range, parabolic weight gain dominates as oxygen diffusion into the MoO_3 determines the oxidation behavior. Parthasarathy et al.[67] reported a parabolic rate constant, $k_p = 3.41 \times 10^5 \exp(-94.5 \text{ kJ mol}^{-1}/RT)$ mg/cm^{2}h$^{0.5}$ in this temperature regime, much smaller than the parabolic rate constant they reported for pure Mo ($k_p = 7.93 \times 10^{10} \exp(-160.6 \text{ kJ mol}^{-1}/RT)$. The simultaneous oxidation of Mo, Si and B serves to slow the oxidation kinetics at 500–600 °C, but the scale is not protective.

Around 700° ± 50 °C, a porous borosilicate scale forms but it offers little oxidation resistance. In this temperature regime, linear weight loss dominates. With respect to the oxidation kinetics, Parthasarathy et al.[67] reported a linear rate constant of 3.3 mg/cm^2 h at 700 °C; no difference was found between Mo-Si-B and pure Mo at this temperature. Indeed, at these intermediate temperatures, the oxidation of Mo into volatile MoO_3 is the rate-limiting step. The porous scale provides easy access for oxygen to reach the substrate material. Little B_2O_3 is thought to volatilize at this temperature, so the B_2O_3 content of the scale is high; as a result, the viscosity of the borosilicate scale is very low[67] (5×10^6 Pa-s), to the point that bubbles can form within the scale since complete fining of silica melts require viscosities in excess of 10^9 Pa-s.[139]

At higher temperatures, parabolic weight loss kinetics are active. An initial stage of rapid MoO_3 formation and evaporation is followed by slow weight loss as B_2O_3 begins to evaporate from the scale, slowing the diffusion of oxygen through the scale. However, at 800 °C, the scale retains a low enough viscosity to allow MoO_3 to form in bubbles within the scale. As a result, MoO_3 egress and inward oxygen diffusion are paradoxically faster at 800 °C than at 1300 °C. At higher temperatures, significant B_2O_3 evaporation occurs, raising the viscosity of the scale by as much as 10 orders of magnitude.[140] The evaporation of B_2O_3 also serves to slow the diffusion rate of oxygen by as much as 6 orders of magnitude.[140] The combination of these two effects leads to a more protective scale at 1300 °C than at 800 °C. Oxygen diffusion, and thus scale growth, is much slower; the oxide scale at 1300 °C is half as thick as the scale that forms at 800 °C. Mendiratta et al.[68] have demonstrated the potential of pre-oxidizing material at 1300 °C for subsequent use at 800 °C, though the lifetime of such a treatment is finite, after which the oxidation kinetics mimicked those for an untreated sample. The oxidation mechanism map developed by

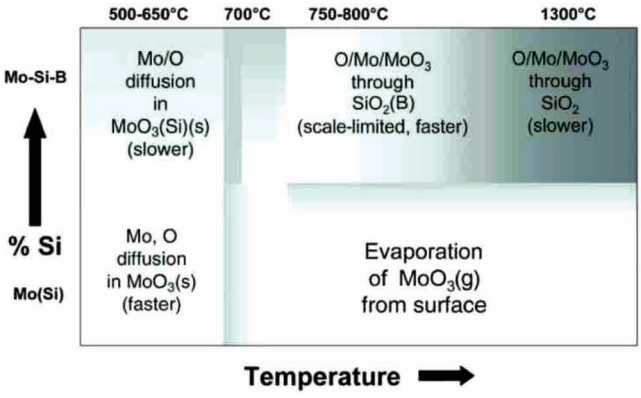

Figure 7. Oxidation mechanism map for Mo-Si-B alloys.[1] At low temperatures, MoO_3(s) forms leading to parabolic weight gain; above ~700 °C, MoO_3 sublimates. The viscosity of SiO_2 at this temperature is too high to form a protective layer. As a result linear weight loss dominates until ~750 °C. Above this temperature regime, a borosilicate layer forms and parabolic weight loss kinetics are active. However, the weight loss at 800 °C is much greater than at 1300 °C. Enhanced oxygen diffusion through the B-rich scale and low scale viscosity lead to rapid weight loss and incomplete fining of the scale. As the temperature increases, B_2O_3 begins to evaporate, raising the viscosity of the scale, thus closing any bubbles that might form, and slowing oxygen transport through the scale. As a result of the higher scale viscosity and lower B content within the scale, parabolic weight loss slows.

Parthasarathy et al.[67] and refined by Dimiduk and Perepezko[1] is shown in **Figure 7**.

Studies of the early stages of oxidation in a Mo-3Si-1B alloy were initiated by Helmick et al.[82] who examined the behavior of both arc-melted and compacted powder alloys when exposed to a number of environments. Specifically, the early stages of formation of the borosilicate scale was examined in static and flowing air, as well as flowing oxygen over the temperature range 700°–1100 °C. In the first minutes of oxidation the component phases were found to oxidize independently, i.e., Mo_5SiB_2 formed MoO_3, SiO_2 and B_2O_3, Mo_3Si formed MoO_3 and SiO_2 and α-Mo formed MoO_3. As the time of oxidation was increased, the borosilicate scale flowed to first cover Mo_3Si and then the α-Mo, but channels were able to form through the scale, mainly at grain boundaries. **Figure 8** is a schematic of this oxidation process.[70] The walls of these channels, as well as the substrate, were coated with MoO_2. The oxygen pressure is thought to have been high enough within the channels to oxidize Mo to form MoO_2, but was not high enough to convert the MoO_2 to MoO_3. These channels are the last to seal, leading to a transition from transient oxidation to steady-state parabolic weight loss. At 700 °C, a porous MoO_3(Si,B) scale formed. This scale was not protective, as evidenced by the observed linear weight loss kinetics. At 816 °C, static environments produced channel-free oxide scales, while channels were seen in the oxide scales formed in flowing-gas environments. While the increased removal of MoO_3 was viewed as beneficial, as it sped the formation of a borosilicate scale, removal of B_2O_3 was also increased. Increased B_2O_3 removal had the effect of lowering the scale viscosity and hindering pore and channel healing. As a result, the oxidation performance in flowing gas was worse than in static air. At 1000 °C, however, little difference in scale morphology was observed for the various environments; a channel-free scale formed for all test conditions. The decrease in scale viscosity was shown to counteract any increase in viscosity from B_2O_3 removal. At this temperature, the scale remained sufficiently fluid to heal any channels that may have formed. At 1100 °C, a channel-free scale formed for the static and slow gas flow rate

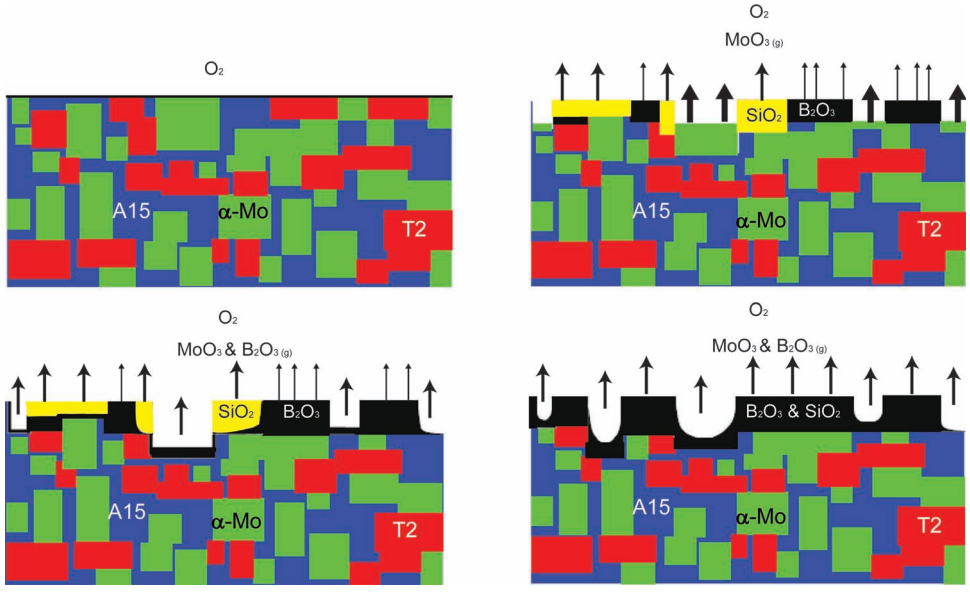

Figure 8. Transient oxidation in an α-Mo-Mo_3Si-Mo_5SiB_2 alloy at 1300 °C.[70] The unoxidized microstructure is shown in (a). In the initial stage, each phase oxidizes independently. α-Mo forms MoO_3 vapor, the Mo_3Si (A15) forms a nanoporous SiO_2 scale and the $MoSiB_2$ (T2) phase forms a borosilicate scale. After some time, (c) B_2O_3 flows to cover α-Mo and diffuses into SiO_2, lowering its viscosity. The lowered viscosity afforded by B_2O_3 additions speeds sintering of SiO_2 and thus passivation. A transition to steady-state oxidation occurs once the entire surface is covered in borosilicate (d).

conditions, but a porous scale was observed for the fastest gas flow rate. The rate of B_2O_3 removal was too great for the highest gas flow rate. As a result, the scale viscosity increased to a point where the scale was unable to flow and heal any channels.

Rioult et al.[70] expanded the this work[82] and probed the effect of microstructural size scale on transient oxidation of Mo-5Si-1.3B at 1100 °C. They examined three slices taken from different sections of an arc-cast ingot; since the bottom of the ingot was in contact with a water-cooled hearth, the bottom of the ingot experienced a higher cooling rate than the top. As a result slices from different heights along the ingot exhibited different microstructural size scales, with the finer microstructures towards the bottom. While the steady-state behavior for each of the microstructures was very similar, the transition time from transient to steady-state oxidation scaled with grain size. As a result, the weight loss during the transient period was lowest for the fine microstructure (10 mg/cm^2), while the intermediate (27 mg/cm^2) and coarse microstructures (32 mg/cm^2) showed significantly more weight loss, by a factor of ~3. As observed by Helmick et al.,[82] each of the constituent phases initially reacted with oxygen individually. A dense borosilicate layer was found over the Mo_5SiB_2 grains, while a nanoporous, non-protective scale was found covering the Mo_3Si grains. No scale was found covering α-Mo, as MoO_3 volatilized at 1100 °C. As the oxidation time increased, flow of the borosilicate scale onto the α-Mo began to protect those grains. Likewise, the porous SiO_2 layer covering the Mo_3Si grains began to sinter, likely aided by boron diffusion from neighboring Mo_5SiB_2 grains. As the transient period progressed, the rate of mass loss decreased. Complete oxidation of the smallest α-Mo and Mo_3Si grains exposed the grains underneath. Some of these grains were Mo_5SiB_2, which formed more protective borosilicate glass. A finer microstructure containing homogenously-distributed Mo_5SiB_2 provided a shorter diffusion distance for B into the SiO_2 scale above Mo_3Si grains. Since the diffusion distance was smaller, sintering of SiO_2 occurred more rapidly, leading to a shorter transient period.

This effect has also been observed by a number of other researchers. Wang et al.[91] reported poor oxidation resistance at 1200 °C for their directionally solidified Mo-3.6Si-2B alloy. The alloy grown at a slower rate, i.e., with a coarser microstructure, performed worse than the faster growth rate material, an effect attributed to large α-Mo particles. Schneibel et al. also reported more than a 38-fold increase in weight loss at 1300 °C for a coarse grained 21 vol.% α-Mo alloy when compared to a finer grain material containing the same amount of α-Mo.[142] Improved oxidation resistance for finer microstructures was also reported by Supatarawanich et al.,[71,72] but the alloys that they tested did not have the same phase distribution, i.e., the α-Mo content and its morphology was different for each of the alloys tested. As a result, it is difficult to interpret the effect of microstructure size scale on the oxidation performance of their alloys.

One important outcome of their work, however, was the identification of Mo_3Si (or a higher-Si-content phase like Mo_5Si_3) as a necessary component for an oxidation-resistant alloy. Without the additional source of silicon provided by Mo_3Si, the boron content of the oxide scale is too high and oxygen diffuses rapidly through the scale.[71,72] A 1:1 Si:B ratio was shown to have the best oxidation resistance at 1300 °C. Alloys with less Si will form scales through which oxygen can diffuse rapidly, while alloys with a higher Si:B ratio may not completely passivate, since the scale viscosity may be too high.

The work of Supatarawanich highlights the necessity of a three-phase alloy for optimal properties. As will be discussed further in Section 5, α-Mo is required for higher toughness. Mo_5SiB_2 can provide some oxidation and creep resistance, but alone it has too high a B content. The 2:1 B:Si ratio in Mo_5SiB_2 forms a scale through which oxygen readily diffuses. As a result, alloying with Mo_3Si is required in order to lower the B:Si ratio to a level where a low viscosity oxide can form through which oxygen diffusion occurs more slowly.

4.2. Oxidation Behavior in Other Environments

Only a few oxidation experiments have been conducted on Mo-Si-B alloys in atmospheres other than laboratory or dry air. Mandal et al.[143] published the first study of the effects of wet air on the oxidation behavior of Mo-Si-B alloys. They tested three alloys (B-Mo_5Si_3-$MoSi_2$-MoB; Mo_5SiB_2-Mo_3Si; α-Mo-Mo_5SiB_2-Mo_3Si) in dry and wet (up to 2 x10^4 Pa H_2O) air at 1000 and 1100 °C. The transient weight loss of the alloys was independent of test temperature and atmosphere; instead, it scaled with increasing Mo weight fraction. Water vapor was seen to promote the formation of a thicker borosilicate scale and enhance growth of a subscale region of Mo and MoO_2, but the authors were unable to explain this behavior. However, the α-Mo-containing alloy exhibited the greatest increase in scale thickness and interlayer formation. Thom et al.[144] expanded on the earlier work of Mandal et al.[143] with their isothermal thermogravimetric analysis of the oxidation rates at 1000 °C of the same three Mo-Si-B alloys in flowing wet air (2×10^4 Pa H_2O). These authors[144] also evaluated the oxidation response of Mo-Si-B alloys in synthetic combustion gas (N_2-13CO_2-10H_2O-4O_2), utilizing the test methods of Mandal et al.[143] The synthetic combustion gas was formulated to simulate the oxidizing flue gas produced by burning fossil fuels, without any sulfidizing agents. The more accurate tests conducted by Thom et al.[144] showed two effects: (i) the oxidation rates for the B-Mo_5Si_3-$MoSi_2$-MoB alloy and the α-Mo-Mo_5SiB_2-Mo_3Si alloy were not greatly affected by wet air, and (ii) the initial weight loss for all three alloys was greater in wet air than in dry air. The Mo_5Si_3-Mo_5SiB_2 alloy exhibited slight weight gain after the initial weight loss. The second result contradicts the earlier results of Mandal et al.,[143] but the imprecision of the earlier tests led to large scatter in the data, and possible obfuscation of any effects of wet air on the initial oxidation behavior. Thom et al.[144] postulated that the similar oxidation rates in dry and wet air for the α-Mo-containing alloy represented no change in the salient weight loss mechanism, i.e., transport of MoO_2 and MoO_3 through the borosilicate scale. It should be noted, however, that only one sample was tested for each condition. The authors also reported an increase in initial weight loss and scale thickness when samples were tested in synthetic combustion gas. Though their test method precluded accurate calculation of oxidation rates, scales nearly twice as thick as the wet air case were found on the α-Mo-Mo_5SiB_2-Mo_3Si and Mo_5SiB_2-

Mo_5Si_3 alloys after exposure to the synthetic combustion gas. The authors reason that the lower Si:B ratio in the Mo_5SiB_2-containing alloys leads to decreased resistance to synthetic combustion gas. No rationale was given as to why this might be the case. The authors also did not relate any justifications for the enhanced mass transport through the oxide scale for the α-Mo-Mo_5SiB_2-Mo_3Si alloy exposed to wet air.

To date, only one paper regarding the sulfidation behavior of Mo-Si-B has been published. Tortorelli et al.[145] studied the isothermal response of an α-Mo-Mo_5SiB_2-Mo_3Si alloy to exposure to an oxidizing-sulfidizing environment at 800 °C. The H_2-H_2S-H_2O-Ar atmosphere to which they exposed their Mo-5Si-1B alloy was meant to mimic the most severe coal gasification conditions. At 800 °C, thermodynamic calculations predicted the partial pressures of S (10^{-6} atm) and O (10^{-22} atm) would result in the formation of SiO_2 and MoS_2. After 150 hr of exposure, only a thin corrosion layer formed on the sample surface. The component phases were observed to independently react with the environment. Very little difference was observed in the oxidation-sulfidation behavior for fine- (~1–5 μm) and elongated, coarse-grained (~30–50 × 7–10 μm) materials. In fact, the sulfidation response of these alloys was comparable to very sulfidation-resistant Fe_3Al, a result that is not wholly unexpected as Mo is known to be very sulfidation-resistant.[146] Schneibel et al.[147] proposed a study of the behavior of a Mo-3Si-1B alloy in a fully-operational coal gasifier but to date no results have been presented.

The effect of low (10^{-6}–10^{-4} bar) and very low (10^{-19}–10^{-12} bar) oxygen partial pressures on the oxidation behavior of a mechanically-alloyed Mo-3Si-1B-1Zr alloy was examined by Burk et al.[131] At these oxygen partial pressures, Si and B are selectively oxidized, while the formation of MoO_2 and MoO_3 is prevented. Isothermal thermogravimetric analysis of the oxidation kinetics between 820 and 1200 °C was performed in both oxygen partial pressure regimes. At very low oxygen partial pressures of 10^{-19}–10^{-12} bar, MoO_x formation is completely suppressed and the oxide growth kinetics are determined solely by the formation of SiO_2 and B_2O_3. At 820 °C, no external scale formed and internal oxidation products of Si were found to a depth of ~20 μm after 100 h. At 1000 °C, a SiO_2 scale began to form, but the viscosity of the scale was too high to allow for complete coverage of the surface; instead, isolated droplets of SiO_2 were found. At 1200 °C, complete wetting of the surface was observed, as individual SiO_2 droplets were created and then flowed to cover the surface after 100 h of exposure. No ZrO_2 was present in the SiO_2, an important implication for the oxidation resistance of this alloy, which will be discussed further in Section 4.3. As a result of the formation of internal SiO_2 precipitates, oxygen transport was slowed and Si diffusion became the rate-limiting step in the formation of an external scale. Internal SiO_2 precipitates formed until some critical volume fraction, based on the oxygen partial pressure, was achieved, at which point an external SiO_2 scale began to form as droplets.

Unlike exposure to very low oxygen partials pressures, the oxide scale that formed upon exposure to low (10^{-6}–10^{-4} bar) partial pressures of oxygen was not protective. At these oxygen partial pressures, the formation of MoO_x was not completely eliminated; indeed, a 1–2 μm MoO_x film formed between a porous SiO_2 scale and the base material. Evaporation of MoO_3 left behind channels within the oxide scale leading to catastrophic oxidation. At 1000 °C, a few dense SiO_2 droplets formed on the oxide surface, but their coverage was minimal. At 1200 °C, the occurrence of SiO_2 increased, but still very little of the oxide surface was covered. ZrO_2 were observed within the porous SiO_2 scale. It is clear from this work that pretreatments at oxygen partial pressures in the range 10^{-6}–10^{-4} bar are ineffective at preventing the incorporation of ZrO_2 into the oxide scale.

4.3. Effects of Alloying Additions

Small additions of a number of alloying additions have been shown to increase the oxidation resistance of Mo-Si-B alloys. Small (<0.3 wt.%) additions of Ti, Hf, Zr and Al have all been found to increase the wetting ability of the borosilicate scale, while larger additions (as much as 10 wt.%) form more refractory oxides underneath the borosilicate scale.[95,96] Additions of as little as 2 wt.% of Fe, Ni, Co, and Cu are also known to improve the oxidation resistance of Mo-Si-B, though no specific mechanisms have been proposed.[97] We focus below on the effects of Al, Nb and Zr alloying additions on the oxidation behavior. The influence of nanoscale Y_2O_3 and La_2O_3 additions will also be reviewed.

The oxidation response of Al-added Mo-Si-B alloys has been extensively studied.[73,74,109–111,148] Paswan et al. investigated both the isothermal[109,110] as well as cyclic and nonisothermal[111] response of reaction hot-pressed Mo-5Si-1.4B, Mo-4.3Si-1.1B-1Al and Mo-4.1Si-1.2B-2.6Al alloys. Isothermal experiments conducted between 400 and 800 °C showed a decrease in oxidation resistance with increasing Al content.[109] At high temperatures, spallation of the oxide scale periodically re-exposed fresh material to the oxidizing atmosphere. This spallation was thought to be the result of internal stresses that develop as a result of the differences in coefficients of thermal expansion of the various components. At lower temperatures, α-Al_2O_3 did form, but it could not completely cover the surface. The formation of α-Al_2O_3 retarded the formation of a borosilicate scale, slowing passivation. During cyclic oxidation at 1150 °C, mullite ($3Al_2O_3$ $2SiO_2$) and crystalline SiO_2 formed.[111] The appearance of these phases was thought to signal reduced oxidation resistance, as the grain boundaries of mullite and crystalline SiO_2 can to act as high diffusivity pathways.[111]

At first glance, this result contradicts the work of Yamauchi et al.[148] who studied the effects of small (≤5 mol.%) Al additions on the isothermal oxidation behavior of a Mo-3.3Si-2.5B two-phase α-Mo-Mo_5SiB_2 eutectic alloy. Over the temperature range 800–1400 °C, the oxidation performance of the Al-containing alloys was superior to the undoped alloy, with the best performance observed for the alloy containing 1 mol.% Al. At 1000 °C, mullite and SiO_2 form a dense, protective scale, while at 1200 °C a more needle-like morphology was observed. Two observations can be made to reconcile the different behaviors observed by Paswan et al.[109–111] and Yamauchi et al.[148] Firstly, Al is known to have a slightly negative influence on the oxidation behavior of Mo-Si-B alloys below 1000 °C.[95,96] The isothermal temperature regimes studied only overlap at 800 °C, so it is likely that Yamauchi et al.[148] observed the beneficial

wetting effect described by Berczik,[95,96] while the lower temperature regime explored by Paswan et al.[109] highlighted the deleterious effects of Al. Secondly, Yamauchi et al.[148] did not probe the cyclic oxidation properties of Al-added Mo-Si-B. It has been proposed that coefficient of thermal expansion mismatches results in large residual stresses during cooling,[111] which leads to cracking and spallation of the oxide scale, an effect that would be minimized during an isothermal experiment. It also should be noted that the two-phase eutectic studied by Yamauchi et al.[148] contained much less Si and more B than the material studied by Paswan et al.[109–111] (5 wt.% Si and 1.4 wt.% B for Paswan et al.; 3.25 wt.% Si and 2.5 wt.% B for Yamauchi et al.) As a result, the viscosity of the oxide scale on the Yamauchi material would be much lower, allowing that scale to self-heal much more rapidly.

Das et al. also studied the effects of Al and Ce additions on the oxidation behavior of Mo-Si-B at low (500–700 °C)[73] and high (1100 °C)[74] temperatures. Here an improvement in the oxidation resistance of Mo-5Si-1.4B was found with the addition of 2.6 wt.% Al. This result would also seem to contradict the findings of Paswan et al.[109] who studied an alloy with the same composition. However, it is important to realize that the microstructural morphologies of the two materials were very different owing to their differing processing methods. The reaction hot-pressed material tested by Paswan et al.[109] exhibited an equiaxed grain structure of nonhomogenously-distributed α-Mo grains ~10 μm in size. The arc-melted material examined by Das et al.,[73] conversely, comprised a primary α-Mo grain structure surrounded by an ultrafine (<0.2 μm interlamellar spacing) three-phase eutectic. Al almost certainly refined the interlamellar spacing in the material used by Das et al.;[73] this grain refinement, coupled with the formation of Al_2O_3, would speed passivation in the low temperature regime. At low temperatures, the addition of Ce did not affect the oxidation behavior. However, at high temperature, the addition of 0.16 at.% Ce to Mo-4.1Si-1.2B-2.6Al (i.e., the alloy tested at low temperature by Das et al.[73]) reduced the total mass loss during a 24 h exposure to oxygen by ~40%.[74] Inhibition of mullite formation by Ce was proposed as the cause of the observed improvement in isothermal oxidation resistance at 1100 °C.

Nb forms a complete solid solution with Mo, so there is potential to combine the superior fracture toughness behavior of Nb-based alloys with the oxidation resistance of Mo-based alloys. Nb-Nb_5Si_3 *in situ* composites have been shown to exhibit reasonable room temperature toughness coupled with strength retention at high temperatures.[149] Unfortunately, Nb forms a porous, non-protective Nb_5O_2 oxide upon exposure to air. As a result, the oxidation resistance of Nb-Nb_5Si_3 is very poor above 500 °C. Unlike MoO_3, which is volatile, Nb_2O_5 does not evaporate, and can slow the formation of a borosilicate scale.[86] Behrani et al.[86] investigated the oxidation behavior of Mo-Si-B and Nb-Mo-Si-B alloys in flowing air at 1000 °C. Of the alloys they examined, the Mo_5Si_3(B)-$MoSi_2$-MoB displayed the best oxidation resistance; this result is not unexpected as this alloy contained the lowest Mo weight fraction of the three Mo-Si-B alloys tested. A dense oxide scale, ~10–50 μm thick, formed on the surface after 100 h of exposure. The thickness of the oxide scale increased with increasing Mo content. The Nb-Mo-Si-B alloys, composed of (Mo, Nb)$_5Si_3$(B)-(Mo, Nb)$_5SiB_2$-$D8_8$, exhibited very poor oxidation resistance. The $D8_8$ phase, (Nb, Mo)$_5Si_3$(B), forms as a hexagonal structure, unlike the body-centered tetragonal T2 (Mo,Nb)$_5SiB_2$ phase, and is not as oxidation-resistant.[150] A highly porous and cracked 600 μm thick SiO_2 scale containing many Nb_2O_5 particles formed after only 10 h. Residual porosity in the base material, volatilization of MoO_3 and the formation of porous Nb_2O_5 were all believed to cause the poor oxidation resistance of the Nb-Mo-Si-B materials. Though the oxidation resistance of this material was very poor, it exhibited marginal improvement over the oxidation resistance of unalloyed Nb-Si-B materials.[86] The research published to date implies that the mechanical property gains that may be realized by alloying Mo-Si-B with Nb would be accompanied by a corresponding decrease in oxidation resistance. The authors are unaware of any work combining studies of the mechanical properties and oxidation resistance of Nb-Mo-Si-B alloys.

As described in Section 2.1, Zr has been demonstrated as an effective ductilizing agent for α-Mo. As such, the oxidation behavior of Zr-added Mo-Si-B (such as Mo-3Si-1B-1Zr) must be understood. As briefly noted in Section 4.2, Zr can be very damaging to the oxidation resistance of these alloys. The initial oxidation studies performed by Burk et al.[132] revealed two temperature regimes displaying vastly differing oxidation behavior. Grain refinement (though no grain sizes were given) was proposed as the mechanism by which slightly improved oxidation resistance was achieved in Zr-added materials at temperatures up to 1100 °C. Above this temperature, the oxidation resistance of the alloy drastically decreased. At 1300 °C, nearly linear weight loss was observed and a scale containing many ZrO_2 inclusions and pores was found. Burk et al.[133] recently published a more comprehensive study on the extremely poor oxidation resistance of Mo-3Si-1B-1Zr above 1200 °C. They found that ZrO_2 inclusions in the borosilicate scale and MoO_3 bubble formation caused the degradation of oxidation resistance above 1200 °C. The ZrO_2 inclusions within the scale underwent a phase transformation above 1100 °C, transforming from a monoclinic to a tetragonal structure. This transformation was accompanied by a volume decrease of approximately 7%;[151] this created voids within the scale allowing the formation of MoO_3 bubbles. These bubbles eventually collapsed, leaving behind partially-closed pores. Oxygen can then easily gain access to unreacted material. It should be noted that this transformation was not instantaneous; the oxidation behavior of Mo-3Si-1B-1Zr closely matched that of Mo-3Si-1B during the first stages of oxidation. The fine microstructural scale of the alloys tested served to increase the number of grain boundaries, which in turn acted as high diffusivity pathways, a beneficial effect for passivation of Mo-3Si-1B but detrimental in the case of Mo-3Si-1B-1Zr, where quick oxygen diffusion enhanced the production of MoO_3. As a result, MoO_3 formation and not oxygen diffusion through the scale became the rate-limiting step, resulting in linear weight loss kinetics. As shown by Burk et al.,[131,133] pre-treatment in extremely low oxygen partial pressures is required to form a borosilicate scale which is free of any ZrO_2 inclusions. Once a Zr-free scale is formed, the bulk material is protected. Subsequent damage to the scale will eventually lead to the formation of ZrO_2, but the deleterious effects of ZrO_2 are minimized by the passivating SiO_2 scale.

Table 1. Oxidation behavior of Al-packed Mo-3Si-1B at elevated temperatures, showing oxidation mass change in mg/cm^2. Numbers in parenthesis indicate the duration of the test.

Material	Oxidation Temperature					
	732 °C	1000 °C	1100 °C	1200 °C	1300 °C	1372 °C
Uncoated Mo-3Si-1B	−427.46 (50 h)	−247.01 (14 h)	−367.35 (2.5 h)	−277.89 (1.47 h)	−320.48 (2.5 h)	No Test
Al-packed Mo-3Si-1B	+0.01	+0.25	+0.27	+1.09	+2.35	+3.50

Nanoscale oxide dispersions of Y_2O_3 and La_2O_3 have also been used to reduce the grain size of Mo-3Si-1B in an effort to increase their ductility.[10,11,132] Jéhanno et al.[11] reported improved oxidation performance at all temperatures for alloys containing 0.1 wt.% La_2O_3. While the addition of 0.1 wt.% Y_2O_3 did improve the oxidation resistance at some temperatures, it was not as effective as La_2O_3. More effective grain boundary pinning by La_2O_3, and thus a more refined grain structure, was believed to be the origin of this behavior. A more comprehensive study by Burk et al.[132] highlighted the improved oxidation resistance of La_2O_3-dispersed Mo-3Si-1B. La_2O_3 was found to improve the fluidity and adhesion of the borosilicate scale. Incorporation of La into the borosilicate layer greatly reduced the coefficient of thermal expansion, reducing the occurrence of cracking. The presence of La_2O_3 on grain boundaries was also thought to slow grain boundary diffusion, reducing the speed at which MoO_3 evaporated. At 1300 °C, these effects combined to slow mass loss; at 820 °C they were even more potent, as the linear weight loss of Mo-3Si-1B at this temperature was replaced by much slower parabolic weight loss.[132] The transition from linear to parabolic weight loss was thought to arise from slower oxygen diffusion through the borosilicate scale.

4.4. Surface Modification Strategies

A number of surface modifications have been used to improve the oxidation resistance of Mo-Si-B alloys. Deposition of Al-Si metallic coatings has proved to be a feasible process.[152] Pre-oxidation at high temperatures is also effective at enhancing the oxidation resistance of Mo-3.9Si-1.5B.[68] Other researchers have deposited SiO_2[75] or borosilicate[93] layers with some success. Wang et al.[90] demonstrated improved oxidation resistance when the surface of their directionally solidified Mo-3.6Si-2B alloy was remelted using a Nd:YAG laser in Ar. Regions remelted with the laser exhibited a much finer three-phase eutectic microstructure than the elongated α-Mo dendrites present in the original material. The oxidation performance of this material was greatly improved by nearly an order of magnitude owing to the refinement in grain size. Behrani et al.[87] were able to achieve a three-fold improvement in the oxidation resistance of their Nb-Mo-Si-B materials by the application of a chlorination treatment. Exposure of pre-oxidized samples to flowing gaseous chlorine selectively removed Nb_2O_5 from the oxide scale, allowing for surface passivation, which was not possible when porous Nb_2O_5 remained in the scale.[86] A chlorination treatment of only 15 minutes was all that was required to remove nearly all the Nb_2O_5 from a 100-200 μm thick oxide scale.[87]

Sakidja et al.[153] examined the effectiveness of aluminum pack cementation as a means for developing an Al_2O_3 surface coating on Mo-3Si-1B. Samples were packed in a mixture of NH_4Cl (1 wt.%, to act as a halide activator), Al-12Si (14 wt.%, the Al source material) and Al_2O_3 (85 wt.%, to act as filler material). The packed samples were then held at 900–1000 °C, depending on desired coating thickness, for 50 h. As a result of this process, a 40-50 μm thick layer of Mo_3Al_8, containing some MoAlB and $Mo(Si,Al)_2$, formed on the material surface. Upon exposure to oxygen (0.2×10^5 Pa) at temperatures between 732 °C and 1372 °C, a dense Al_2O_3 layer formed. This layer afforded extraordinary oxidation resistance, as is apparent in from the weight change of the alloys after oxidation, as related in **Table 1**.

As the Al_2O_3 formed, a $Mo_3(Al,Si)$ containing ~30 vol.% Mo_5SiB_2, grew between the Mo_3Al_8 layer and the base material. The growth of this interlayer limited the availability of Al to heal any cracks that appeared, and thus compromising the lifetime of the coating. Rioult et al.[69] defined the coating lifetime as a complex function of the coating thickness (h), densities of the various layers (d_{Mo3Al8}, d_{Al2O3} & $d_{Mo3(Al,Si)}$), molar masses of the various constituents (M_{Mo3Al8}, M_{Al2O3} & $M_{Mo3(Al,Si)}$), the Al:Si ratio in the $Mo_3(Al,Si)$ phase (r), the proportion of $Mo_3(Al,Si)$ in the interlayer (F) and constants determined from the parabolic growth rates of the Al_2O_3 (A_x & h_{ax}) and $Mo_3(Al,Si)$ (A_y & h_{ay}) layers. Their model for the lifetime of an Al_2O_3 coating is given by:

$$t_{\text{lifetime}} = \left[7\frac{h \times d_{Mo_3Al_8}}{M_{Mo_3Al_8}} \frac{1}{2\frac{d_{Al_2O_3}}{M_{Al_2O_3}}\sqrt{A_x \exp\left(\frac{-h_{ax}}{RT}\right)} + \frac{r}{1+r} \times \frac{F \times d_{Mo_3}(Al,Si)}{M_{Mo_3}(Al,Si)}\sqrt{A_y \exp\left(\frac{-h_{ay}}{RT}\right)}} \right] \quad (3)$$

The calculated lifetimes for various coating thicknesses at various temperatures are given in **Figure 9**. Below 950 °C, lifetimes are expected to suffer as a result of the formation of the less protective θ-Al_2O_3 phase. Under thermal cycling, the lifetime of these coatings is also expected to decrease, as coefficient of thermal expansion mismatch can lead to cracking and spallation of the Mo_3Al_8 coating.[69] Despite these limitations, Al pack cementation has the potential to radically improve the oxidation resistance of Mo-Si-B. The analysis by Rioult et al.[69] suggested that a 100 μm thick Mo_3Al_8 coating could provide more than 1000 h of enhanced oxidation resistance at 1300 °C. This lifetime

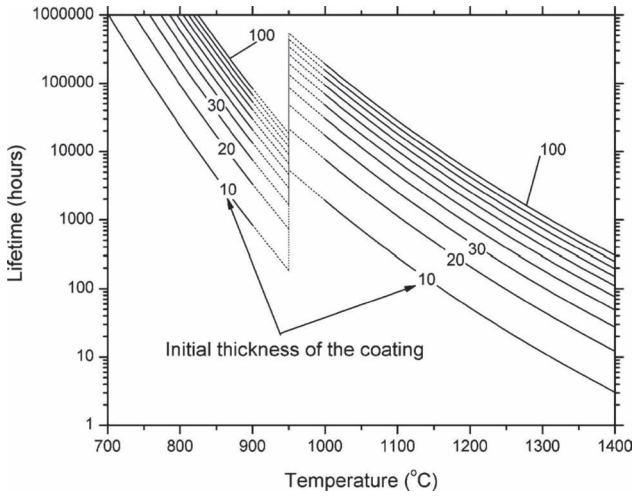

Figure 9. Lifetime of an aluminum pack cemented coating on Mo-Si-B vs. temperature for various initial coating thicknesses.[69] The lifetime of these coatings is dictated by depletion of Al by the formation of an $Mo_3(Si,Al)$ interlayer between the base material and the Al_2O_3 scale. Relatively thick initial coatings are required to provide long lives at elevated temperatures.

could be further improved if a B-rich layer can be formed on the base material before Al-pack cementation, as this layer has been shown to inhibit diffusion of Al into the base material.[153]

Pack cementation of Si has also been employed[83,89,154,155] as a means of improving the oxidation resistance of Mo-Si-B alloys. The process for creating an oxidation resistant coating is similar to the process used for Al pack cementation. A Mo-Si-B substrate is packed in a powder mixture of NaF (5 wt.%, to act as the halide activator), Si (25 wt.%, source material) and Al_2O_3 (70 wt.%, to act as filler material).[155] On heating to 900 °C, Si reacts with NaF to form SiF_4 gas, which interacts with the surface of the substrate to deposit a uniform layer of Si; the resulting surface enrichment leads to the *in situ* formation of a $MoSi_2$ coating. As $MoSi_2$ cannot exist in thermodynamic equilibrium with either α-Mo or Mo_3Si, an interlayer containing B-doped Mo_5Si_3 is formed. When exposed to an oxidizing atmosphere, a SiO_2 scale forms on the outer surface of the coating, while the Mo_5Si_3 interlayer continued to grow. Boron atoms ejected during the transition of Mo_5SiB_2 to Mo_5Si_3(B) react with α-Mo grains to form particles of MoB.[156] Sakidja et al.[155] have reported complete transformation of $MoSi_2$ to Mo_5Si_3 and SiO_2 after only 25 h in air at 1300 °C. Underneath the Mo_5Si_3 layer, a two-phase region of Mo_5SiB_2 and MoB forms, which can act as a barrier to Si transport.[89,154] As a result, the growth of the Mo_5Si_3 layer is halted. The underlying Mo_5SiB_2-MoB layer continuously supplies boron to the Mo_5Si_3 layer by maintaining the protective capabilities of this layer. Ito et al.[89,154] reported no weight change for Mo-3.4Si-2.6B alloys tested at 1300 and 1400 °C for 50 h. A slight weight gain was reported for tests performed at 1500 °C for 50 h, though slight weight loss was observed in a 100 h test. Ito et al.[89] also reported a slight degradation in the cyclic oxidation response of their material, although the slight weight loss was curtailed after 40 h.

While the Si pack strategy has proven to be effective at protecting alloys with small volume fractions of α-Mo,[89,154,155] it is less successful at protecting Mo-3Si-1B alloys, as the B content is not high enough to cause the formation of a continuous Mo_5SiB_2-MoB layer.[155] Sakidja et al.[155] proposed co-deposition of Si and B as a means to create a Mo_5SiB_2-MoB layer. The mechanics of such a deposition were explored further by Tang et al.[83] by examining the oxidation resistance afforded by deposition of Si, Si and B, or B then Si on a Mo-4Si-1B substrate. Si deposition resulted in a coating that transformed completely into Mo_5Si_3 after a 12 h exposure at 1600 °C. As a result, the sample was completely oxidized after only 50 h at this temperature. Co-deposited B and Si resulted in the formation of a similar coating structure as the solely Si deposition, though the porosity of the coating increased with increasing B content. The coating was again completely transformed within 12 h at 1600 °C, with the sample completely oxidized after 50 h. The initial porosity of the coating was not thought to affect the long term oxidation behavior, as any pores were sealed by the oxide during the experiment. The two-step process formed a more complex coating; specifically, after the initial B deposition, a Mo_2B_5 layer containing MoB particles was observed on the sample surface, while a Mo_5SiB_2-MoB layer formed between the outer coating and the substrate material. After the second step, the outer Mo_2B_5 layer had been converted into $MoSi_2$, while the Mo_5SiB_2-MoB interlayer had increased in thickness. This process was unsuccessful at improving the lifetime of a $MoSi_2$ coating at 1600 °C. Though these deposition techniques could not extend the life of a $MoSi_2$ coating on Mo-4Si-1.1B at 1600 °C, a lifetime on the order of thousands of hours was predicted for coatings oxidized at 1100 °C. Si diffusion, and the resulting transformation of $MoSi_2$ into much less oxidation-resistant Mo_5Si_3, limits the lifetime of these coatings.

5. Mechanical Properties

Because Mo-Si-B alloys are potential candidates for next-generation ultra-high temperature structural materials, an understanding of the mechanical response of these materials both at ambient and elevated temperatures is essential. The mechanical properties of these alloys are reviewed specifically with respect to the issues of creep, fracture and fatigue. However, we first examine high temperature tension, compression and bending behavior, with particular focus on α-Mo-Mo_5SiB_2-Mo_3Si alloys, as alloys consisting of only intermetallic phases (i.e., Mo_5Si_3-Mo_5SiB_2-Mo_3Si) are simply too brittle to act in load-bearing applications (for this reason, there is little published research on the mechanical properties of these purely intermetallic phase alloys.[81]) α-Mo is a required component if any significant ductility is desired, as few mobile dislocations and hence little plasticity can be realized in the highly-ordered intermetallic phases, especially at lower temperatures (*cf.,* Sections 2.2-4).

5.1. Tension/Compression Constitutive Behavior

Only a few studies of the basic tension, compression or bending constitutive behavior of Mo-Si-B alloys at elevated temperatures have been published.[9,10,14,15,94,114,134–137] However, the elastic

Table 2. Elastic Constants of Mo-4Si-1B at 24–1200 °C.

Temperature (°C)	*E* (GPa)	μ (GPa)	*B* (GPa)	ν
24	325	125	252	0.285
300	313	121	248	0.289
600	298	115	241	0.294
900	284	109	241	0.304
1200	269	102	239	0.312

constants of the Mo-4Si-1B alloy are known, determined by finite element modeling (FEM) simulations and confirmed by the resonant beam technique; these are listed, specifically Young's modulus, *E*, the shear modulus μ and the bulk modulus *B*, in **Table 2**.[134]

Nieh et al.[114] published the first tensile data for an α-Mo-Mo_5SiB_2-Mo_3Si alloy; they examined the high temperature deformation behavior of a three-phase, α-Mo-rich Mo-3.4Si-1.9B alloy, manufactured by hot-pressing blended elemental powders. The resulting alloy comprised ~50 vol.% α-Mo as a continuous matrix phase containing a fine dispersion of intermetallic phases; the grain size of all phases was ~3 μm. Nieh et al.[114] observed marked temperature and strain rate sensitivities for their alloy. At 1400 °C, a peak stress of 222 MPa and a tensile elongation of 150% were recorded at a strain rate of 10^{-4} s^{-1}, while the peak stress at a strain rate of 10^{-3} s^{-1} were 480 MPa and 23%, respectively. A significant decrease in strength was observed at 1450 °C, with peak stresses of 138 MPa at a strain rate of 10^{-4} s^{-1} and 275 MPa at a strain rate of 10^{-3} s^{-1}. The authors attributed this behavior a combination of creep of the α-Mo phase and grain-boundary sliding. Plastic deformation of the α-Mo phase accommodated grain boundary sliding of the intermetallic phases without the formation of cavities. For their material, Nieh et al.[114] reported a stress exponent, $n = 2.8$ (highlighting the combined influence of grain-boundary sliding ($n = 2$) and creep of α-Mo ($n = 5$)) and an activation energy of 740 kJ/mol. Similar behavior, in compression, has been observed by Mitra et al. for a Mo-5Si-1.4B alloy,[107,108] though higher strength retention was found at elevated temperatures which was attributed to the lower α-Mo content in their alloy (33 vol.%, distributed as discontinuous particles in an intermetallic matrix).

The remarkable high temperature deformation behavior observed by Nieh et al.[114] has also been observed by Jéhanno et al.[135,136] for their Mo-3Nb-3Si-1B mechanically-alloyed material. In this latter alloy, Nb was added as a solid solution strengthening agent for the α-Mo phase. Like Nieh et al.,[114] Jéhanno et al.'s material[135,136] contained a continuous α-Mo matrix, although the volume fraction of α-Mo was slightly higher (55 vol.%). However, the grain size in the Jéhanno material was even smaller than that of the Nieh material; this can result in a diminished toughness particularly at lower temperatures. Jéhanno et al.[135,136] reported submicron grain sizes for all three phases present in their material. At 1400 °C and a strain rate of 10^{-4} s^{-1}, a maximum stress of 45 MPa and a plastic strain to failure of ~400% were reported.[136] Unlike the Nieh material, substantial plasticity was observed at faster strain rates at 1400 °C (200% elongation at a strain rate of 10^{-3} s^{-1} and 25% elongation at a strain rate of 10^{-2} s^{-1}). In fact, more than 300% elongation was observed at 1300 °C at a strain rate of 10^{-4} s^{-1}.[136] This result is noteworthy, as the alloys tested by Jéhanno et al.[135,136] and Nieh et al.[114] both contain ~50 vol.% brittle intermetallic phases. After deformation, all phases remained in the submicron range as equiaxed grains, satisfying the requirements of superplasticity[157] as a potential deformation mechanism. Jéhanno et al.[136] reported a stress exponent $n = 2.3$ and an activation energy of 470 kJ/mol. The authors credit bulk diffusion of Mo atoms, as evidenced by their observed activation energy for deformation (the activation energy of Mo self-diffusion is 405 kJ/mol[158]), for maintaining grain cohesion during plastic deformation.

Similar behavior in compression, though at much slower strain rates, was noted by Alur et al.[98] and Kumar and Alur[101] for a Mo-2Si-1B two-phase powder-processed alloy containing an α-Mo matrix surrounding an α-Mo-Mo_5SiB_2 eutectic. These alloys were isothermally forged at 1760 °C with compression samples cut such that the long axis of the sample (i.e., the compression direction) matched the forging direction. Between 25 and 800 °C, this material was found to be relatively insensitive to strain rate in the range 10^{-7}-10^{-4} s^{-1}. The flow stress in this regime (~1100 MPa) was comparable to the room temperature yield stress (1280 MPa). Above 1000 °C, a significant strength drop and increase in strain rate sensitivity was observed; specifically, yield strengths between 790 MPa (at a strain rate of 10^{-4} s^{-1}) and 320 MPa (at a strain rate of 10^{-7} s^{-1}) were measured at this temperature. At 1400 °C, the yield strength fell to 130 MPa and 15 MPa for strain rates of, respectively, 10^{-4} s^{-1} and 10^{-7} s^{-1}. Very similar strength levels were reported for a three-phase Mo-2.9Si-1.1B alloy consisting of an α-Mo matrix interspersed with intermetallic phases. At 1000 °C, the material had a stress exponent $n = 7.1$, which was unaffected by strain rate; at 1400 °C, the stress exponent had fallen to $n = 5.2$ for strain rates as slow as 10^{-5} s^{-1}. Below this strain rate a possible shift in deformation mechanism was observed, as the stress exponent in this regime was reported to be $n = 2.5$. Activation energies in the range 415 - 445 kJ/mol were found for all test conditions, again implying self-diffusion of Mo as an important deformation mechanism. The high yield strengths of these materials, especially at lower temperatures, were at least partially attributable to the high initial dislocation densities in these materials as a result of the forging process.

FEM simulations performed by Alur et al.[98] help to elucidate the deformation mechanisms in this temperature/strain rate regime. Assuming an elastic-plastic matrix and an elastic intermetallic phase, Alur et al.[98] found a high degree of strain localization in the matrix phase. At low temperatures, the matrix phase was highly strained, while the Mo_5SiB_2 phase was relatively unstrained. This behavior was the result of the comparatively low yield stress and high work hardening rate of the matrix phase, such that the applied deformation was accommodated by matrix plastic deformation. At the lowest temperatures and highest strain rates, cracking of Mo_5SiB_2 particles was observed, highlighting the inability of this phase to accommodate strain. At high temperatures the strains were more homogeneously distributed. A significant decrease in the strain level in each phase was achieved by allowing plastic

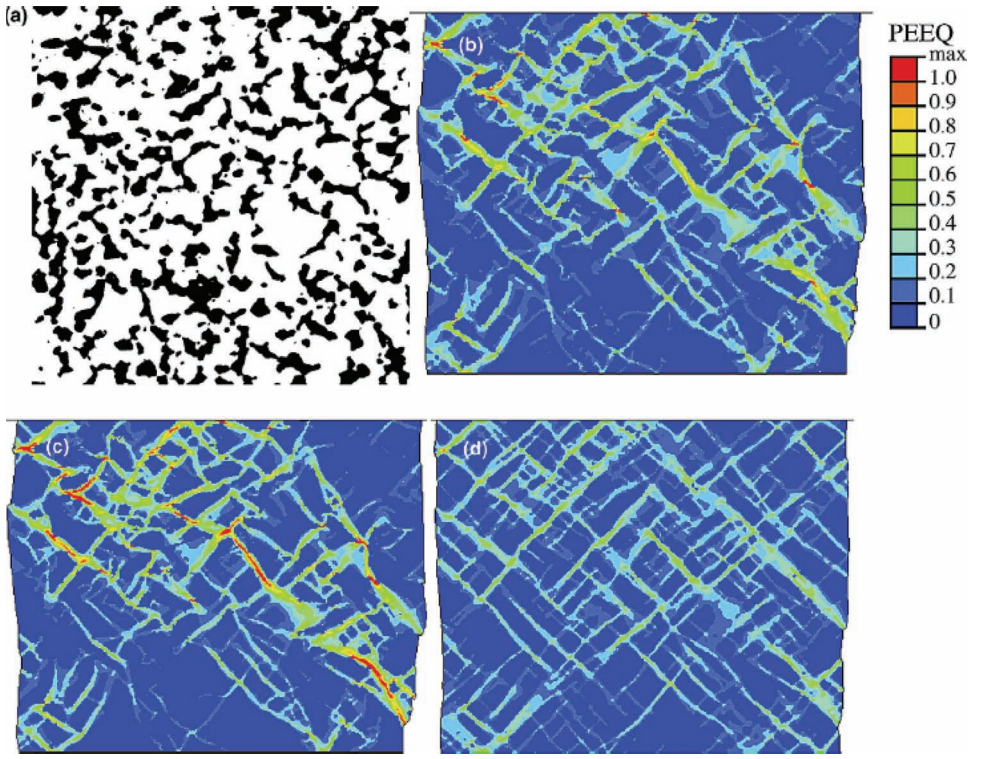

Figure 10. FEM simulation of the strain localization at a global strain of 10% in a Mo-2Si-1B two phase alloy.[98] The color scale represents relative strain. The microstructure from which a mesh was created is shown in (a). The material consisted of Mo_5SiB_2 (black) within a continuous α-Mo matrix (white). (b) At room temperature, the strain is highly localized in the much softer and more ductile α-Mo phase. (c) At intermediate temperatures (~750 °C), the localization of strain in the matrix phase increases. (d) At even higher temperatures (1550 °C), where Mo_5SiB_2 can plastically deform, a much more homogeneous distribution of strain is observed.

deformation of the intermetallic phase. This shift in modeling behavior was justified by the presence of dislocations in the post-deformation Mo_5SiB_2 phase. Deformation was accommodated by both the matrix and the intermetallic phase, as highlighted in **Figure 10**.

The importance of the matrix phase on the mechanical response of Mo-Si-B alloys was confirmed by Jéhanno et al.[94] They examined the tensile response of two Mo-3Si-1B alloys: one alloy, consolidated from rapidly solidified gas atomized powders, was comprised of an intermetallic matrix surrounding large α-Mo particles, and the second, consisting of a continuous α-Mo matrix surrounding small intermetallic particles, was created by a 6:1 extrusion at 1800 °C. A higher volume fraction of α-Mo was observed in the extruded material, but only one measurement was taken from each alloy condition, so this effect may be an artifact. Below 1200 °C, all intermetallic-matrix samples, tested in tension at an initial strain rate of 1.1×10^{-4} s^{-1}, failed in a brittle manner; at 1200 °C, however, some measureable plasticity at failure (7.3% elongation) was observed. The brittle-ductile transition temperature for the intermetallic-matrix alloy was estimated to be ~1150 °C. By contrast, significant plasticity (21.5% elongation) was found in the extruded, α-Mo-matrix material at 1093 °C. The authors estimated the brittle-ductile transition temperature of the extruded material to be ~950 °C–1000 °C, a drop of ~200 °C. It is likely that some of the strength gain observed after extrusion was a result of the increased initial dislocation density of the post-extrusion material.

The incorporation of a continuous α-Mo phase can greatly affect the brittle-ductile transition temperature in Mo-Si-B alloys. Krüger et al.[14] developed ultra-fine grained (grain size ~ 1 μm) three-phase Mo-3Si-1B alloys via mechanical alloying, as described in Section 3.2 In bending, these alloys achieved at least 8% strain at 1000 °C, matching the behavior exhibited by the extruded material tested by Jéhanno et al.[93] In contrast, the intermetallic-matrix gas-atomized material required temperatures in excess of 1200 °C to accomplish the same result. A cast and annealed, intermetallic-matrix, Mo-4.2Si-1.1B alloy, containing ~40 vol.% discontinuous α-Mo exhibited negligible ductility, even at 1520°C and a strain rate of 7×10^{-6} s^{-1} in flowing nitrogen.[84] Meanwhile, an α-Mo-matrix Mo-2.2Si-1B powder-processed alloy containing ~49 vol.% continuous α-Mo achieved a fracture strain of 1.8% at 1200 °C *in vacuo* at a much faster loading rate (3.3×10^{-3} s^{-1}).[116]

Grain size reduction also has the potential to increase the ductility of Mo-Si-B and lower the brittle-ductile transition temperature. α-Mo, as a bcc metal, is highly susceptible to cleavage fracture. High stresses ahead of a dislocation pileup can initiate a cleavage failure. If the grain size is reduced to such a degree that a sufficient dislocation pileup cannot form, failure by cleavage will not occur and higher ductility can be realized at lower temperatures. With this framework in mind, a number of oxide dispersions have been utilized[9,11,25–29] to pin grain boundaries and limit grain growth during processing. The effects of $MgAl_2O_4$ spinel additions were discussed in

Section 2.1. Jéhanno et al.[11] observed a substantial reduction in the brittle-ductile transition temperature with the addition of 0.1wt% Y_2O_3 or La_2O_3 to a Mo-3Si-1B alloy, though the alloy to which their data were compared did not have a continuous α-Mo matrix. As a result of their test methods, it is difficult to separate the effects of a continuous α-Mo from the effects of a reduced grain size. These authors measured the brittle-ductile transition temperature by compressing cylinders until 10% plastic strain was reached. Large (100 °C) temperature steps were used, so identification of a precise brittle-ductile transition temperature was not possible. As a result, the added benefit of a reduced grain size for the studied materials, pertaining to the brittle-ductile transition, is unclear. However, the work of Heilmaier et al.[9] clearly shows the benefit of a submicron grain size as 8% plastic strain (the chosen benchmark for ductility) was reached for a mechanically-alloyed, submicron-grained Mo-3Si-1B alloy at 1000 °C, while negligible ductility was observed for a micron-grained, La_2O_3-doped alloy. The reported low strength and ductility of the La_2O_3-doped alloy seems to contradict the results of Jéhanno et al.[11] for seemingly exactly the same material, but no explanation was given by the authors for this discrepancy.[9]

Alloying additions such as Zr have been shown[137] to affect the brittle-ductile transition temperature of Mo-3Si-1B and Mo-1.9Si-0.6B. Krüger et al.[137] observed significant plasticity in bending at 954 °C at a displacement rate of 0.01 mm/min in Ar. While a micron-grained Mo-3Si-1B alloy exhibited ~0.5% strain under these conditions, a Mo-3Si-1B-1Zr alloy exhibited ~1.5% strain. At lower Si and B contents, this effect was magnified. At 954 °C, a Mo-1.9Si-0.6B-1Zr alloy exhibited ~4% strain as compared to the ~0.5% strain displayed by the Zr-free material. Limited plasticity was observed in the Mo-1.9Si-0.6B-1Zr material at temperatures as low as 800 °C. It was postulated that the brittle-ductile transition temperature of continuous α-Mo-matrix Mo-Si-B materials could be reduced another 150 °C with the addition of Zr.[137]

5.2. Constant-Load Creep Behavior

Mo-Si-B alloys are potential replacements for current Ni-based superalloys because, among other beneficial properties, they demonstrate excellent creep resistance and strength retention at high temperatures. A number of studies on the creep behavior of these materials has recently been published.[9,10,18,100,135,141,142,159,160] The effects of creep on crack growth, as studied by Alur et al.,[100] will be deferred until the discussion of high temperature fracture toughness and fatigue behavior in Sections 5.2 and 5.3.

Schneibel and Lin[160] measured the creep response of a cast Mo-4.2Si-1.1B alloy at 1200 °C in flowing Ar. Owing to insufficient gettering of the Ar environment, oxidation of the material occurred during testing. MoO_3 crystals deposited on the quartz window used for laser extensometry of the sample; as a result, the authors were only able to successfully test one sample in tension. Compression tests were also performed in flowing Ar at temperatures between 1220° and 1420 °C. A steady-state creep stress was determined from the flow stress at 5% plastic strain. The activation energy (338 kJ/mol) and stress exponent (n = 2.7) were found to be insensitive to temperature or strain rate. The power-law creep equation developed by Schneibel and Lin[160] was given by:

$$\dot{\varepsilon} = 2.2 \times 10^{14} s^{-1} (\sigma / E)^{2.7} \exp([-338 kj/mol]/RT), \quad (4)$$

where R is the Gas constant and E is the room temperature Young's modulus of this material (327 GPa).[80] The authors claimed Mo_3Si to be the rate-controlling phase, as the calculated creep rate for single phase Mo_3Si using the compression data of Rosales et al.[34] compared favorably to the observed behavior. However, the relatively low volume fraction of this phase (32 vol.%) implies a contribution from the Mo_5SiB_2 phase (30 vol.%) as well. α-Mo was not thought to be rate-controlling.

Schneibel[159] also investigated the effects of alloying additions of Nb and W on the creep response of a Mo-X(Nb,W)-4.2Si-1.1B alloy between 1200 and 1400 °C. He identified the creep stress as the compressive engineering flow stress at 2% plastic deformation. For an unalloyed material, he reported a stress exponent of 3.2 and an activation energy of 295 kJ/mol. The addition of 36.7 wt.% (19.5 at.%) W was found to only slightly raise the activation energy to 319 kJ/mol, whereas Nb additions had a much stronger effect on the creep behavior. While the stress exponent was unaffected, the addition of 11 wt.% (9.5 at.%) or 22.7 wt.% (19.5 at.%) Nb raised the activation energy to 345 kJ/mol or 489 kJ/mol, respectively. The potency of Nb was attributed to its much larger atomic radius than either Mo or W. As a result of its larger size, Nb was postulated to inhibit diffusion and dislocation motion. The effect of Nb and W on the creep behavior of Mo-4.2Si-1.1B is shown in **Figure 11**.

In the same study, Schneibel[159] looked at the influence of the morphology and scale of the microstructure on the creep behavior of Mo-6.1Si-1.1B and Mo-4.9Si-1.5B alloys. Two Mo-6.1Si-1.1B alloys both comprising 21 vol.% discontinuous α-Mo but with differing α-Mo grain sizes were processed. The Mo-4.9Si-1.5B alloy contained ~30 vol.% continuous α-Mo,

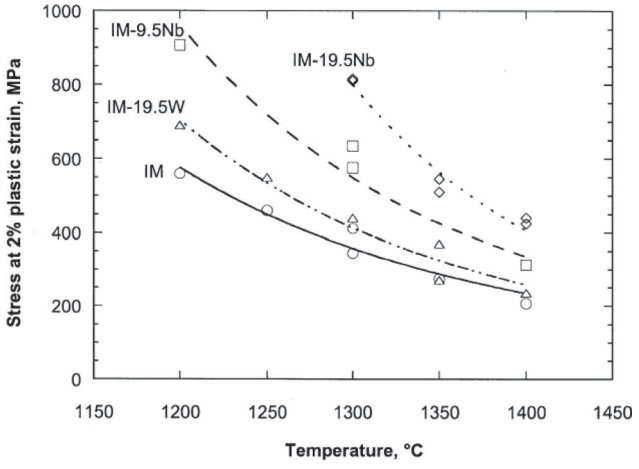

Figure 11. Influence of W and Nb on the creep behavior of Mo-Si-B.[159] While the effects of W additions are slight, significant gains in creep resistance can be realized by alloying Mo-Si-B with Nb. Substitution of Mo by the larger Nb atoms is thought to slow diffusion and dislocation motion, improving the creep response of these alloys.

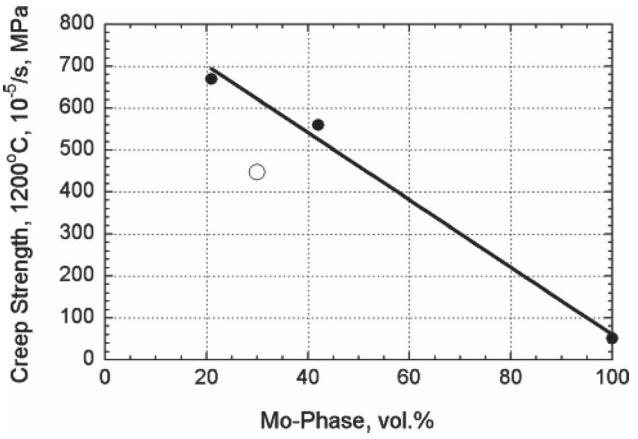

Figure 12. Influence of α-Mo volume fraction on the creep strength of Mo-Si-B.[141] As the weakest and most ductile phase, increasing the volume fraction of α-Mo will severely decrease the creep strength. This effect is even greater for a continuous α-Mo matrix (open circle), as the α-Mo is not as plastically constrained by the intermetallic grains, as is the case for discontinuous α-Mo grains within an intermetallic matrix (closed circles).

achieved using the process described in Section 3.1. Both microstructural scale and grain morphology were observed to have a profound effect on the creep behavior in the studied temperature regime. A detectable increase in the stress exponent (n = 2.8 *vs.* n = 2.1 for the finer microstructure) and decrease in the activation energy (327 kJ/mol *vs.* 376 kJ/mol) at 1300 °C were observed for the coarser-grained of the two Mo-6.1Si-1.1B alloys. Likewise, a significant increase in the stress exponent (n = 3.9) and decrease in activation energy (328 kJ/mol) were found for the continuous α-Mo Mo-4.9Si-1.5B alloy, although the reported values were calculated at 1400 °C. As α-Mo is the softest phase at these temperatures, the higher volume fraction of α-Mo in the Mo-4.9Si-1.5B material led to lower creep strength. Similarly, the continuity of the α-Mo phase in this material lowered the creep strength as plastic deformation of this phase was not as constrained. Finer microstructures provided more high-diffusivity pathways, speeding diffusion of Mo, and thus lowered the creep resistance of the material.[141,142,159] The combined effects of α-Mo volume fraction and continuity are shown in **Figure 12**.

Though the ultra-fine grained materials developed via mechanical alloying exhibit attractive oxidation resistance and formability, the preponderance of grain boundaries in these materials would be expected to harm their creep resistance.[135] Jéhanno et al.[135] studied the effect of microstructure size scale on the constant stress compression behavior of an ultra-fine grained Mo-3Nb-3Si-1B alloy between 1050° and 1315 °C. In order to assess the influence of grain size, both as-processed (submicron grains) and annealed (~7 μm α-Mo grains, ~4 μm intermetallic grains) samples were tested. 10 hour annealing treatments at 1700 °C were required to sufficiently coarsen the microstructure. The authors found that the stress exponent for each microstructure was approximately n = 2, indicating that grain-boundary sliding could be a possible creep mechanism. The activation energies for each microstructure were also similar (477 kJ/mol for the as-processed alloy, 444 kJ/mol for the annealed material), again implying the role of Mo diffusion in the high temperature deformation behavior of Mo-Si-B alloys, as reported by Alur et al.,[98] Kumar and Alur[101] and Jéhanno et al.[136] Although the mechanism and activation energy for creep were similar for the as-processed and annealed microstructures, the coarser-grained annealed alloy exhibited a creep rate that was more than one order of magnitude slower than the ultra-fine grained material. Similar behavior to the ultra-fine grained material was reported for La_2O_3-doped Mo-3Si-1B alloys by Heilmaier et al.,[9,10] who showed that the high temperature properties of his alloys compared very favorably with a Ni-based single crystal alloy, CMSX-4 below 1100 °C and vastly outperformed the Ni alloy above 1200 °C.[9,10] Thermal instability of the CMSX-4 above 1200 °C, coupled with the excellent thermal stability of Mo-3Si-1B up to 1600 °C, was thought to be the origin of the Mo-Si-B alloy's superior creep resistance.

The most comprehensive study of the creep behavior of Mo-Si-B alloys was recently published by Jain and Kumar.[18] As part of this work, they examined a Mo-0.9Si-0.2B material with the objective of studying the α-Mo solid solution phase (see also Section 2.1). These authors principally investigated the tensile load creep behavior of Mo-2Si-1B two-phase and Mo-3Si-1B three-phase alloys between 1000 °C and 1300 °C at both constant load and at a strain rate of 10^{-4} s^{-1}. Below 1200 °C, both the two- and three-phase alloys fractured after very little detectable plasticity. Above 1200 °C, no substantial difference between the creep behavior of the two- and three-phase alloys could be detected. For both materials, a stress exponent of n = 7 was calculated at 1200 °C when the tensile data of Jain and Kumar[18] and the compression data of Alur et al.[98] were combined to increase the range of strain rates examined. Creep voids did not form until very late in the creep lifetime; as a result, the creep behavior in tension and compression was assumed to be nearly identical, such that data from tension and compression tests could be combined. At 1300 °C, a stress exponent of n = 4.6 was reported for both multi-phase alloys, although corresponding values could not be extracted from the 1300 °C tension tests. Mo_5SiB_2 particles were observed as grain boundary precipitates in samples tested above 1200 °C; the quantity and coarseness of these particles was found to scale with temperature and applied stress. The authors postulated that the formation of these precipitates served to alleviate the grain boundary Si and B segregation observed in the as-processed alloy. This reasoning was bolstered by the lack of any precipitates within grains or on recrystallized grain boundaries that formed during the experiment (and thus would not be sites of Si or B segregation). The formation of Mo_5SiB_2 occurred both in the gauge section and within the grip section of the samples, implying that stress (and thus plastic strain) was not required for precipitation, though the application of stress did speed their coarsening. The higher Si content (and thus higher strength) of the matrix phase of the multiphase alloys, as well as the much higher volume fraction of intermetallic phases, were credited for providing the superior creep resistance of the two- and three-phase alloys. The alloys tested by Jain and Kumar[18] also outperformed Ni-based alloys over the temperature and stress regime investigated.

5.3. Toughness

While many researchers have performed toughness tests on Mo-Si-B alloys (*cf.*,**Table 3**), only a few have investigated the operative fracture mechanisms in these alloys. We will discuss the fracture behavior of these alloys at both ambient and elevated temperatures. While the proposed operating temperature for these alloys exceeds 1200 °C, it is unrealistic to think that fracture events cannot occur at lower temperatures. In any event, the high brittle-ductile transition temperature shown by these materials means that the brittle behavior observed at room temperature will persist until at least 1000 °C, and possibly higher, depending on the alloy choice and grain morphology.

At room temperature, Mo-Si-B alloys are inherently brittle. The high intermetallic content required for good oxidation resistance, coupled with solid solution strengthening of the α-Mo phase, limits the ability of these alloys to plastically deform. As a result, they all exhibit low room temperature

Table 3. Published Fracture Toughness Values for Various Mo-Si-B Alloys. This table represents a collection of all the published fracture toughness values for Mo-Si-B alloys. These values have not previously been tabulated and are provided here as a central reference. Various geometries have been used by different researchers. Test geometries include three-point bend (3PB), four-point bend (4PB), compact tension (C(T)) and disc-shaped compact tension (DC(T)). Note that where chevron-notching has been used, this can truncate the early portion of the R-curve and slightly elevate the observed initiation toughness.

Ref.	Material	Processing Technique	α-Mo vol.%	α-Mo Morphology	Test Geometry	Fracture Toughness, K_Q, [MP$\alpha\sqrt{m}$]
[112]	Mo-5.2Si-0.7B	Reaction Hot-pressed	1.2	Discontinuous	3PB	7.5
[112]	Mo-5.5Si-1.4B	Reaction Hot-pressed	4.5	Discontinuous	3PB	6.6
[112]	Mo-5.8Si-2.2B	Reaction Hot-pressed	8.4	Discontinuous	3PB	5.2
[88]	Mo-3.4Si-2.6B	Directional Solidification (5 mm/h)	28	Discontinuous	3PB	11
[113]	Mo-3Si-1.2B	Hot-pressed powder	50	Discontinuous	4PB	9.5
[113]	Mo-5.4Si-1.3B	Hot-pressed powder	20	Discontinuous	4PB	6.1
[84]	Mo-4.2Si-1.1B	Cast and Annealed (1600 °C/24 h)	38	Discontinuous	3PB, Chevron-notched	9.5
[107]	Mo-5.1Si-1.4B	Reaction Hot-Pressed	33	Discontinuous	3PB	5.0
[107]	Mo-1.1Al-4.3Si-1.1B	Reaction Hot-Pressed	35	Discontinuous	3PB	5.8
[107]	Mo-2.8Al-4.1Si-1.1B	Reaction Hot-pressed	39	Discontinuous	3PB	6.6
[141]	Mo-4.2Si-1.1B	Cast and Annealed (1600 °C/24 h)	42	Discontinuous	3PB, Chevron-notched	9.0
[141]	Mo-4.2Si-1.1B-1.1Zr	Cast and Annealed (1600 °C/24 h)	42	Discontinuous	3PB, Chevron-notched	12.4
[141]	Mo-4.2Si-1.1B-1.7Zr	Cast and Annealed (1600 °C/24 h)	42	Discontinuous	3PB, Chevron-notched	13.5
[141]	Mo-4.2Si-1.1B-3.5Zr	Cast and Annealed (1600 °C/24 h)	42	Discontinuous	3PB, Chevron-notched	12.6
[77]	Mo-4.2Si-1.1B-0.9Ti	Cast and Annealed (1600 °C/24 h)	42	Discontinuous	3PB, Chevron-notched	10.0
[85]	Mo-4.2Si-1.1B	Arc-cast	38	Discontinuous	DC(T) 25 °C	7.2
[85]	Mo-4.2Si-1.1B	Arc-cast	38	Discontinuous	DC(T) 25 °C	7.8[#]
[85]	Mo-6.1Si-1.2B	HIPped Powder	21	Discontinuous	DC(T) 25 °C	4.1
[85]	Mo-6.1Si-1.2B	HIPped Powder	21	Discontinuous	DC(T) 1300 °C	8.1
[85]	Mo-6.1Si-1.2B	HIPped Powder (Mo & Mo-20Si-10B (at.%))	21	Discontinuous	DC(T) 25 °C	5.7
[85]	Mo-6.1Si-1.2B	HIPped Powder (Mo & Mo-20Si-10B (at.%))	21	Discontinuous	DC(T) 1300 °C	7.5
[85]	Mo-6.1Si-1.2B	HIPped Powder (Mo & Mo-20Si-10B (at.%))	21	Discontinuous	DC(T) 1300 °C	7.7[#]
[85]	Mo-12.1Nb-4.2Si-1.1B	Arc cast	38	Discontinuous	DC(T) 25 °C	6.3
[85]	Mo-12.1Nb-4.2Si-1.1B	Arc cast	38	Discontinuous	DC(T) 25 °C	6.7[#]
[85]	Mo-4.2Si-1.1B	Arc Cast	38	Discontinuous	DC(T) 1300 °C	9.7
[85]	Mo-4.2Si-1.1B	Arc Cast	38	Discontinuous	DC(T) 1300 °C	11.7[#]
[104]	Mo-16.2Si-1.6B	Plasma-Sprayed	0[†]	n/a	4PB, Chevron-notched	4.1
[115]	Mo-7.6Si-1.5B[*]	Vacuum Annealed Powder	30	Continuous	3PB, Chevron-notched	14
[113]	Not Reported	Hot-pressed powder	78	Continuous	4PB	13.4
[84]	Mo-4.2Si-1.1B	Hot-pressed powder	38	Continuous	3PB, Chevron-notched	14.8
[99]	Mo-2Si-1B	PREP powder, isothermal forged	62	Continuous	3PB, 25 °C	8
[99]	Mo-2Si-1B	PREP powder, annealed (1600 °C/48 h)	62	Continuous	3PB, 25 °C	9
[99]	Mo-2Si-1B	PREP powder, isothermal forged	62	Continuous	3PB, 600 °C	13

Table 3. Continued.

Ref.	Material	Processing Technique	α-Mo vol.%	α-Mo Morphology	Test Geometry	Fracture Toughness, K_Q, [MPa$\sqrt{m}$]
[99]	Mo-2Si-1B	PREP powder, isothermal forged	62	Continuous	3PB, 1200 °C	18
[99]	Mo-2Si-1B	PREP powder, isothermal forged	62	Continuous	3PB, 1400 °C	25
[117]	Mo-4.1Si-1.6B	Vacuum Annealed Powder	37.5	Continuous	DC(T), 25 °C	8.0
[117]	Mo-4.1Si-1.6B	Vacuum Annealed Powder	37.5	Continuous	DC(T), 25 °C	~9
[117]	Mo-4.0Si-1.5B	Vacuum Annealed Powder	37.5	Continuous	DC(T), 25 °C	7.5
[117]	Mo-4.0Si-1.5B	Vacuum Annealed Powder	37.5	Continuous	DC(T), 25 °C	~9[#]
[117]	Mo-4.0Si-1.5B	Vacuum Annealed Powder	37.5	Continuous	DC(T), 1300 °C	12.6
[117]	Mo-4.0Si-1.5B	Vacuum Annealed Powder	37.5	Continuous	DC(T), 1300 °C	~15[#]
[117]	Mo-5.5Si-1.6B	Vacuum Annealed Powder	18.3	Continuous	DC(T), 25 °C	5.0
[117]	Mo-5.5Si-1.6B	Vacuum Annealed Powder	18.3	Continuous	DC(T), 25 °C	~8[#]
[117]	Mo-5.5Si-1.6B	Vacuum Annealed Powder	18.3	Continuous	DC(T), 1300 °C	8.3
[117]	Mo-5.5Si-1.6B	Vacuum Annealed Powder	18.3	Continuous	DC(T), 1300 °C	~9[#]
[117]	Mo-3.3Si-1.3B	Vacuum Annealed Powder	49.1	Continuous	DC(T), 25 °C	9.8
[117]	Mo-3.3Si-1.3B	Vacuum Annealed Powder	49.1	Continuous	DC(T), 1300 °C	35 (23)[‡]
[117]	Mo-2.2Si-1.0B	Vacuum Annealed Powder	~50	Continuous	DC(T), 25 °C	12.0
[123]	Mo-3Si-1B	Reaction Synthesis	~55	Continuous	Notched C(T), 25 °C	7.1
[123]	Mo-3Si-1B	Reaction Synthesis	~55	Continuous	Notched 4PB, 1300 °C	26[§]
[123]	Mo-3Si-1B-0.1Y	Mechanical Alloying	~55	Continuous	Notched DC(T), 25 °C	7.8
[123]	Mo-3Si-1B-0.1Y	Mechanical Alloying	~55	Continuous	Notched DC(T), 1300 °C	22[§]

[*]The material tested by Schneibel et al.[115] had an initial powder composition of Mo-20Si-10B (at.%). During processing, Si was removed from the powder particles surface by vacuum annealing. No composition after vacuum annealing was reported by the authors; [†]The plasma-sprayed Mo-Si-B alloy tested by Okumus et al.[104] did not contain any α-Mo. It was composed instead of Mo_5Si_3, MoB and $MoSi_2$; [‡] The toughness value reported by Kruzic et al.[117] for their alloy was an overestimate as it was based on a "rule of mixtures" calculation using the room temperature elastic modulus values. Moreover, the authors assumed a d_n of unity in Eq. 5, corresponding to plane stress loading of a perfectly plastic material, whereas a more accurate value for their material is 0.586. Accordingly, the more appropriate recalculated toughness values given by Lemberg et al.[123] is also given here, in parenthesis; [#]Steady-state or maximum reported toughness after stable crack growth; [§]The initiation toughnesses at 1300 °C reported by Lemberg et al.[123] represent equivalent K values which would have been obtained had samples large enough to satisfy the requirements of linear elasticity. Instead, J-integral (i.e., nonlinear elastic fracture toughness) values were estimated based on crack tip opening displacements at crack initiation, as given by Eq. 5.

toughness. Incorporating the α-Mo phase into an intermetallic matrix as a second phase can allow some room temperature plasticity; indeed, the volume fraction and distribution of α-Mo greatly affects the fracture behavior of Mo-Si-B alloys. As a crack extends, it will encounter a region of α-Mo; as this is softer phase, the crack can become blunted and trapped, increasing the so-called *intrinsic toughness* of the material. (Toughening in materials can be considered as a mutual competition between intrinsic and extrinsic mechanisms. Intrinsic toughening mechanisms dominate in ductile materials; they operate ahead of the crack tip to generate resistance to microstructural damage, with the most prominent mechanism being that of plastic deformation. Extrinsic toughening mechanisms, conversely, operate primarily in the wake of the crack tip to inhibit cracking by "shielding" the crack from the applied driving force.[161-164] Whereas intrinsic toughening mechanisms are effective in inhibiting both the initiation and growth of cracks, extrinsic mechanisms, such as crack bridging, are only effective in inhibiting crack growth.[162–164])

Extrinsic toughening can also be generated by the presence of the α-Mo phase; prominent mechanisms in this regard are crack deflection and uncracked ligament bridging, which can lead to crack-resistance curve (R-curve) behavior. (The R-curve provides an assessment of the fracture toughness in the presence of subcritical crack growth. It involves measurements of the crack-driving force, e.g., the linear-elastic stress intensity K, the strain energy release rate G or nonlinear elastic J-integral, as a function of crack extension (Δa). The value of the driving force as Δa tends to 0 provides a measure of the crack-initiation toughness whereas the slope and/or the maximum value of the R-curve can be used to characterize the crack-growth toughness.) As a crack extends and encounters a more ductile α-Mo grain, depending on the relative toughnesses of the phases, their relative elastic moduli and the angle of incidence, the crack can either penetrate the α-Mo grain (and fracture the grain transgranularly) or deflect into the grain boundary and propagate around the grain.[165] This deflection event raises the toughness of the material, as the preferred microstructural path no longer coincides with the direction of maximum driving force. As a result, more stress must be applied to continue crack propagation. At some point the crack must either propagate "backwards" up the flank of the grain, or it will stall, creating a highly stressed region in the proximity of the crack tip.[166] As the remotely-applied stress (and thus the local stresses near the crack tip) are increased, a region ahead of the crack tip can become stressed enough that the crack will reinitiate and continue propagating (**Figure 13**). This process leaves regions behind the crack tip which remain uncracked (so called "uncracked ligaments") which can carry load that would otherwise be used to propagate the crack, *i.e,* they shield the crack tip from the full extent of the remotely applied stress. As

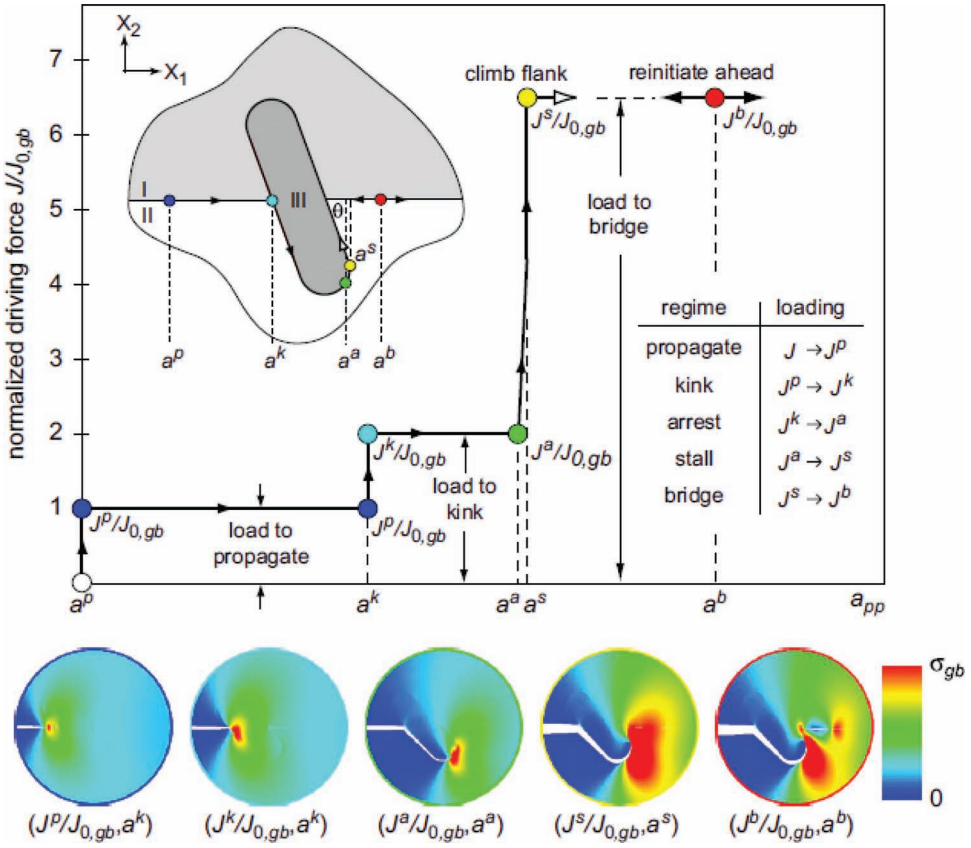

Figure 13. Schematic of toughening associated with uncracked grain bridge formation.[166] A crack traveling within the boundary between two grains (I & II) requires a certain driving force to propagate, J^p. Upon interacting with a more ductile grain (III), the crack can kink and deflect along the preferred path of a grain boundary. This preferred microstructural path is not aligned with the direction of maximum driving force, so additional driving force, J^k, is necessary to propagate the crack. Eventually, the crack will arrest at a driving force, J^a. The crack can climb backwards up the flank of the grain, a process known as stalling, but this process is highly energetically unfavorable and a large driving force is required, J^s. The stresses that build during the stall phase can be large enough to reinitiate a crack in the boundary ahead of the ductile grain (III). The crack will proceed, leaving behind an uncracked ligament. Such uncracked ligaments result in rising R-curve behavior in Mo-Si-B alloys.

the crack extends, more bridges are left in the wake, increasing the shielding effect, which leads to rising R-curve toughening behavior.

5.3.1. Ambient Temperature Behavior

The room temperature fracture behavior of Mo-Si-B alloys has been thoroughly investigated by Choe et al.,[78,79,85] Kruzic et al.,[116–118] Lemberg et al.[123] and Alur et al.[99] for various alloy compositions, phase distributions and processing methods. Choe et al.[85] studied the room temperature fracture behavior of two cast alloys (Mo-4.2Si-1.1B and Mo-12.1Nb-4.2Si-1.1B) and two hot-pressed powder alloys (both Mo-6.1Si-1.2B, differing starting powders). The cast alloys contained 38 vol.% discontinuous α-Mo as a second phase in an intermetallic matrix. The powder processed alloys contained 21 vol.% discontinuous α-Mo. The average grain size of the cast alloys (10.4 μm for Mo-4.2Si-1.1B, 7 μm for Mo-12.1Nb-4.2Si-1.1B) was significantly larger than the powder alloys (respectively, 2.1 and 4.4 μm), although the coarser-grained powder processed alloy contained a number of elongated 50 μm grains. Choe et al.[85] performed fracture toughness experiments, as per the ASTM E561 standard,[167] using fatigue pre-cracked disk-shaped tension specimen. Stable crack growth was measured *in situ* utilizing the unloading compliance technique prescribed by the testing standard. Stable crack growth and the accompanying rise in toughness were used to create crack growth R-curves. They found that the initiation toughness of their alloys scaled with mean grain size and volume fraction and contiguity of the α-Mo phase. The highest initiation toughness, K_o = 7.2 MPa$\sqrt{m}$, was exhibited by the Mo-4.2Si-1.1B alloy, which had the largest and most continuous grains. This alloy exhibited a slight rise in toughness with crack extension. After 800 μm of crack growth, a peak (plateau) toughness of K_{ss} = 7.8 MPa$\sqrt{m}$ was reported. The finer-grained Mo-12.1Nb-4.2Si-1.1B alloy exhibited lower initiation (6.3 MPa$\sqrt{m}$) and peak (6.7 MPa$\sqrt{m}$) toughnesses. Both powder-processed alloys displayed significantly lower initiation toughnesses (5.7 MPa$\sqrt{m}$ for the larger-grained alloy, 4.3 MPa$\sqrt{m}$ for the smallest-grained, least continuous material) and no stable crack growth was observed. In fact, the authors were unable to fatigue-precrack the smaller-grained material, so the value reported for that alloy was probably somewhat of an over-estimate.

Fracture at room temperature in these materials is essentially totally brittle and occurs mostly by transgranular cleavage

of the intermetallic matrix. The crack predominately travels through the intermetallic matrix or within the grain boundaries surrounding the α-Mo phase. Cracks were observed to deflect around or crack through small α-Mo regions, but became trapped at larger α-Mo grains. A small number of unbroken α-Mo grains were found in the crack wake, but these uncracked ligaments displayed minimal plastic deformation, which was attributed to plastic constraint of the α-Mo grains by the intermetallic matrix. The dominant toughening mechanism reported for these intermetallic-matrix materials was crack trapping, an *intrinsic* toughening mechanism.

While Choe et al.[85] showed the influence of grain size, volume fraction of α-Mo and the contiguity of the α-Mo phase (large-grained microstructures containing a large volume fraction of contiguous α-Mo provide the most resistance to crack extension), they did not study the effects of a continuous α-Mo-matrix material. To address this issue, Kruzic et al.[117] measured R-curve toughness behavior for a number of alloys with varying α-Mo volume fractions and grain sizes; all of the alloys tested comprised intermetallic second phases distributed within a continuous α-Mo matrix, using the processing method developed by Schneibel et al.[115] to produce a continuous α-Mo phase, even at very low volume fractions of α-Mo. The authors varied both the initial starting size ("fine" ≡ <45 μm, "medium" ≡ 45-90 μm, "coarse" ≡ 90-180 μm) of their vacuum-anneal Mo-7.6Si-1.5B powders and the volume fraction of α-Mo in their "coarse" alloy (17 vol.%, 46 vol.% and 49 vol.%). Utilizing the notation of Kruzic et al.,[117] the alloys are labeled F34, M34, C17, C46 and C49 where the letter represents the initial powder size and the number represents the volume fraction of α-Mo.

All of the alloys tested by Kruzic et al.[117] exhibited significant rising R-curve behavior, with the largest degree of toughening with crack extension observed for the coarse-grained materials. While the C17 alloy had an initiation toughness (K_o = ~5 MPα√m) comparable to the discontinuous α-Mo alloys studied by Choe et al.,[85] after 3 mm of crack extension, the peak toughness of the C17 alloy had increased to ~7 MPα√m, a much larger increase in toughness than exhibited by the alloys studied by Choe et al.[85] which contained twice as much α-Mo, although distributed as a discontinuous second phase. The alloys containing a similar volume fraction of α-Mo to Choe, et al's alloys, namely F34 and M34, exhibited similar initiation toughnesses (~7.5 MPα√m), but the increase in toughness with crack extension (K_{ss} = ~9 MPα√m) was approximately 12% greater than seen by Choe et al. (K_{ss} = ~7.9 MPα√m).[85] The high volume fraction α-Mo materials exhibited initiation toughnesses as high as 12.5 MPa√m and peak toughnesses in excess of 20 MPa√m after 3 mm of crack extension, as shown in **Figure 14**. The values reported by Kruzic et al.[117] are the highest reported room-temperature toughnesses for any Mo-Si-B alloy.

The transition to a continuous α-Mo matrix greatly improves the room temperature toughness of Mo-Si-B alloys. Crack trapping remains an important toughening mechanism, although crack bridging by uncracked α-Mo ligaments occurs much more frequently with the continuous α-Mo matrix, and provides the primary source of *extrinsic* toughening and hence rising R-curve behavior. As shown in **Figure 15**, cracks cannot avoid a continuous α-Mo phase, so the effectiveness of crack trapping and uncracked ligament bridging is improved when an α-Mo matrix is utilized.

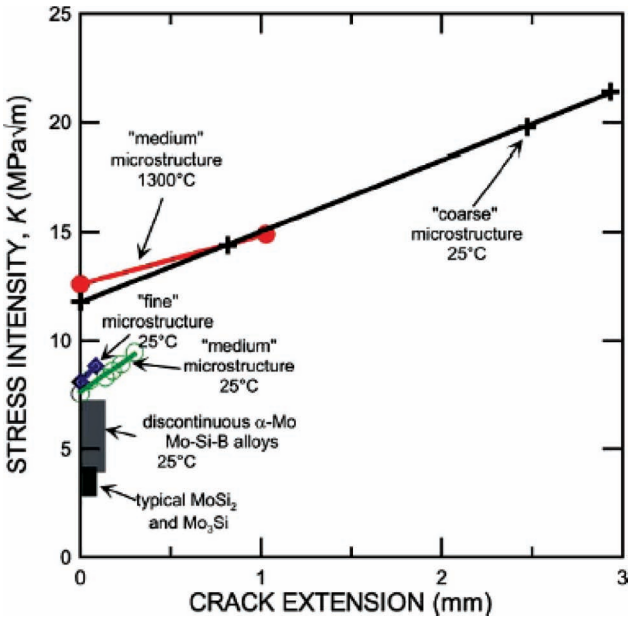

Figure 14. Room temperature R-curves for continuous α-Mo-matrix Mo-Si-B alloys.[116] A higher volume fraction of α-Mo (~49 vol.% in the coarse alloy, ~34 vol.% in the fine and medium alloys) leads to more *intrinsic* toughening, as the α-Mo can plastically deform and raise the initiation toughness of the alloy. *Extrinsic* toughening, afforded by uncracked ligament bridging, is more potent for coarser-grained materials. A continuous α-Mo phase forces the crack to interact with this ductile phase, where it can become blunted and trapped, raising the toughness of the material. In fact, a continuous α-Mo matrix allows for significant *extrinsic* toughening, while discontinuous α-Mo does not. At 1300 °C the toughness of this alloy is increased, highlighting the contribution of α-Mo ductility to toughness.

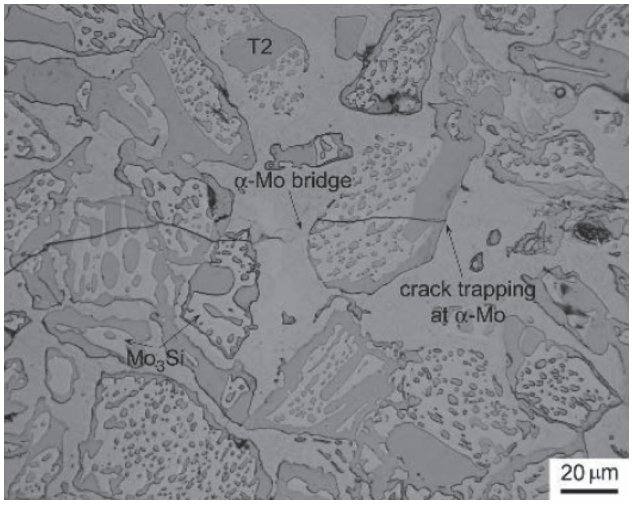

Figure 15. Crack trapping and bridging in a continuous α-Mo-matrix Mo-Si-B alloy.[117] As it is continuous, cracks cannot avoid the α-Mo phase. Uncracked ligaments can form, raising the *extrinsic* toughness of the material by shielding the crack tip. Cracks blunt at the plastically-deformable α-Mo phase and must reinitiate to continue propagating. This process serves to raise the *intrinsic* toughness of the material.

A larger volume fraction of α-Mo provides more traps and potential crack-bridging sites, so both the initiation toughness (as the result of more plasticity) and the peak toughness (as the result of more *extrinsic* toughening) will increase.

When comparing alloys with the same volume fraction of α-Mo but differing microstructural size scales, it becomes apparent that grain size has little effect on the initiation toughness. Both the F34 and M34 alloys tested by Kruzic et al.[117] had initiation toughnesses K_o = 7 MPa$\sqrt{}$m, similar to the initiation toughness of the cast material tested by Choe et al.[85] While little difference was observed for the initiation toughnesses of these materials, a higher peak toughness at a larger crack extension was reported for the M34 alloy, implying an increased level of *extrinsic* toughening in that material. Kruzic et al.[117] reported improved crack stability and easier bridge formation in coarser-grained alloys. That the authors were able to achieve significant stable crack growth accompanied by rising toughness in a coarse-grained alloy containing only 17 vol.% α-Mo highlights the influence of microstructural size scale on the rising R-curve behavior of these alloys.

Lemberg et al.[123] confirmed the importance of microstructural size scale and morphology with their study of the fracture behavior of two ultra-fine-grained Mo-3Si-1B alloys, one mechanically alloyed and the other reaction synthesized, comparing their results to the earlier work of Kruzic et al.[117] on coarse grained Mo-3Si-1B alloys. Each of the Lemberg alloys contained ~55 vol.% continuous α -Mo and but unlike the Kruzic alloys, the grain size was far smaller, on the order of 5 μm. Lemberg et al.[123] found that the initiation toughness of the mechanically alloyed and reaction synthesized alloys was approximately 33% lower than the coarse-grained Kruzic material. They reported initiation toughnesses from radiused micronotches of 7.8 and 7.2 MPa$\sqrt{}$m for the mechanically alloyed and reaction synthesized alloys, respectively. More importantly, no stable crack growth was observed, similar to some of the powder-processed alloys tested by Choe et al.,[85] although this could have been in part due to the use of radiused micronotches with root radii less than 20 μm. (Fatigue pre-cracking very brittle materials, such as the current Mo-Si-B alloy, can be extremely difficult without fracturing the sample. Ceramic materials have similar problems which has led to the use of the radiused micronotching technique. However, the presence of a stress concentrator with a micron-sized root radius, rather than a fatigue crack with a root radius closer to atomic dimensions, has the effect of truncating the early portion of the R-curve and thereby slightly elevating the crack-initiation toughness.)

The critical point here is that at low temperatures, Mo-Si-B alloys are truly brittle materials as the α-Mo phase can only provide for very limited ductility. *Brittle materials can only be toughened extrinsically*, and as such the coarser microstructures are able to generate toughness (more precisely crack-growth resistance) through such shielding processes as crack deflection and ductile-ligament bridging. The much smaller grains in the mechanically alloyed and reaction synthesized alloys cannot act as such impediments to crack propagation. Though a large volume fraction of α-Mo would imply a very high probability of the more ductile grains interacting with a moving crack and trapping it, the extremely small grain size provides a pathway so that a crack can avoid the more ductile grains without a large increase in energy.

Two additional factors were proposed by Lemberg et al.[123] as limitations to the toughness of the ultra-fine-grained alloys. Plastic constraint of α -Mo grains by the hard intermetallic phases, as well as embrittlement of the grain boundaries by Si and O, was reasoned to reduce the damage tolerance of the mechanically alloyed and reaction synthesized alloys tested. Specifically, the presence of hard particles can limit the ductility of α-Mo grains, thereby lowering their effectiveness as crack traps and bridges. Chan and Davidson[168] developed a model to account for the decrease in toughness caused by plastically-constrained ductile particles. In the case of constrained ductile particles, they proposed that the toughness of a ductile-phase toughened brittle material could be expressed by:

$$K_C = K_C^{Brittle} \sqrt{\left(1 + \sqrt{1-f}\left[\left(\frac{K_C^{Ductile}}{K_C^{Brittle}}\right)^2 \exp\left(-\frac{8q}{3}\left(\frac{f}{1-f}\right)\right) - 1\right]\right)}, \quad (5)$$

where $K_C^{Brittle}$ and $K_C^{Ductile}$ are the toughnesses of the brittle and ductile phases, f is the volume fraction of brittle phase and q is a geometric factor here taken to be unity (representative of spheroidal particles). For an unconstrained ductile phase, the corresponding toughness is given by:[168]

$$K_C = K_C^{Brittle} \sqrt{\left(1 + \frac{2}{\sqrt{\pi}}\sqrt{1-f}\left[\left(\frac{K_C^{Ductile}}{K_C^{Brittle}}\right)^2 - 1\right]\right)} \quad (6)$$

Using toughness values of ~3 MPa$\sqrt{}$m for the brittle (intermetallic) phase(s)[34,65] and ~15 MPa$\sqrt{}$m for the ductile (α-Mo) phase, these models predict that the toughness of an alloy containing ~55 vol.% α-Mo would be reduced from ~13.8 MPa$\sqrt{}$m for an unconstrained ductile phase to ~4.8 MPa$\sqrt{}$m for a constrained ductile phase. While not particularly predictive of the absolute toughness values of the alloys studied by Lemberg et al.[123] (Eqs. 3 & 4 are especially sensitive to the volume fraction at which hard particles begin to contact the ductile phase as the strengthening contribution afforded by hard particles is constant once contact between particles is established[168]), these models do serve to illustrate the loss in extrinsic toughening, by a factor of ~3, associated with the constraint imposed by the hard intermetallic grains on the more ductile α-Mo phase. In fact, in the terminology adopted by Chan and Davidson,[168] both the mechanically alloyed and reaction synthesized alloys suffer from "brittle-phase embrittlement" where the high degree of plastic constraint imposed by the high volume fraction of intermetallic (Mo_3Si and Mo_5SiB_2) grains acts to counteract the potential ductile-phase toughening afforded by the α-Mo grains. As a result, any α-Mo grains that interact with a crack will break, or cause deflection of the crack into the grain boundaries, rather than exhibit the crack trapping-reinitiation mechanism necessary to form a ductile ligament bridge. This issue is exacerbated by small grain sizes, as the mean free path between two intermetallic grains is shorter, thereby increasing the amount of constraint on each α-Mo grain. Indeed, Lin and

Chan[169] showed that the maximum effective plastic strain occurs within the interface between a strengthening particle and the surrounding matrix (here the grain boundaries between the harder intermetallic phases and the α-Mo matrix). Consequently, grain boundaries will fail prematurely, lowering the toughness of the material.

Another consideration limiting the effectiveness of α-Mo as a ductile phase is solid-solution strengthening of molybdenum by silicon. The α-Mo phase in these alloys can contain as much as 4 at.% Si, as the α-Mo remains supersaturated with Si which after precipitation of the intermetallic increases the strength of α-Mo phase by as much as a factor of 6, but at the cost of reduced ductility and toughness.[19,20] The lack of plasticity afforded by the solid solution phase magnifies the effects of plastic constraint, as the contact stresses caused by the intermetallic grains cannot be alleviated by plastic deformation. As a result, the values used for the toughness of the "ductile" phase in Eqs. 3 and 4 are likely overestimates. As an illustration of this, Sturm et al.[20] found a drop in room temperature toughness from 24 MPa√m for pure molybdenum to ~5 MPα√m for a solid solution containing 2 at.% Si.

Scanning Auger electron spectroscopy was performed by Lemberg et al.[123] in an effort to locate any oxygen or silicon impurities in both of their fine-grained alloys, as well as the coarse-grained Kruzic alloy. Oxygen is known[21,22] to have has a deleterious effect on the strength of grain boundaries in molybdenum alloys. Free oxygen has a greater potential to weaken the grain boundaries than oxygen tied up in silica or other glassy inclusions, so the location of any oxygen impurities is vitally important to these alloys' structural performance. Silicon is also well known as a solid solution strengthener of Mo at the expense of toughness; however, it can segregate to grain boundaries, greatly reducing their cohesive strength.

Though some degree of oxygen segregation was apparent in the reaction-synthesized and Kruzic alloys, the authors found it difficult to comment on the severity of this segregation based on their results. The presence of Si on the grain boundaries of these materials, as shown in **Figure 16**, was thought to be problematic, especially in the case of the fine-grained alloys, which have a much larger grain boundary volume than the Kruzic material. Much higher levels of Si were found on the grain boundaries than in the bulk of all three materials, although a standardless test method prevented the determination of exact impurity levels; qualitative comparisons, however, clearly showed much higher Si levels in the mechanically-alloyed and reaction-synthesized materials.[123]

The disparity in Si levels was a result of the processing methods used to manufacture each alloy. The powders used to make the Kruzic alloy were vacuum annealed to enrich the powder particle surfaces in Mo by driving off Si as volatile SiO.[115,117] Hot-isostatic pressing these surface modified powders created a continuous α-Mo microstructure with very low Si content in the grain boundaries, as the particle interfaces (which become grain boundaries upon sintering) were silicon-depleted. The processing methods used to create the mechanically alloyed and reaction synthesized alloys could result in excess Si in the α-Mo phase. Specifically, supersaturation of the α-Mo phase during mechanical alloying can lead to segregation of Si to grain boundaries during precipitation of the

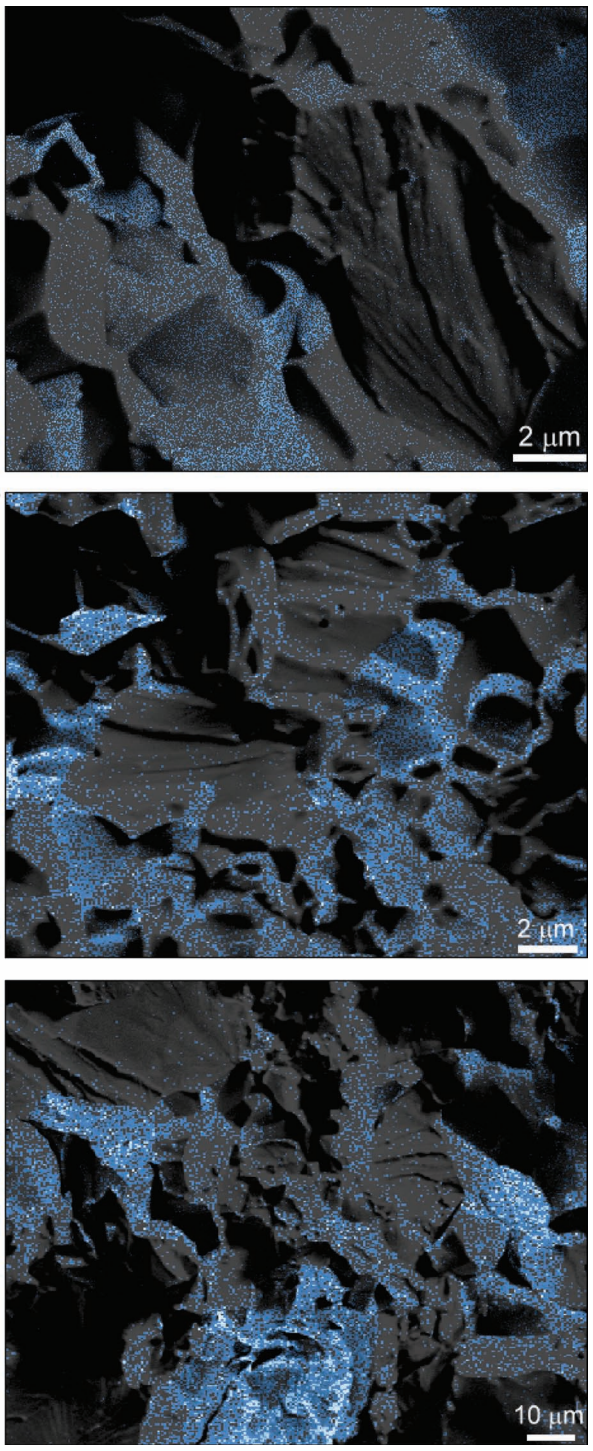

Figure 16. Auger electron spectroscopy maps of impurity content on grain boundaries overlaid on the corresponding room-temperature fracture surfaces for the (a) mechanically alloyed, (b) reaction synthesized and (c) coarse-grained Mo-3Si-1B alloys.[123] Areas of high silicon content (blue) are shown. Si segregates to grain boundaries, reducing interfacial strength and increasing the occurrence of intergranular fracture. Note the high concentrations of Si in the regions that fractured intergranularly, while almost no Si is found in regions that fractured transgranularly. Note the difference in scale for (c) as this alloy material[117] had grains more than one order of magnitude larger than either (a) or (b).

intermetallic phases. Likewise, incomplete reaction of Mo and Si_3N_4 to form Mo_3Si and Mo_5SiB_2 can lead to excess free silicon, which then segregates to grain boundaries, lowering their cohesive strength.

Alur and Kumar[99] observed limited room temperature ductility and no rising R-curve behavior for their isothermally-forged Mo-2Si-1B alloys. Even though the volume fraction of α-Mo in the materials studied by Alur and Kumar[99] was even larger (62 vol.% α-Mo) than any of the materials studied by Kruzic et al.,[117] their initiation toughnesses were approximately 36% lower. The largest initiation toughness observed by Alur and Kumar[99] was only 9 MPa$\sqrt{m}$ for an annealed alloy. The more brittle behavior and lack of extrinsic toughening observed for these materials can be attributed to the differing processing methods used to create the two materials. The powders used by Kruzic et al.[117] were processed in such a way as to create regions of α-Mo nearly free of Si; by contrast, the alloys used by Alur and Kumar[99] contained as much as 4 at.% Si within the grains and 12 at.% within the grain boundaries.[18] Since Si is a well-known solid solution strengthener and embrittling agent of Mo grain boundaries, the lower toughness observed by Alur and Kumar[99] is not unexpected. The presence of some recrystallized grains in these two-phase materials served to further embrittle the materials, since recrystallized Mo grain boundaries are weaker.

This body of work clearly shows the influence of microstructure on the room temperature damage tolerance of Mo-Si-B alloys. Clearly the pertinent microstructural feature here is the presence, volume fraction and connectivity of the α-Mo phase. Although it is possible to create a continuous α-Mo matrix with a small volume fraction of α-Mo,[115] the most common processing methods result in high α-Mo volume fractions. A continuous α-Mo matrix imparts the highest toughnesses via two means: (i) a highly contiguous α-Mo phase increases the probability of a crack interacting with the more ductile α-Mo phase, increasing the incidence of crack trapping and ductile ligament bridging (extrinsic toughening), and (ii) the presence of the more ductile α-Mo phase can promote crack blunting thereby promoting the intrinsic toughness.

5.3.2. Elevated Temperature Behavior

At elevated temperatures, the toughness of these alloys is significantly improved, by as much as a factor of 3. As noted in Section 5.2, the ductile-brittle transition temperature of these alloys can be lowered by ~150 °C by transitioning to a continuous α-Mo matrix. In particular, the ability of the α-Mo phase to plastically deform is drastically increased at elevated temperatures; as a result, the crack blunting and trapping ability of the material is much improved. Choe et al.[85] observed a sizeable increase in the initiation toughness of both their cast and their powder-processed alloys. At 1300 °C, the cast alloy exhibited an initiation toughness K_o = 9.7 MPa$\sqrt{m}$ *vs.* K_o = 7.2 MPa$\sqrt{m}$ at room temperature. The powder processed alloys exhibited lower toughnesses at both room and elevated temperatures (K_o = 4.1 MPa$\sqrt{m}$ and 5.7 MPa$\sqrt{m}$ at room temperature, 8.1 MPa$\sqrt{m}$ and 7.5 MPa$\sqrt{m}$ at 1300 °C), though this effect was likely the result of the lower volume fractions and contiguities of the α-Mo phase in the powder processed alloys. At elevated temperatures, significant microcracking was observed in the Mo_5SiB_2 phase.

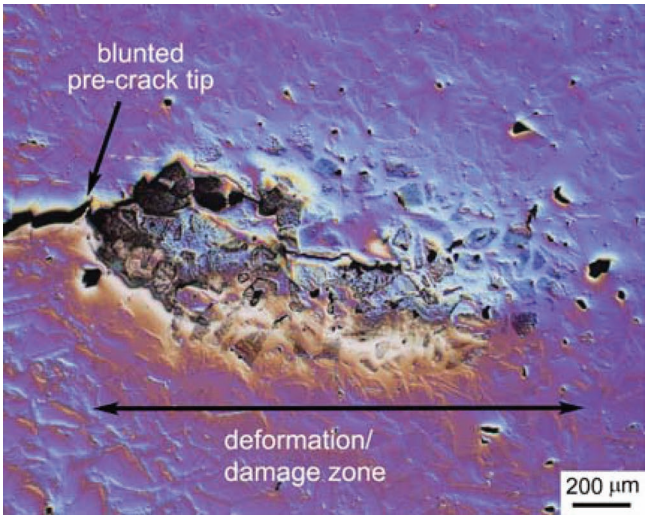

Figure 17. Crack profile near crack initiation at 1300 °C for a coarse-grained Mo-3Si-1B alloy.[117] Large-scale plastic deformation at the crack tip led to crack blunting and a significant increase in toughness.

Microcracking, and the associated dilatation, acts as an additional crack-tip shielding mechanism, as the compressive forces caused by the dilated microcracked region must be overcome before the critical stress to fracture the material can achieved.[162] The additional toughening effect afforded by microcracking of Mo_5SiB_2 is relatively small, specifically, ~2 MPa$\sqrt{m}$ from the dilatation of the microcracked region and ~1 MPa$\sqrt{m}$ from the change in compliance as a result of the microcracks.[85]

A much larger increase in toughness with temperature was observed for α-Mo-matrix alloys. Kruzic et al.[117] found that the initiation toughness of a coarse grained (~100 μm grain size) Mo-3.3Si-1.3B alloy increased from 9.8 MPa$\sqrt{m}$ at room temperature to ~35 MPa$\sqrt{m}$ at 1300 °C, although the value reported for elevated temperature was valid for a plane stress condition, and is thus not directly comparable. In fact, the increase in ductility of the α-Mo phase at 1300 °C was so profound that linear elastic fracture mechanics (i.e., the *K*-based approach) no longer applied and the nonlinear elastic fracture mechanics *J*-integral approach had to be used, as is evident from the excessive degree of damage present in **Figure 17.** (*J* is the nonlinear strain-energy release rate, i.e., the rate of change in potential energy for a unit increase in crack area in a nonlinear elastic solid. It is the nonlinear elastic equivalent of the strain energy release rate *G*. It characterizes the stress and displacement fields at a crack tip in such a solid, and as such can be used to define the onset of fracture there.) After their tests were completed, Kruzic et al.[117] optically measured the crack-tip opening displacement (CTOD) at crack initiation. Using the CTOD-*J* relationships derived by Shih,[170] they estimated the fracture toughness in terms of a J_{ic} value which was then converted to an equivalent K_{JC} value (which would have been observed had a sample large enough to satisfy the applicability requirements for plane strain and the linear-elastic fracture mechanics condition of small-scale yielding). The *J*-integral can be estimated from the CTOD by:[170]

$$J = d_n \sigma_\gamma \delta_t, \tag{7}$$

where σ_y is here the flow stress (the average of the yield and ultimate stresses), and d_n is a dimensionless parameter, varying from 0.3 to 1, which is dependent upon the strain-hardening exponent, n, the yield strain, and whether a state of plane stress or plane strain prevails. From the calculated J values, it is possible to calculate K_{JC} values using a Mode I approximation, *viz.*:

$$K_{JC} = (J\,E')^{1/2} \tag{8}$$

where $E' = E$, the elastic (Young's) modulus) in plane stress and $E/(1-\nu^2)$ in plane strain (ν is Poisson's modulus). Such K_{JC} values represent the fracture toughnesses that would have been obtained if a sample large enough to maintain small-scale yielding could have been used. Using this method, it is possible to overcome the size constraints of meeting small-scale yielding conditions while still properly accounting for the extension of the crack. (Note here that as documented in ASTM Standard E-1820,[171] for linear-elastic K_{IC} measurements the crack-tip plastic-zone size must be typically an order of magnitude smaller than (i) the in-plane dimensions of crack length a and remaining uncracked ligament b (small-scale yielding condition) and (ii) the out-of-plane thickness dimension B (a condition of plane strain); i.e., a, b, $B \geq 2.5\,(K_{IC}/\sigma_y)^2$, where σ_y is the yield (or flow) strength. For nonlinear elastic J measurements, similar validity criteria exist although the size requirements are much less restrictive; specifically b, $B \geq 10\,(J_C/\sigma_y)$.)

However, the toughness value reported by Kruzic, et al.[117] for their alloy, using the CTOD method, was an overestimate as it was based on a "rule of mixtures" calculation using the room temperature elastic modulus values. Moreover, the authors assumed a d_n value of unity in Eq. 7, corresponding to plane stress loading of a perfectly plastic material, whereas a more accurate value for their material is 0.586. Accordingly, a more appropriate value of ~23 MPa√m was recalculated by Lemberg, et al.[123]

With these alloys, again the continuous α-Mo matrix forces the crack to interact with the ductile phase. The increased ductility of α-Mo at 1300 °C increases the effectiveness of crack blunting and trapping. Similar to the observations at room temperature, a coarse microstructure increases the effectiveness of crack bridging at elevated temperature.

Lemberg et al.[123] found that the distribution of α-Mo becomes less critical above the ductile-brittle transition temperature. The enhanced ductility of the α-Mo phase allows for significant plastic deformation, and under some testing conditions superplasticity is possible. As the alloys can now be considered as ductile, *intrinsic* toughening associated with plasticity provides the dominant contribution to the toughness. This is primarily governed by the volume fraction of the ductile α-Mo phase, rather than the grain morphology, with the result that at 1300 °C, the fine-grained mechanically alloyed and reaction synthesized alloys, with their high volume fraction of α-Mo, now display comparable toughness to the coarse-grained Kruzic materials (**Figure 18**). Lemberg et al.[123] reported plane stress K_{JC} values of 22 MPa√m and 26 MPa√m for their mechanically alloyed and reaction synthesized materials, respectively, values which compare very favorably with the calculated initiation toughness for the coarse-grained material tested by Kruzic et al.[117]

At temperatures as low as 300 °C, pure molybdenum can have an initiation toughness greater than 60 MPa√m[172] with the toughness at 1300 °C expected to be much higher. The

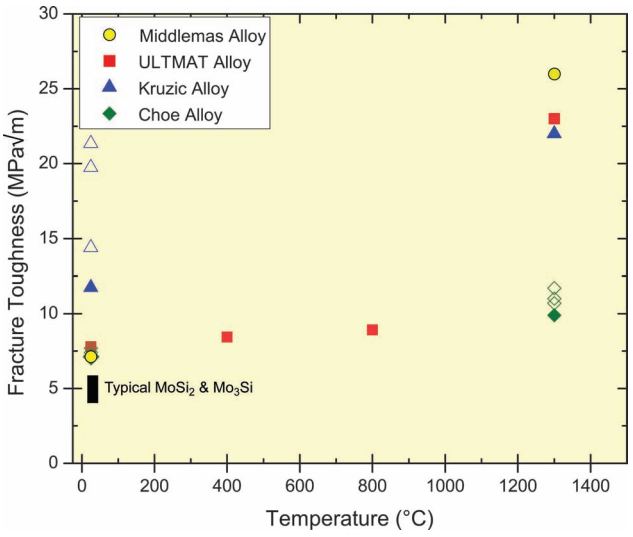

Figure 18. Fracture toughness as a function of temperature for Mo-3Si-1B alloys.[123] Crack-initiation toughnesses (closed symbols) are plotted along with any increases in toughness with crack extension (open symbols). At low temperatures, neither the ULTMAT (mechanically alloyed) nor the Middlemas (reaction synthesized) alloy exhibited any stable crack growth prior to unstable fracture. At 1300 °C, the enhanced ductility of the α-Mo phase markedly improves the initiation toughness of alloys containing ~50 vol.% α-Mo. At this temperature, the volume fraction of α-Mo becomes a more important factor in developing toughness (*intrinsically* from plasticity) than the distribution and morphology of α-Mo grains (which leads to *extrinsic* toughening from mechanisms such as crack bridging).

toughness of the silicon-containing α-Mo phase will not be as high as that for pure Mo (owing to the effects of solid solution strengthening), but it should be clear that the adverse effects of plastic constraint can be overcome once the ductile-brittle transition temperature is surpassed. At elevated temperatures, uncracked grain ligaments are much easier to form, even for ultra-fine-grained materials. The reduced strength of α-Mo at elevated temperatures lowers the barriers to plastic deformation, allowing for significant crack blunting. As a result of this blunting, crack reinitiation must occur, leaving behind an uncracked grain ligament. It is unclear at this time how the contribution to toughening by uncracked ductile ligaments will differ between the fine-grained and coarser-grained materials. The additional toughness afforded by uncracked ductile ligaments can be understood by an examination of the strain-energy release rate, G, which is another measure of toughness that defines the amount of strain-energy dissipated by an advancing crack. Sigl et al.[173] described the toughening contribution of uncracked ligaments, in terms of the strain energy release rate $G = K^2/E$, by:

$$\Delta G = V_f\,\sigma_y\,t\,\chi, \tag{9}$$

where V_f is the volume fraction of bridges, σ_y is the yield strength, t is the size of the bridges and χ is a work of rupture, dependent on the ductility, plastic constraint and strain hardening of the ductile phase.

At elevated temperatures, the ductility of these alloys is increased, but the yield strength is much lower. As a result, the crack-growth toughness (i.e., the slope of the R-curve) will not

be affected as greatly as the initiation toughness, although some gains are expected.[117] While the smaller grains of the mechanically alloyed and reaction synthesized materials would imply smaller bridges (as were in fact observed by Lemberg et al.), a larger number of grains can act as bridges. Campbell et al.[174] demonstrated that a large volume of many small bridges may be nearly as effective at promoting crack growth toughness in γ-TiAl as a smaller volume of fewer large bridges. The latter authors[174] observed the largest toughness increase in materials containing high-aspect ratio lamellae, while the increase toughness caused by bridging was more limited in material containing equiaxed grains. The potential attractiveness of ultra-fine grained Mo-3Si-1B alloys as structural materials is due, in part, to the possibility of producing a large number of small bridges in these alloys. However, further study is needed to quantify the additional crack-growth toughness afforded by uncracked ductile ligaments in these finer-grained, equiaxed materials. Nevertheless, the drastic improvement in damage tolerance exhibited by the ultrafine grained materials at high temperatures is promising.

Alur and Kumar[99] also observed similar behavior at elevated temperatures for their Mo-2Si-1B two-phase powder-processed alloy. The reported initiation toughnesses for their alloy rose from ~9 MP$\alpha\sqrt{}$m at room temperature to 25 M$\alpha\sqrt{}$m at 1400 °C *in vacuo*, with the largest gains in toughness observed over the 1200 °C (18 MP$\alpha\sqrt{}$m) to 1400 °C (25 MP$\alpha\sqrt{}$m) regime. At 1400 °C, the authors observed a large amount of microcracking of the Mo_5SiB_2 phase not seen at room temperature. They also observed a much more tortuous crack path at 1400 °C. The crack deflections were thought to be the result of the formation of a microcracked region ahead of the crack tip.

Alur et al.[100] observed that the initiation toughness in three-point bending exhibited some loading rate sensitivity at elevated temperatures. While the initiation toughness increased monotonically with temperature at a loading rate of 10^{-3} mm/s, a toughness maximum was observed at 1200 °C at a loading rate of 10^{-5} mm/s. The lower toughness at 1400 °C compared to 1200 °C was attributed to creep cavitation and grain recrystallization. The much longer exposures to temperature at the slower loading rate (525 min to test at 10^{-5} mm/s *vs.* 12 min to test at 10^{-3} mm/s) led to creep effects such as grain boundary sliding (and thus creep cavities). These cavities provide a preferred microstructural path, thereby reducing the initiation toughness. Cavities form on recrystallized grain boundaries, which are known to be weaker. Plastic constraint by the hard metallic particles and the presence of silica were also proposed mechanisms for creep cavity formation. While creep effects were detrimental to the initiation toughness at 1400 °C, at lower temperatures where creep cavitation does not occur, creep can relax the local stresses at the crack tip, thereby increasing the toughness. However, without comparable hold times at temperature for the differing loading rates, it is difficult to decouple the effects of creep and loading rate.

5.4. Fatigue

Since Mo-Si-B alloys are toughened extrinsically, fatigue of these alloys is governed by degradation of the effectiveness of these mechanisms under cyclic loading.[162,164] Mechanistically, early fatigue "damage" consists of the rapid formation of many uncracked bridging ligaments. Continued cyclic loading causes a breakdown of some bridges, while new bridges form as the crack extends. Eventually a steady-state behavior is reached, where a dynamic zone of bridge formation and destruction is carried along with the growing crack. Near the end of the fatigue life, bridge destruction far outstrips bridge formation and failure proceeds rapidly. An example of this mechanism is illustrated in **Figure 19**, though the bridge depicted is a rarely-formed intermetallic bridge. The mechanism operates in the same manner for α-Mo bridges.

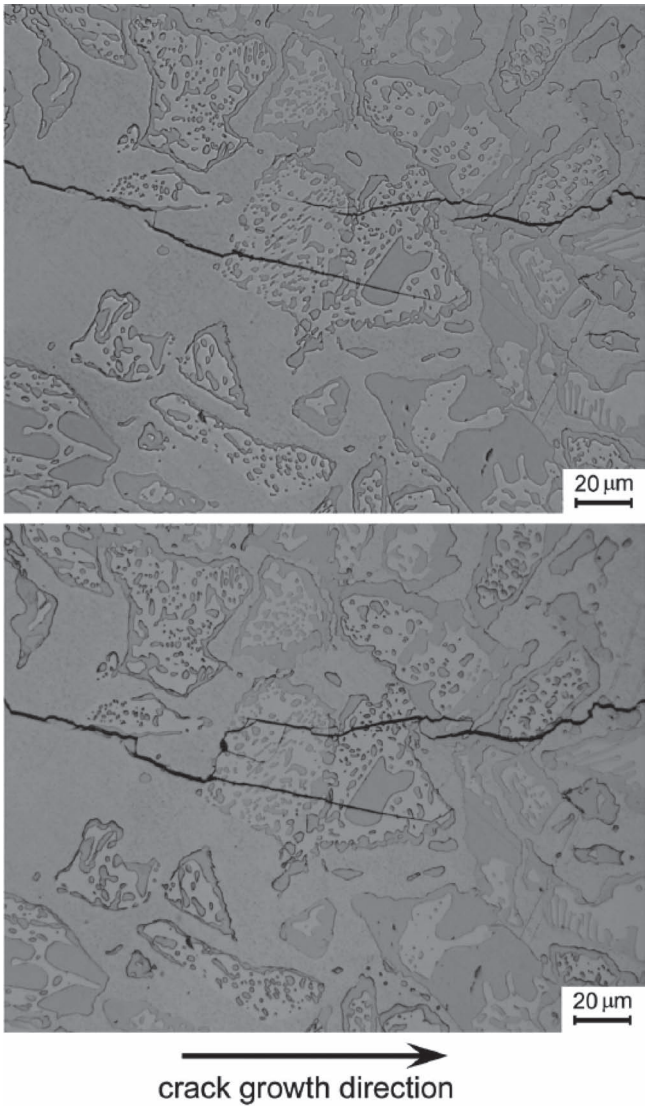

Figure 19. Formation (a) and subsequent destruction (b) of an uncracked ligament bridge during cyclic loading of coarse-grained Mo-3Si-1B.[117] Fatigue in these brittle materials occurs as a result of the failure of these bridges, a mechanism very different than fatigue in a ductile material.[162] As a result, these materials exhibit high fatigue thresholds and low susceptibility to fatigue. However, when a fatigue crack is initiated, it very quickly propagates to critical size. These materials display very large room temperature Paris law exponents (>75) unlike the Paris law exponents found in ductile materials (2-4).

In the steady-state regime, fatigue behavior can be described in simple terms by Paris' Law, $da/dN \propto \Delta K^m$, where da/dN is the incremental crack growth per cycle, ΔK is the stress-intensity factor range (K_{max}–K_{min}) and m is the Paris exponent. Ductile materials typically exhibit Paris exponents in the range of 2-4, while brittle materials exhibit much larger Paris exponents, often greater than 20. The extremely large Paris exponent values for brittle materials highlight their limited damage tolerance and rapid progression to failure once a crack is initiated.

As a result of the brittle mechanisms for fatigue crack growth, the fatigue thresholds and Paris law exponents for Mo-Si-B alloys are quite large, especially at room temperature. Thus the majority of the fatigue lifetime of these alloys is spent initiating a flaw that that once formed quickly grows to a critical size. Increased α-Mo ductility generates more extrinsic toughening, and thus slows crack growth and improves the fatigue resistance of these materials. However, increased α-Mo ductility leads to increased susceptibility to fatigue, as the plastic deformation required for the typical "ductile" fatigue-crack growth mechanism of alternating crack-tip blunting and resharpening can occur more readily. Thus, lower α-Mo ductility implies a reduced susceptibility to fatigue (insomuch as a larger minimum stress-intensity factor can be supported without initiating a crack), but once a crack is initiated, unstable fracture soon follows. Higher α-Mo contents will lead to fatigue crack growth at lower loads, but the increased damage tolerance of the material allows for some measure of stable crack growth before final fast fracture occurs.

5.4.1. Room Temperature Behavior

Only a few researchers have studied the fatigue crack growth behavior of Mo-Si-B alloys. Choe et al.[85] investigated the tension-tension fatigue crack growth behavior of their cast Mo-4.2Si-1.1B and powder-processed Mo-6.1Si-1.2B alloys under stress-intensity control (K-control) at a load ratio (maximum load/minimum load) of $R' = 0.1$ and a testing frequency of 25 Hz. These authors obtained crack growth rates, da/dN, between 10^{-11} and 10^{-5} m/cycle under K-increasing and K-decreasing conditions, with a normalized K-gradient of ± 0.1 mm^{-1}, as per ASTM Standard E647.[175] Since these materials are very brittle, they exhibit a higher sensitivity to the maximum stress intensity at the fatigue threshold, $K_{max,th}$ than to ΔK.[162] (The fatigue threshold represents the magnitude of the stress intensity, either ΔK or K_{max}, where the crack growth rate can be assumed to be vanishingly small. It is often operationally defined as the stress intensity to give a growth rate of 10^{-11} m/cycle.) In brittle solids such as Mo-Si-B alloys, $K_{max,th}$ threshold values were deemed more appropriate for gauging the fatigue resistance. The relationship between $K_{max,th}$ values and the more usual ΔK_{th} thresholds can be equated in terms of the load ratio R' by the expression:

$$\Delta K_{th} = K_{max,th}(1 - R') \tag{10}$$

Both the cast Mo-4.2Si-1.1B and coarser-grained powder-processed Mo-6.1Si-1.2B alloy (*cf.,* Section 5.2.1) exhibited a fatigue threshold of $K_{max,th} \sim 5$ MPα√m, i.e., lower than the room temperature fracture toughness for these materials. By contrast, the slightly finer-grained Mo-12.1Nb-4.2Si-1.1B alloy displayed a slightly lower threshold, $K_{max,th} \sim 4$ MPα√m. The fine-grained powder processed alloy, which did not have any elongated grains, failed catastrophically at $\Delta K = 4$ MPα√m such that no fatigue crack growth data could be obtained. The Paris law exponent for all three materials was approximately $m = 60$, comparable to many brittle (*e.g.*, ceramic) materials.[176] The relatively high threshold values (K_{th} = ~70% of K_o for the cast alloys) and large Paris exponents demonstrates the heightened sensitivity to flaw size and stress that these intermetallic-matrix materials display. While some uncracked ligament bridges form, over time they degrade under cyclic loading and eventually crack. However, the minimal bridge formation exhibited by these alloys means that little *extrinsic* toughening exists in the first place to be degraded; the result of this is that, akin to ceramics, these materials are essentially insensitive to fatigue. The specific fatigue mechanism involves cracks extending each loading cycle, mechanistically as under monotonic loading, before local arrest occurs; any bridges that form continue to carry load, but eventually fail by fatigue. As a result, the crack-microstructure interactions under cyclic loading mimic those seen under monotonic loading, with the coarser microstructures providing better fatigue resistance.

Alloys containing a continuous α-Mo matrix exhibit similar fatigue behavior to that displayed by intermetallic-matrix alloys. Kruzic et al.[117] studied the fatigue crack growth response of their five alloys (F34, M34, C17, C46, C49, *cf.,* Section 5.2.1) under the same conditions used by Choe et al.[85] At room temperature, owing to the relatively brittle response of the α-Mo phase, very large (>78) Paris law exponents were observed. Fatigue thresholds, $K_{max,th}$, as large as 10.6 MPα√m were reported for the coarse-grained material containing 49 vol.% α-Mo. The fatigue threshold was found to scale with microstructural size scale and volume fraction of α-Mo, while the Paris law exponent, m, decreased with increasing α-Mo content or grain size. In all cases, the fatigue threshold was approximately the same as the initiation toughness in monotonic loading, implying that the mechanisms for crack growth do not change under cyclic or monotonic loading, similar to the behavior observed by Choe et al.[85] Utilization of a α-Mo matrix improved the fatigue threshold, as compared to the intermetallic-matrix materials studied by Choe et al.[85] Kruzic et al.[117] reported a room temperature fatigue threshold for their F34 alloy of $K_{max,th} = 6.8$ MPα√m, an increase of 36% compared to the fatigue threshold reported by Choe et al.[85] That the fatigue threshold increased with higher α-Mo volume fractions is not surprising since in these materials, where the cracking mechanisms are so similar under monotonic and cyclic loading, the fatigue thresholds scale with the (crack initiation) toughnesses. The fatigue thresholds for the F34 and M34 alloys (6.8 MPα√m and 7.2 MPα√m, respectively) were nearly the same, implying minimal influence on the fatigue threshold exerted by microstructural size scale, at least over the size regime studied in these alloys. However, the Paris slopes for the two alloys were quite different (125 for F34, 87 for M34). Since room temperature fatigue in these materials proceeds by the degradation of *extrinsic* toughening mechanisms, e.g., the cyclic degradation of grain bridging, the increased number and potency of uncracked ligament bridges (i.e., increased *extrinsic* toughness) exhibited by the coarser-grained M34 alloy leads to an increased

susceptibility to fatigue, as expressed by the lowered Paris law slope for this alloy.

Alur and Kumar[99] studied both the stress-life (*S-N*) and fatigue crack-growth (*da/dN* versus ΔK) response of their Mo-2Si-1B isothermally forged alloy. Tension-tension *S-N* tests were performed in accordance with ASTM E466[177] at 5 Hz and a load ratio $R' = 0.1$, with the loading direction aligned with the forging direction. Fatigue crack growth experiments were performed using pre-cracked compact-tension specimen at load ratios $R' = 0.1$ and 0.2 (although no difference in behavior was detected between the two load ratios) and a testing frequency of 5 Hz. The forging direction was aligned with the plane of the sample as the geometry of the forged ingot precluded alignment of the notch with the forging direction. Tests were performed at constant ΔK and were interrupted every 25,000 cycles in order to optically measure any crack growth.

Although the material tested by Alur and Kumar[99] contained more α-Mo (62 vol.%) than the maximum of 49 vol.% tested by Kruzic et al.[117], the fatigue response of this alloy was characteristic of a brittle material. A failure stress of 565 MPa was observed for a 30,000 cycle life, which fell to 500 MPa for a 1, 000, 000 cycle life. The observed crack morphologies and fracture surfaces closely resembled the behavior of monotonically loaded samples. The authors reported a relatively low fatigue threshold ($\Delta K_{th} = 5$ MP$\alpha\sqrt{m}$) considering the high α-Mo content of their alloy. The low fatigue threshold exhibited by this alloy was the result of solid solution strengthening of Mo by Si and work hardening caused by isothermal forging during processing. Hardening of Mo limited its ductility and thus its ability to form uncracked ligament bridges; the degradation of these bridges is the mechanism by which fatigue cracking occurs in Mo-Si-B alloys. It is important to note, however, that the room temperature Paris law exponent reported by Alur and Kumar ($m = 17$) is the lowest yet reported. While not in the regime characteristic of ductile materials (m = 2-4[162]), the relatively low value of the Paris law exponent for these materials highlights the influence of a large volume fraction of continuous, ductile α-Mo on fatigue susceptibility of Mo-Si-B alloys.

As stated at the beginning of this section, a larger volume fraction of α-Mo leads to a higher fatigue susceptibility, but the alloy exhibits a higher damage tolerance. Thus, while a crack will initiate at a lower stress-intensity factor in a high-α-Mo alloy, the crack growth rate will be significantly slower. Restated, a low-α-Mo alloy can withstand a larger load than a high-α-Mo alloy without initiating a crack, but once a crack initiates in a low-α-Mo alloy, it fractures unstably almost immediately. By contrast, some measure of stable crack growth is attainable in a high-α-Mo alloy, allowing for detection of a crack before it grows to a critical size.

5.4.2. Elevated Temperature Behavior

At elevated temperatures, the fatigue resistance of Mo-Si-B alloys is improved. The improved ductility of α-Mo above ~1000 °C clearly results in larger fatigue thresholds. Above the ductile-brittle transition temperature, uncracked α-Mo bridges are much easier to form and act as more potent extrinsic toughening agents. The increased ductility of these bridges enhances their fatigue lifetimes as the material exhibits Paris law behavior more akin to ductile metals than the characteristic brittle behavior exhibited at room temperature. As a result, a larger portion of the fatigue life is spent growing a fatigue crack (as opposed to initiating a flaw that then grows) until it reaches a critical size large enough to initiate unstable fracture. Choe et al.[85] saw the fatigue threshold of their Mo-4.2Si-1.1B alloy increase from 5 MP$\alpha\sqrt{m}$ at 25 °C to ~ 8 MP$\alpha\sqrt{m}$ at 1300 °C while the Paris law exponent fell from m = ~60 to $m = 44$. While significant microcracking of the Mo_5SiB_2 phase provided some measure of crack-tip shielding, the ductility of the α-Mo phase was limited by its discontinuity and constraint by the surrounding intermetallic matrix; few α-Mo bridges formed as a result.

More impressive fatigue resistance gains have been realized in alloys containing a continuous α-Mo phase, as this guarantees interaction with the crack path and increases the effectiveness of crack trapping and uncracked ligament bridging. Kruzic et al.[117] reported a transition to more ductile fatigue behavior at 1300 °C for their C49 alloy. While the authors were unable to accurately measure fatigue thresholds at this temperature, they found that the Paris law exponent for this alloy had dropped from $m = 78$ to $m = 4$, a characteristic value for fatigue of ductile materials. These results highlight the importance of a large volume fraction of continuous α-Mo when developing a damage tolerant Mo-Si-B material. The role of microstructural size scale on the high temperature fatigue behavior of these alloys has not yet been explored, as the fine-grained and coarse-grained materials studied by Kruzic et al.[117] had different volume fractions of α-Mo. Kruzic et al. did not explore the fatigue behavior of two alloys with the same volume fraction of α-Mo. Lemberg et al.[123] showed a convergence of the 1300 °C initiation toughness values for coarse and ultrafine grained alloys containing 55 vol% α-Mo. It is reasonable then to predict that the ultrafine-rained materials studied by Lemberg et al.[123] would exhibit similar fatigue behavior at 1300 °C, but to date no study of the fatigue response of these ultrafine-grained materials has been conducted.

The most comprehensive work on the high temperature fatigue behavior of Mo-Si-B was performed by Alur and Kumar[99] and Alur et al.,[100] although they only studied the behavior of a two-phase Mo-2Si-1B alloy. Alur and Kumar[99] reported improved *S-N* behavior for their alloy *in vacuo* at 1200 °C. The authors observed an endurance limit, which they defined as survival of the sample after 10^7 cycles at a given stress, of ~550 MPa; this was an improvement over the endurance limit (~500 MPa) that they observed at room temperature. Their material was more susceptible to fatigue at 1200 °C, since plastic deformation was much more prevalent at this temperature; for example, plastic stretching of α-Mo grains was evident before failure, indicating more ductile behavior.

Alur and Kumar[99] also explored the fatigue crack growth behavior of their alloy in air (up to 600 °C) and vacuum (up to 1400 °C). To date, this study represents the only exploration of the combined effects of environment and temperature on the fatigue behavior of a Mo-Si-B alloy. In air, little difference was observed in the fatigue threshold (~5 MP$\alpha\sqrt{m}$), but a slight increase in the Paris law exponent ($m = 17$ at room temperature, $m = 23$ at 600 °C) was seen with increase in temperature. Tests performed at 600 °C *in vacuo* revealed a Paris

law exponent $m = 17$, implying the difference in Paris law exponents in air and vacuum was caused by the environment. In this temperature regime, α-Mo in this alloy oxidizes to form solid MoO_3,[99] a brittle oxide. Thus, it is reasonable to believe an increase in the content of brittle phases at the expensive of more ductile α-Mo would lead to more brittle-like fatigue and thus larger Paris law exponents. It is important to note that the effect of the testing environment on the fatigue behavior of Mo-2Si-1B was significantly smaller than that of a commercial Mo alloy, which exhibited a two-fold decrease in the fatigue threshold when tested at 600 °C in air as compared to vacuum. The improved oxidation resistance of an α-Mo-Mo_5SiB_2 alloy, as compared to the nominally pure Mo matrix of TZM (*e.g.*, Mo-0.5Ti-0.08Zr-0.02C), was thought to minimize the effects of oxidation on the fatigue crack growth behavior of Mo-2Si-1B. However, the authors argued that the formation of a borosilicate layer leads to slip irreversibility, thus speeding up crack growth; moreover, the temperature dependence of the formation of a borosilicate layer leads to the observed temperature dependence of the fatigue behavior in air up to 600 °C. One aspect, acknowledged by Alur and Kumar,[99] which has never been studied is the effect of oxygen segregation and subsequent embrittlement on the fatigue behavior of their alloy.

Above 1200 °C *in vacuo*, the fatigue threshold remained approximately the same as the room temperature value, but the Paris law exponent continued to decrease, falling as low as $m = 3.5$ at 1400 °C. Fatigue striations were observed on some grains, highlighting the improved ductility of their alloy at 1400 °C. The authors did observe some creep effects, like creep cavitation, and dynamic recrystallization ahead of the growing fatigue crack. The formation of a recrystallized region provides a preferred microstructural path and accelerates crack growth. However, recrystallization only occurred at 1400 °C and at a ΔK value (~9 MP$\alpha\sqrt{m}$), i.e., much higher than the fatigue threshold.

The combined effects of creep (via the formation of creep cavities) and fatigue (via the degradation of ductile α-Mo bridges) are thought to accelerate crack growth and increase the fatigue susceptibility of Mo-Si-B alloys. Alur et al.[100] compared the fatigue crack growth rates of a Mo-2Si-1B alloy exposed to 4 Hz sinusoidal waveforms as well as trapezoidal waveforms including a tensile hold for various dwell times (5–15 seconds) at 1200 °C and 1400 °C. At 1200 °C, crack growth rates increased with a dwell time of at least 10 s; at 1400 °C, the deterioration of the fatigue resistance of this alloy was even greater. A marked increase in the fatigue crack growth rate was observed for all of the tested non-zero dwell times. The rapid increase in crack growth implied the formation of recrystallized grains and creep cavities ahead of the crack tip. The deterioration in the fatigue response increased with increasing ΔK, highlighting the influence of stress on the formation and eventual linking of creep cavities, which enhance crack growth.

6. Concluding Remarks: Optimization of Mo-Si-B Alloys for Structural Applications

The design and development of new materials for ultrahigh temperature applications is invariably a competition between achieving excellent oxidation resistance and creep/fatigue strength at service temperatures and maintaining adequate ductility and toughness at both low and high temperatures. Unfortunately, the microstructural requirements to achieve acceptable behavior in all categories are generally mutually exclusive. This is a particularly difficult problem in Mo-Si-B alloys where the microstructures for optimal oxidation resistance, creep strength and damage tolerance (strength and toughness) are so contradictory. Specifically, for oxidation resistance, the three-phase alloys with very small discontinuous grains are best as the small grains limit the probability that an α-Mo grain will be exposed to oxygen; likewise, the small grains provide a short diffusion pathway allowing for faster passivation than in coarser-grained alloys.[70] In direct contrast, optimal room-temperature damage tolerance is afforded by large, continuous α-Mo grains that promote extrinsic toughening by the generation of ductile ligament bridges that act to "shield" a crack tip from the full force of an applied stress, thereby inhibiting crack advance.[85,116,117] Corresponding high-temperature toughness is also promoted by a high volume fraction of α-Mo as the ductility of this phase generates extensive plasticity which toughens the alloy intrinsically. In further contrast, optimal creep response is provided by alloys with large intermetallic grains surrounding small islands of α-Mo, which limits the number of high-diffusivity pathways such as grain boundaries;[141] a low volume fraction of α-Mo is also desirable, as the relative ease of deformation of α-Mo at high temperatures allows individual intermetallic particles to rearrange easily. **Figure 20** shows schematic illustrations of the microstructural morphologies necessary to maximize material response for each property.

There has been much recent interest to address the combined necessity of optimizing Mo-S-B alloys to come to terms with the fact that a large α-Mo is required for damage tolerance yet a fine grain size is needed for oxidation resistance.[14,15,119–122,137] Although the oxidation resistance of fine-grained materials is clearly superior, a high volume fraction of ductile phase is by itself not a sufficient requirement for high toughness. As shown by Lemberg et al.,[123] fine-grained microstructures do not provide adequate impediment to crack advance at room temperature. Plastic constraint of the ductile phase in these alloys limits their ability to plastically deform and thus blunt any cracks which interact with the ductile phase. Grain boundary segregation of Si and O further inhibited toughness by lowering grain boundary adhesion, thus embrittling the grain boundaries.

While some degree of grain boundary weakness (and thus intergranular fracture) is advantageous to the toughness of these alloys (and is in fact necessary for the formation of interlocking grain bridging ligaments), a purely intergranular fracture of severely weakened grain boundaries would severely limit any such (*extrinsic*) crack-growth resistance. In such a situation, the toughness of the alloy is governed by the toughness of the grain boundary, and not the toughnesses of the constituent phases. Conversely, increased interfacial strength can lead to premature failure of uncracked ligaments[169] or crack penetration and transgranular cleavage instead of deflection,[165] again limiting the ability of the material to be toughened extrinsically. As a result, akin to many ceramic materials,[178] precise control of the concentration of grain-boundary impurities, such oxygen and silicon which lower grain boundary strength, is vitally important for insuring enhanced damage tolerance in these alloys.

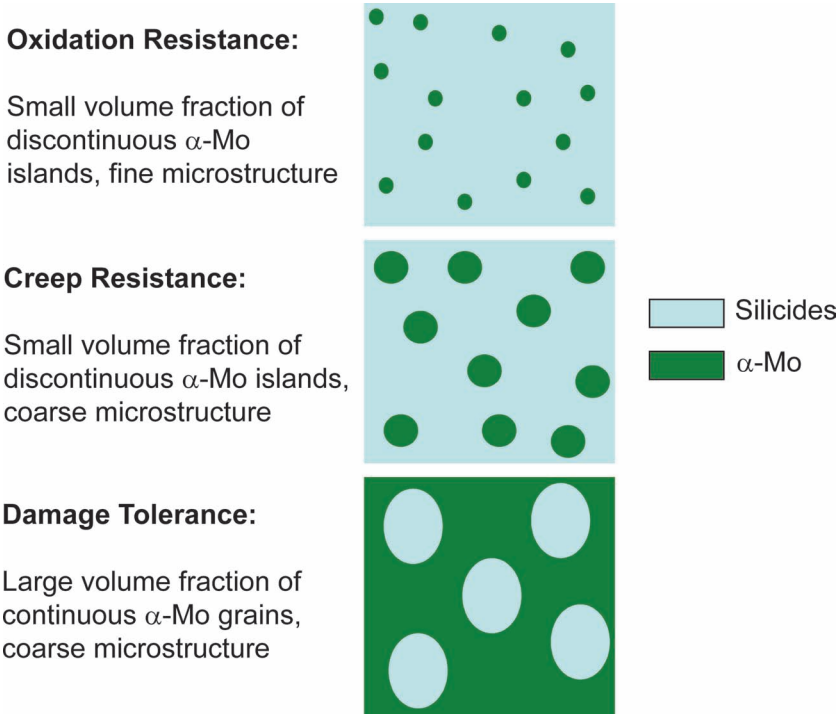

Figure 20. Schematic illustrations of the ideal microstructures to improve oxidation resistance, creep resistance and damage tolerance of Mo-Si-B alloys. The morphological considerations for improvement in each area are mutually exclusive, so optimization of the properties of each phase is necessary.[141]

If damage tolerant Mo-Si-B alloys are ever to be manufactured on an industrial scale, the issue of the segregation of Si and O to grain boundaries needs to be addressed. The most damage-tolerant alloys reported to data all require complex processing routes involving vacuum annealing of arc-melted and ground Mo-Si-B powders, which produced material with very little Si in the grain boundaries. Clearly the complexity and processing steps necessary to create these alloys limits the shapes that can be produced by this method, as well as the quantities that can be manufactured. The mechanical alloying and reaction synthesis methods, described in Section 3.2, can provide a path forward, provided the segregation of Si and O can be limited. One way to reduce the amount of Si segregation is to remove elemental Si as one of the initial alloy constituents. In this regard, new research on Mo-SiO_2-B alloys has shown promising results, but much work still remains to optimize the oxidation resistance and mechanical response of these alloys.[179]

At elevated temperature (above ~ 1150 °C), the ductility of α -Mo is greatly increased, to the point that the distribution of this phase becomes secondary to the volume fraction of ductile phase in the development of toughness.[123] High volume fractions of continuous a-Mo allow for stable crack growth, both in fatigue and under monotonic loading. At 1300 °C, the initiation toughness of ultrafine-grained materials has been shown to be comparable to that of a coarse-grained alloy containing a similar volume fraction of α-Mo.[123] While the high temperature damage tolerance and oxidation resistance of these alloys are impressive, the minimal damage tolerance exhibited by the fine-grained alloys at room temperature limits their usefulness. As a result, improving the room temperature ductility of α-Mo is one way to produce industrially-viable Mo-Si-B alloys.

Surface modification or thermal barrier coating of these alloys will likely be necessary to achieve the best combination of oxidation resistance and damage tolerance. The outer layer would provide oxidation resistance, while a coarse-grained interior could provide damage tolerance. Al[69,153] and Si[83,89,154,155] pack cementation have each proven successful at depositing an oxidation resistant coating on Mo-Si-B alloys, but the lifetime of such coatings is diffusion-limited. Diffusion barriers can extend the lifetime of a coating, but care is required to ensure good adhesion. Laser-remelting has also been shown to improve the oxidation resistance by reducing the grain size in the near-surface region,[90] but the oxidation resistance of such a coating is limited by its initial thickness. The most promising surface modification for developing oxidation resistance is the preoxidation treatment in extremely oxygen partial pressures pioneered by Burk et al.[131] but so far, the utility of this technique has only been shown for ultrafine-grained materials.

Realistically, a combination of a coarse-grained core coupled with a fine-grained exterior will likely be required to satisfy the all of the mechanical and oxidation response requirements for the anticipated service conditions for these alloys. Laser-remelting of the surface of a coarse-grained alloy will provide a fine-grained "crust", while leaving a coarse-grained core. Pretreatment in extremely low oxygen partial pressures, as suggested by Burk et al.[131] can be used to form a SiO_2 scale before entering service. In this way, the alloy is passivated, but still maintains an intermediate layer of fine-grained material which can quickly repair the oxide scale should it become damaged.

As explained by Rioult et al.,[70] finer grains lead to shorter B diffusion lengths, which in turn lead to less transient weight loss. Once a passive scale is formed, grain size becomes much less important. By utilizing a "duplex" structure, the oxidation resistance of a fine-grained material can be gained without a large decline in the room temperature damage tolerance. The coarse core, protected from oxidation by both the oxide scale and the quick-healing afforded by the fine grained surface, would no longer be a liability at high temperatures.

To improve the creep resistance of these materials, less α-Mo should be used. Alloying additions, like Zr, have the potential to increase the ductility of α-Mo. By increasing the plastic response capability of the α-Mo phase, it is possible to achieve high toughness utilizing far less α-Mo. As a result, the oxidation and creep resistance of these materials can be improved. Unfortunately, Zr causes drastic deterioration of the oxidation resistance above ~1100 °C.[133] Again, pretreatment in extremely low partial pressures of oxygen has been shown to combat this degradation.[131]

Acknowledgements

This work was supported at the Lawrence Berkeley National Laboratory by the Director, Office of Science, Office of Basic Energy Research, Division of Materials Sciences and Engineering of the U.S. Department of Energy under contract No. DE-AC02-05CH11231. JAL also would like to acknowledge several years of graduate student support from a National Defense Science and Engineering Graduate (NDSEG) Fellowship.

Received: February 22, 2012
Revised: April 19, 2012
Published online: June 19, 2012

[1] D. M. Dimiduk, J. H. Perepezko, *MRS Bull.* **2003**, *28*, 639.
[2] J. H. Perepezko, R. Sakidja, K. S. Kumar, in *Advanced Structural Materials: Properties, Design Optimization, and Applications*, (Ed: W. Soboyejo), CRC Press, Boca Raton, FL **2007**, 437.
[3] S. Drawin, *Mater. Res. Soc. Symp. Proc.* **2009**, *1128*, 1128.
[4] M. Heilmaier, M. Krüger, H. Saage, J. Rösler, D. Mukherji, U. Glatzel, R. Völkl, R. Huttner, G. Eggler, C. Somsen, T. Depka, H.-J. Christ, B. Gorr, S. Burk, *JOM* **2009**, *61*, 61.
[5] J. H. Perepezko, Science **2009**, 326, 1068.
[6] A. K. Vasudévan, J. J. Petrovic, *Mater. Sci. Eng.* **1992**, *A155*, 1.
[7] J.-C. Zhao, J. H. Westbrook, *MRS Bull.* **2003**, *28*, 622.
[8] J. H. Perepezko, R. Sakidja, *JOM* **2010**, *62*, 13.
[9] M. Heilmaier, M. Krüger, H. Saage, *Mater. Sci. Forum* **2010**, *633-634*, 549.
[10] M. Heilmaier, H. Saage, M. Krüger, P. Jéhanno, M. Böning, H. Kestler, *Mater. Res. Soc. Symp. Proc.* **2009**, *1128*, 1128-U07-07.
[11] P. Jéhanno, M. Böning, H. Kestler, M. Heilmaier, H. Saage, M. Krüger, *Powder Metallurgy* **2008**, *51*, 99.
[12] M. Yamaguchi, H. Inui, K. Ito, *Acta Mater.* **2000**, *48*, 307.
[13] H. Nowotny, E. Dimakopoulou, H. Kudielka, *Mh. Chem.* **1957**, *88*, 180.
[14] M. Krüger, S. Franz, H. Saage, M. Heilmaier, J. H. Schneibel, P. Jéhanno, M. Böning, H. Kestler, *Intermetallics* **2008**, *16*, 933.
[15] M. R. Middlemas, J. K. Cochran, P. Jain, K. S. Kumar, TMS 2010 139th Annual Meeting & Exhibition - Supplemental Proceedings, Vol 1: Materials Processing and Properties **2010**, 859.
[16] C. A. Nunes, R. Sakidja, Z. Dong, J. H. Perepezko, *Intermetallics* **2000**, *8*, 327.
[17] N. Floquet, O. Bertrand, J. J. Heizmann, *Oxidation of Metals* **1992**, *37*, 253.
[18] P. Jain, K. S. Kumar, *Acta Mater.* **2010**, 58.
[19] P. Jain, K. S. Kumar, *Scripta Mater.* **2010**, *62*, 1.
[20] D. Sturm, M. Heilmaier, J. H. Schneibel, P. Jéhanno, B. Skrotzki, H. Saage, *Mater. Sci. Eng. A* **2007**, *463*, 107.
[21] M. K. Miller, E. A. Kenik, M. S. Mousa, K. F. Russell, A. J. Bryhan, *Scripta Mater.* **2002**, *46*, 299.
[22] M. K. Miller, A. J. Bryhan, *Mater. Sci. Eng.* **2002**, *A327*, 80.
[23] H. Saage, M. Krüger, D. Sturm, M. Heilmaier, J. H. Schneibel, E. George, L. Heatherly, C. Somsen, G. Eggeler, Y. Yang, *Acta Mater.* **2009**, *57*, 3895.
[24] S. R. Agnew, T. Leonhardt, *JOM* **2003**.
[25] D. Sun, in *Department of Mechanical Engineering*, Vol. Master of Science, University of West Virginia, Morgantown, WV **2003**.
[26] C. K. Lee, in *Department of Mechanical Engineering*, Vol. Master of Science, University of West Virginia, Morgantown, WV **2005**.
[27] D. M. Scruggs, *United States Patent* number 3,320,036, **1967**.
[28] J. H. Schneibel, M. P. Brady, J. J. Kruzic, R. O. Ritchie, *Z. Metallkunde* **2005**, *96*, 632.
[29] I. M. Gunter, J. H. Schneibel, J. J. Kruzic, *Mater. Sci. Eng.* **2007**, *A458*, 275.
[30] M. P. Brady, I. M. Anderson, M. L. Weaver, H. M. Meyer, L. R. Walker, M. K. Miller, D. J. Larson, I. G. Wright, V. K. Sikka, A. Rar, G. M. Pharr, J. R. Keiser, C. A. Walls, *Mater. Sci. Eng.* **2003**, *A358*, 243.
[31] A. Kumar, B. L. Eyre, *Proc. R. Soc. Lond.* **1980**, *A 370*, 431.
[32] P. Jain, A. P. Alur, K. S. Kumar, *Scripta Mater.* **2006**, *54*, 13.
[33] N. A. Christensen, *Acta Chem. Scandinavica* **1983**, *A37*, 519.
[34] I. Rosales, J. H. Schneibel, *Intermetallics* **2000**, *8*, 885.
[35] I. Rosales, *J. Crystal Growth* **2008**, *310*, 3833.
[36] J. G. Swadener, I. Rosales, J. H. Schneibel., *Mater. Res. Soc. Symp. Proc.* **2001**, *646*, N4.2.1.
[37] I. Rosales, J. H. Schneibel, L. Heatherly, J. A. Horton, L. Martinez, B. Campillo, *Scripta Mater.* **2003**, *48*, 185.
[38] I. Rosales, H. Martinez, *Mater. Sci. Eng.* **2004**, *A379*, 245.
[39] S. Ochiai, *Materials Science Forums* **2003**, *426-432*, 1771.
[40] I. Rosales, H. Martinez, D. Bahena, J. A. Ruiz, R. Guardian, J. Colin, *Corrosion Science* **2009**, *51*, 534.
[41] C. L. Fu, J. H. Schneibel, *Acta Mater.* **2003**, *51*, 5083.
[42] J. H. Schneibel, C. J. Rawn, T. R. Watkins, E. A. Payzant, *Physical Review B* **2002**, *65*, 134112.
[43] H. L. Zhao, M. J. Kramer, M. Akinc, *Intermetallics* **2004**, *12*, 493.
[44] J. B. Berkowitz-Mattuck, R. R. Dils, *J. Electrochem. Soc.* **1965**, *112*, 583.
[45] M. K. Meyer, A. J. Thom, M. Akinc, *Intermetallics* **1999**, *7*, 153.
[46] M. K. Meyer, M. Akinc, *J. Am. Ceram. Soc.* **1996**, *79*, 2763.
[47] M. K. Meyer, M. Akinc, *J. Am. Ceram. Soc.* **1996**, *79*, 938.
[48] M. Meyer, M. Kramer, M. Akinc, *Advanced Materials* **1996**, *8*, 85.
[49] K. Natesan, S. C. Deevi, *Intermetallics* **2000**, *8*, 1147.
[50] E. F. Riebling, *J. Am. Ceram. Soc.* **1964**, *47*, 478.
[51] J. Schlichting, *J. Non-Crystalline Solids* **1984**, *63*, 173.
[52] E. Ström, *Mater. Characterization* **2005**, *55*, 402.
[53] M. Akinc, M. K. Meyer, M. J. Kramer, A. J. Thom, J. J. Huebsch, B. Cook, *Mater. Sci. Eng.* **1999**, *A261*, 16.
[54] M. K. Meyer, M. J. Kramer, M. Akinca(sic), *Intermetallics* **1996**, *4*, 273.
[55] K. Yoshimi, M. H. Yoo, A. A. Wereszczak, S. M. Borowicz, E. P. George, E. Miura, S. Hanada, *Mater. Sci. Eng.* **2002**, A329-331, 228.
[56] C. J. Rawn, J. H. Schneibel, C. M. Hoffman, C. R. Hubbard, *Intermetallics* **2001**, *9*, 209.
[57] R. Sakidja, J. H. Perepezko, S. Kim, N. Sekido, *Acta Mater.* **2008**, *56*, 5223.
[58] K. Ito, K. Ihara, K. Tanaka, M. Fujikura, M. Yamaguchi, *Intermetallics* **2001**, *9*, 591.
[59] R. D. Field, D. J. Thoma, J. C. Cooley, F. Chu, C. L. Fu, M. H. Yoo, W. L. Hults, C. M. Cady, *Intermetallics* **2001**, *9*, 863.
[60] R. Sakidja, H. Sieber, J. H. Perepezko, *Philosophical Magazine Letters* **1999**, *79*, 351.
[61] R. Sakidja, J. H. Perepezko, *Metallurg. Mater. Trans. A* **2005**, *36A*, 507.
[62] Y. Yang, H. Bei, S. Chen, E. P. George, J. Tiley, Y. A. Chang, *Acta Mater.* **2010**, *58*, 541.
[63] R. Sakidja, J. Myers, S. Kim, J. H. Perepezko, *International J. Refractory Metals & Hard Materials* **2000**, *18*, 193.
[64] T. Hayashi, K. Ito, K. Ihara, M. Fujikura, M. Yamaguchi, *Intermetallics* **2004**, *12*, 699.
[65] K. Ihara, K. Ito, K. Tanaka, M. Yamaguchi, *Mater. Sci. Eng.* **2002**, *A329-331*, 222.
[66] K. Yoshimi, S. Nakatani, T. Suda, S. Hanada, H. Habazaki, *Intermetallics* **2002**, 10.
[67] T. A. Parthasarathy, M. G. Mendiratta, D. M. Dimiduk, *Acta Mater.* **2002**, *50*, 1857.
[68] M. G. Mendiratta, T. A. Parthasarathy, D. M. Dimiduk, *Intermetallics* **2002**, *10*, 225.

[69] F. Rioult, N. Sekido, R. Sakidja, J. H. Perepezko, *J. Electrochem. Soc.* **2007**, *154*, C692.
[70] F. A. Rioult, S. D. Imhoff, R. Sakidja, J. H. Perepezko, *Acta Mater.* **2009**, *57*, 4600.
[71] V. Supatarawanich, D. R. Johnson, C. T. Liu, *Mater. Sci. Eng.* **2003**, *A344*, 328.
[72] V. Supatarawanich, D. R. Johnson, C. T. Liu, *Intermetallics* **2004**, *12*, 721.
[73] J. Das, R. Mitra, S. K. Roy, *Intermetallics* **2011**, *19*, 1.
[74] J. Das, R. Mitra, S. K. Roy, *Scripta Mater.* **2011**, *64*, 486.
[75] J. S. Park, R. Sakidja, J. H. Perepezko, *Scripta Mater.* **2002**, *46*, 765.
[76] V. S. Dheeradhada, D. R. Johnson, M. A. Dayananda, *J. Phase Equilibria and Diffusion* **2006**, *27*, 582.
[77] J. H. Schneibel, J. J. Kruzic, R. O. Ritchie, *"Mo-Si-B alloy development", presented at Proceedings of the 17th Annual Conference on Fossil Energy Materials*, Knoxville, TN, **2003**.
[78] H. Choe, D. Chen, J. H. Schneibel, R. O. Ritchie, in *Fatigue and Fracture Behavior of High Temperature Materials*, (Ed: P. K. Liaw), TMS, Warrendale, PA **2000**, 17.
[79] H. Choe, D. Chen, J. Schneibel, R. O. Ritchie, *Intermetallics* **2001**, *9*, 319.
[80] J. H. Schneibel, C. T. Liu, D. S. Easton, C. A. Carmichael, *Mater. Sci. Eng.* **1999**, *A261*, 78.
[81] J. H. Schneibel, C. T. Liu, L. Heatherly, M. J. Kramer, *Scripta Mater.* **1998**, *38*, 1169.
[82] D. A. Helmick, G. H. Meier, F. S. Pettit, *Metallurg. Mater. Trans. A* **2005**, *36A*, 3371.
[83] Z. Tang, A. J. Thom, M. J. Kramer, M. Akinc, *Intermetallics* **2008**, *16*, 1125.
[84] J. H. Schneibel, M. J. Kramer, Ö. Ünal, R. N. Wright, *Intermetallics* **2001**, *9*, 25.
[85] H. Choe, J. H. Schneibel, R. O. Ritchie, *Metallurg. Mater. Trans. A* **2003**, *34A*, 225.
[86] V. Behrani, A. J. Thom, M. J. Kramer, M. Akinc, *Intermetallics* **2006**, *14*, 24.
[87] V. Behrani, A. J. Thom, M. J. Kramer, M. Akinc, *Metallurg. Mater. Trans. A* **2005**, *36A*, 609.
[88] K. Ito, M. Kumagai, T. Hayashi, M. Yamaguchi, *Scripta Mater.* **2003**, *49*, 285.
[89] K. Ito, T. Murakami, K. Adachi, M. Yamaguchi, *Intermetallics* **2003**, *11*, 763.
[90] F. Wang, A. Shan, X. Dong, J. Wu, *Scripta Mater.* **2007**, *56*, 737.
[91] F. Wang, A. Shan, X. Dong, J. Wu, *J. Alloys Compounds* **2008**, *462*, 436.
[92] S. M. Koohpayeh, D. Fort, J. S. Abell, *Progr. Crystal Growth Characterization Mater.* **2008**, *54*, 121.
[93] P. Jéhanno, M. Heilmaier, H. Kestler, *Intermetallics* **2004**, *12*, 1005.
[94] P. Jéhanno, M. Heilmaier, H. Kestler, M. Böning, A. Venskutonis, B. Belway, M. Jackson, *Metallurg. Mater. Trans. A* **2005**, *36A*, 515.
[95] D. Berczik, *United States Patent* number 5,595,616, **1997**.
[96] D. Berczik, *United States Patent* number 5,693,156, **1997**.
[97] S. R. Woodward, R. Raban, J. F. Myers, D. M. Berzcik, *United States Patent* number 6,652,674, **2003**.
[98] A. P. Alur, N. Chollacoop, K. S. Kumar, *Acta Mater.* **2004**, *52*, 5571.
[99] A. P. Alur, K. S. Kumar, *Acta Mater.* **2006**, *54*, 385.
[100] A. P. Alur, N. Chollacoop, K. S. Kumar, *Acta Mater.* **2007**, *55*, 961.
[101] K. S. Kumar, A. P. Alur, *Intermetallics* **2007**, *15*, 687.
[102] M. J. Kramer, S. C. Okumus, M. F. Besser, Ö.Ünal, M. Akinc, *J. Spray Technol.* **2000**, *9*, 90.
[103] S. C. Okumus, M. J. Kramer, A. J. Thom, M. Akinc, *Key Eng. Mater.* **2004**, *264–268*, 509.
[104] S. C. Okumus, Ö. Ünal, M. J. Kramer, M. Akinc, in *Innovative Processing and Synthesis of Ceramics, Glasses, and Composites II*, (Eds: N. P. Bansal, J. P. Singh), The American Ceramic Society, Westerville, Ohio **1999**, 347.
[105] N. Nomura, T. Suzuki, K. Yoshimi, S. Hanada, *Intermetallics* **2003**, *11*, 735.
[106] A. C. D. Chaklader, *Nature* **1965**, *206*, 392.
[107] R. Mitra, A. K. Srivastava, N. E. Prasad, S. Kumari, *Intermetallics* **2006**, *14*, 1461.
[108] R. Mitra, K. Chattopadhyay, A. K. Srivastava, K. K. Ray, N. E. Prasad, *Key Eng. Mater.* **2009**, *395*, 179.
[109] S. Paswan, R. Mitra, S. K. Roy, *Mater. Sci. Eng.* **2006**, *A424*, 251.
[110] S. Paswan, R. Mitra, S. K. Roy, *Intermetallics* **2007**, *15*, 1217.
[111] S. Paswan, R. Mitra, S. K. Roy, *Metallurg. Mater. Trans. A* **2009**, *40A*, 2644.
[112] Z. Li, L. M. Peng, *Mater. Lett.* **2008**, *62*, 2229.
[113] V. Supatarawanich, D. R. Johnson, M. A. Dayananda, C. T. Liu, *Mater. Sci. Forums* **2003**, *426–432*, 4301.
[114] T. G. Nieh, J. G. Wang, C. T. Liu, *Intermetallics* **2001**, *9*, 73.
[115] J. H. Schneibel, M. J. Kramer, D. S. Easton, *Scripta Mater.* **2002**, *46*, 217.
[116] J. J. Kruzic, J. H. Schneibel, R. O. Ritchie, *Scripta Mater.* **2004**, *50*, 459.
[117] J. J. Kruzic, J. H. Schneibel, R. O. Ritchie, *Metallurg. Mater. Trans. A* **2005**, *36A*, 2293.
[118] J. J. Kruzic, J. H. Schneibel, R. O. Ritchie, *Mater. Res. Soc. Symp. Proc.* **2005**, *842*, S2.9.1.
[119] M. R. Middlemas, J. K. Cochran, *JOM* **2008**, *28*, 19.
[120] M. R. Middlemas, J. K. Cochran, *TMS* 2008 Annual Meeting Supplemental Proceedings, Vol 3: General Paper Selections **2008**, 177.
[121] M. R. Middlemas, J. K. Cochran, *JOM J. Minerals, Met. Mater. Soc.* **2010**, *62*, 20.
[122] M. R. Middlemas, J. K. Cochran, A. M. Gokhale, TMS 2009 138th Annual Meeting & Exhibition - Supplemental Proceedings, Vol 1: Materials Processing and Properties **2009**, 177.
[123] J. A. Lemberg, M. R. Middlemas, T. Weingärtner, B. Gludovatz, J. K. Cochran, R. O. Ritchie, *Intermetallics* **2011**.
[124] O. Hassomeris, G. Schumacher, M. Kruger, M. Heilmaier, J. Banhart, *Intermetallics* **2011**, *19*, 470.
[125] A. R. Abbasi, M. Shamanian, *Mater. Sci. Eng. A* **2011**, *A528*, 3295.
[126] A. R. Abbasi, M. Shamanian, *J. Alloys Compounds* **2010**, *508*, 152.
[127] A. R. Abbasi, M. Shamanian, *J. Alloys Compounds* **2011**, doi:10.1016/j.jallcom.2011.05.066.
[128] A. Yamauchi, K. Yoshimi, K. Kurokawa, S. Hanada, *J. Alloys Compounds* **2007**, *434–435*, 420.
[129] S. R. Bakhshi, M. Salehi, H. Edris, G. H. Borhani, *Powder Metallurgy* **2008**, *51*, 119.
[130] S. R. Bakhshi, M. Salehi, H. Edris, G. H. Borhani, *Powder Metallurgy* **2011**, *54*, 108.
[131] S. Burk, B. Gorr, H.-J. Christ, *Acta Mater.* **2010**, *58*, 6154.
[132] S. Burk, B. Gorr, V. B. Trindade, U. Krupp, H.-J. Christ, *Corrosion Engineering, Science and Technology* **2009**, *44*, 168.
[133] S. Burk, B. Gorr, V. B. Trindade, H.-J. Christ, *Oxid. Met.* **2010**, *73*, 163.
[134] P. G. Biragoni, M. Heilmaier, *Advanced Engineering Materials* **2007**, *9*, 882.
[135] P. Jéhanno, M. Heilmaier, H. Saage, M. Böning, H. Kestler, J. Freudenberger, S. Drawin, *Mater. Sci. Eng.* **2007**, *A463*, 216.
[136] P. Jéhanno, M. Heilmaier, H. Saage, H. Heyse, M. Böning, H. Kestler, J. H. Schneibel, *Scripta Mater.* **2006**, *55*, 525.
[137] M. Krüger, H. Saage, M. Heilmaier, M. Böning, H. Kestler, *J. Physics: Conference Series* **2010**, *240*, 012087.
[138] P. S. Gilman, J. S. Benjamin, *Ann. Rev. Materials Science* **1983**, *13*, 279.

[139] J. E. Gardner, M. Hilton, M. R. Carroll, *Geochimica et Cosmochimica Acta* **2000**, *64*, 1473.
[140] N. P. Bansal, R. H. Doremus, *Handbook of Glass Properties*, Academic Press, Orlando, FL **1986**.
[141] J. H. Schneibel, R. O. Ritchie, J. J. Kruzic, P. F. Tortorelli, *Metallurg. Mater. Trans. A* **2005**, *36A*, 525.
[142] J. H. Schneibel, P. F. Tortorelli, M. J. Kramer, A. J. Thom, J. J. Kruzic, R. O. Ritchie, *Mater. Res. Soc. Symp. Proc.* **2003**, *753*, BB2.2.1.
[143] P. Mandal, A. J. Thom, M. J. Kramer, V. Behrani, M. Akinc, *Mater. Sci. Eng.* **2004**, *A371*, 335.
[144] A. J. Thom, M. J. Kramer, P. Mandal, M. Akinc, *Scripta Mater.* **2005**, *53*, 915.
[145] P. F. Tortorelli, J. H. Schneibel, K. L. More, B. A. Pint, *Mater. Sci. Forums* **2004**, *461–464*, 1063.
[146] S. Mrowec, *Oxidation of Metals* **1995**, *44*, 177.
[147] J. H. Schneibel, J. J. Kruzic, R. O. Ritchie, "*Development of Ultra-High Temperature Molybdenum Borosilicides*", presented at *Proceedings of the 20th Annual Conference on Fossil Energy Materials*, Knoxville, TN, **2006**.
[148] A. Yamauchi, K. Yoshimi, Y. Murakami, K. Kurokawa, S. Hanada, *Solid State Phenomena* **2007**, *127*, 215.
[149] M. G. Mendiratta, J. J. Lewandowski, D. M. Dimiduk, *Metallurg. Transactions A* **1991**, *22*, 1573.
[150] V. Behrani, Vol. *Master of Science*, Iowa State University, Ames, IA **2004**.
[151] C. T. Lynch, F. W. Vahldiek, L. B. Robinson, *J. Am. Ceram. Soc.* **1961**, *44*, 147.
[152] J. E. Jackson, D. L. Olson, B. Mishra, A. N. Lasseigne-Jackson, *Int. J. Hydrogen Energy* **2007**, *32*, 3789.
[153] R. Sakidja, F. Rioult, J. Werner, J. H. Perepezko, *Scripta Mater.* **2006**, *55*, 903.
[154] K. Ito, T. Hayashi, M. Yokobayashi, T. Murakami, H. Numakura, *Metallurg. Mater. Trans. A* **2005**, *36A*, 627.
[155] R. Sakidja, J. S. Park, J. Hamann, J. H. Perepezko, *Scripta Mater.* **2005**, *53*, 723.
[156] T. Hayashi, K. Ito, H. Numakura, *Intermetallics* **2005**, *13*, 93.
[157] O. D. Sherby, J. Wadsworth, *Progr. Mater. Sci.* **1989**, *33*, 169.
[158] H. J. Frost, M. F. Ashby, *Deformation Mechanism Maps*, Pergamon Press, New York, NY **1982**.
[159] J. H. Schneibel, *Intermetallics* **2003**, *11*, 625.
[160] J. H. Schneibel, H. T. Lin, *Materials at High Temperature* **2002**, *19*, 25.
[161] A. G. Evans, *J. Am. Ceram. Soc.* **1990**, *73*, 187.
[162] R. O. Ritchie, *Int. J. Fracture* **1999**, *100*, 55.
[163] R. O. Ritchie, *Mater. Sci. Eng., A* **1988**, *103*, 15.
[164] M. E. Launey, R. O. Ritchie, *Adv. Mater.* **2009**, *21*, 2103.
[165] M.-Y. He, J. W. Hutchinson, *Int. J. Solids Structures* **1989**, *25*, 1053.
[166] J. W. Foulk, R. M. Cannon, G. C. Johnson, P. A. Klein, R.O.Ritchie, *J. Mech. Phys. Solids* **2007**, *55*, 719.
[167] ASTM E561-98. *Annual Book of ASTM Standards, Vol. 03.01: Metals- Mechanical Testing; Elevated and Low-temperature Tests; Metallography*, ASTM, West Conshohocken, Pennsylvania, USA **1998**.
[168] K. S. Chan, D. L. Davidson, *Metallurg. Mater. Trans. A* **2003**, *34A*, 1833.
[169] G. Y. Lin, K. S. Chan, *Metallurg. Mater. Trans. A* **1999**, *30*, 3239.
[170] C. F. Shih, *J. Mech. Phys. Solids* **1981**, *29*, 205.
[171] ASTM E1820-08. *Annual Book of ASTM Standards, Vol. 03.01: Metals - Mechanical Testing; Elevated and Low-temperature Tests; Metallography*, ASTM International, West Conshohocken, Pennsylvania, USA: **2008**.
[172] J. A. Shields, P. Lipetzky, A. J. Mueller, "Fracture toughness of 6.4 mm (0.25 inch) arc-cast molybdenum and molybdenum-TZM plate at room temperature and 300 °C", presented at *Proceedings of the 15th International Plansee Seminar*, Reutte, Austria, **2001**.
[173] L. S. Sigl, P. A. Mataga, B. J. Dalgleish, R. M. McMeeking, A. G. Evans, *Acta Metallurg.* **1988**, *36*, 945.
[174] J. P. Campbell, R. O. Ritchie, K. T. Venkateswara Rao, *Metallurg. Mater. Trans. A* **1999**, *30*, 563.
[175] ASTM E647-00. *Annual Book of ASTM Standards, Vol. 03.01: Metals - Mechanical Testing; Elevated and Low-temperature Tests; Metallography*, ASTM International, West Conshohocken, Pennsylvania, USA: **2000**.
[176] R. O. Ritchie, R. H. Dauskardt, *J. Ceram. Soc. Jpn.* **1991**, *99*, 1047.
[177] ASTM E446-76. *Annual Book of ASTM Standards, Vol. 03.01: Metals - Mechanical Testing; Elevated and Low-temperature Tests; Metallography*, ASTM International, West Conshohocken, Pennsylvania, USA: **1976**.
[178] A. Ziegler, J. C. Idrobo, M. K. Cinibulk, C. Kisielowski, N. D. Browning, R. O. Ritchie, *Science* **2004**, *306*, 1768.
[179] J. K. Cochran, W. L. Daloz, P. E. Marshall, unpublished.